

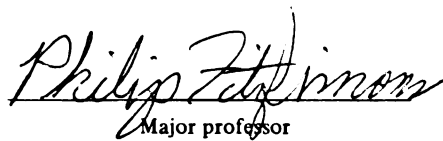


3 1293 00913 4812

This is to certify that the
thesis entitled
Characterization and Enhancement
of the Damping Within Composite Beams

presented by
Daniel John Trahan

has been accepted towards fulfillment
of the requirements for
Master of Science degree in Mechanical Engineering


Major professor

Date February 21, 1991

LIBRARY
Michigan State
University

PLACE IN RETURN BOX to remove this checkout from your record.
TO AVOID FINES return on or before date due.

DATE DUE	DATE DUE	DATE DUE
_____	_____	_____
_____	_____	_____
_____	_____	_____
_____	_____	_____
_____	_____	_____
_____	_____	_____
_____	_____	_____

MSU is An Affirmative Action/Equal Opportunity Institution

c:\cric\datedue.pm3-p.1

**CHARACTERIZATION AND ENHANCEMENT OF THE
DAMPING WITHIN COMPOSITE BEAMS**

By

Daniel John Trahan

A THESIS

**Submitted to
Michigan State University
in partial fulfillment of the requirements
for the degree of**

MASTER OF SCIENCE

Department of Mechanical Engineering

1991

ABSTRACT

CHARACTERIZATION AND ENHANCEMENT OF THE DAMPING WITHIN COMPOSITE BEAMS

By

Daniel John Trahan

The dynamics relating the transverse motions of a clamped-free graphite/epoxy beam are investigated. A Bernoulli-Euler beam model incorporating viscoelastic damping is used to predict the transfer function relating clamped end displacement to the displacement of the free end. Three damping strategies are considered. One strategy relies upon the internal damping abilities of the fiber and matrix. A second approach utilizes strips of viscoelastic damping material within the laminate. A third design considers optimal placement of the damping material to achieve the greatest damping enhancement with minimum strength and stiffness reductions. Each strategy is applied to two layup geometries, unidirectional and crossply. The experimental apparatus is configured to measure specimen end displacements resulting from random excitement of the clamped end. Collected data are analyzed to evaluate the utility of the model structure for capturing the essential system dynamics and the effectiveness of the damping strategies considered.

DEDICATION

To my parents for their enduring and continued love, understanding, and support during my years of study. Their help was genuinely appreciated although it often appeared that I was oblivious to the assistance.

ACKNOWLEDGEMENTS

During the past year my research has been assisted by numerous people whose help was essential in completion of this project. I am indebted to the 3M company for the donation of the carbon/epoxy prepreg and the viscoelastic material, and to the Composite Materials and Structures Center at Michigan State University for assistance in specimen fabrication. Naturally I owe a world of thanks to my advisor, Dr. Philip FitzSimons, who provided countless hours of advice and support as well as an understanding of the “big” research picture. Thanks are in order for Dr. Clarke Radcliffe who offered timely advice regarding experimental matters. Lastly, special thanks to Scott Emery for assistance with the Macintosh computers and enjoyable nerf games.

TABLE OF CONTENTS

LIST OF TABLES	vii
LIST OF FIGURES	ix
NOMENCLATURE	x
1.0 INTRODUCTION.....	1
2.0 DAMPING IN COMPOSITE LAMINATES	4
2.1 Laminate Methods of Internal Energy Dissipation.....	4
2.2 Laminate Shear Analysis.....	5
2.3 Damping Strategies.....	6
2.3.1 Undamped Specimens	7
2.3.2 Generally Damped Specimens	7
2.3.3 Optimally Damped Specimens	8
3.0 DEVELOPMENT OF THE CANTILEVER BEAM MODEL.....	15
3.1 Bernoulli-Euler Model	15
3.2 Boundary Conditions	17
3.3 Eigenfunction Solution.....	17
3.4 Eigenfunction Selection and Normalization of Constants.....	19
3.5 Solving for $z(x,t)$	22
3.6 Transfer Function Solution Process.....	25
3.7 Modal Parameter Values	26
3.8 Analysis of Results.....	26
4.0 EXPERIMENTAL MATERIALS	28
4.1 Experimental Materials.....	28
4.1.1 Material Aging	28
4.1.2 Aging Effects Upon Specimens.....	30
4.2 Specimen Fabrication	30
4.2.1 Lay-up Orientations and Damping Material Locations	30
4.2.2 Fabrication Equipment	32
4.2.3 Fabrication Methods.....	32
4.2.4 Problems Unique To Fabrication	33
5.0 EXPERIMENTAL PROCESS.....	34
5.1 Experimental Set-up.....	34
5.2 Equipment descriptions	34

5.3	Excitation Method	37
5.4	Specimen Linearity	37
5.5	System Damping.....	38
5.5.1	Apparatus Damping	39
5.5.2	Aerodynamic Damping.....	39
5.6	Input Displacement Content.....	40
5.7	Specimen Quality	41
6.0	EXPERIMENTAL RESULTS.....	42
6.1	Data Collection.....	42
6.1.1	Sampling Rate.....	42
6.1.2	Sampling Process.....	42
6.2	Data Manipulation	43
6.2.1	Laser Calibration.....	43
6.2.2	Kaman Calibration.....	43
6.3	Parameter Identification.....	44
6.4	Results.....	47
6.4.1	Parameter Values	48
6.4.2	Parameter Magnitude.....	52
6.4.3	Analysis of Time Responses	53
6.4.4	Damping Parameter Convergence To Zero	56
7.0	CONCLUSIONS and RECOMMENDATIONS.....	57
7.1	Conclusions.....	57
7.2	Recommendations.....	57
	REFERENCES.....	59
	Appendix A.....	63
	Appendix B.....	64
	Appendix C.....	65
	Appendix D.....	66
	Appendix E.....	69
	Appendix F.....	97

LIST OF TABLES

<u>Number</u>	<u>Title</u>	<u>Page</u>
2-1	Position of optimal damping strips.	14
3-1	Eigenvalues and truncation error.	20
5-1	Specimen linearity.	38
6-1	Crossply-generally damped dimensionless damping parameter and natural frequency values values.	48
6-2	Unidirectional-generally damped dimensionless damping parameter and natural frequency values values.	48
6-3	Crossply-optimally damped dimensionless damping parameter and natural frequency values values.	48
6-4	Unidirectional-optimally damped dimensionless damping parameter and natural frequency values values.	48
6-5	Crossply-undamped dimensionless damping parameter and natural frequency values values.	49
6-6	Unidirectional-undamped dimensionless damping parameter and natural frequency values values.	49
6-7	Damping enhancement ratios.	50
6-8	Aluminum 6061 modal dimensionless damping parameter values and natural frequency values, test A.	51
6-9	Aluminum 6061 modal dimensionless damping parameter values and natural frequency values, test B.	51
6-10	Aluminum 6061 modal dimensionless damping parameter values and natural frequency values, test C.	51
6-11	Aluminum 6061 modal dimensionless damping parameter values and natural frequency values, total case.	52
6-12	Crossply-generally damped modal dimensionless damping parameter values and natural frequency values, test case A.	52
6-13	Crossply-generally damped modal dimensionless damping parameter values and natural frequency values, test case B.	52
6-14	Crossply-generally damped modal dimensionless damping parameter values and natural frequency values, test case C.	52
6-15	Crossply-generally damped modal dimensionless damping parameter values and natural frequency values, total case.	52
6-16	2-norm of measured displacement signal.	54
6-17	2-norm of the one mode approximation error signal.	54

6-18	2-norm of the two mode-one damping parameter approximation error signal.	54
6-19	2-norm of the two mode-two damping parameter approximation error signal.	55
6-20	2-norm of measured free end displacement and the error between predicted free end displacements and measured free end displacements, crossply-generally damped specimen.	56
6-21	2-norm of measured free end displacement and the error between predicted free end displacements and measured free end displacements, aluminum 6061 specimen.	56

LIST OF FIGURES

<u>Number</u>	<u>Title</u>	<u>Page</u>
2-1	Laminate side view for the generally damped strategy.	7
2-2	Beam configuration for energy analysis.	9
2-3	Beam element free body diagram.	10
2-4	Moment magnitude along clamped-free beam of normalized length.	12
3-1	Differential beam element.	16
3-2	Four mode approximation of magnitude and phase responses with varying dimensionless damping parameter values.	27
5-1	Experimental set-up.	35

NOMENCLATURE

a	\equiv	specimen cross sectional area
a_0	\equiv	calibration removal scale factor for Kaman measuring system
a_1	\equiv	Kaman measuring system “guage” factor
B	\equiv	viscoelastic damping parameter
b	\equiv	specimen width
C_i	\equiv	constant used in the eigenfunction
E	\equiv	Young’s modulus
E_e	\equiv	square of 2-norm of error signal
E_{ym}	\equiv	square of 2-norm of measured signal
F	\equiv	matrix representation for the eigensolution
$f(x,t)$	\equiv	load per unit length applied to specimen
$H_i(s)$	\equiv	beam transfer function
I	\equiv	area moment of inertia
i	\equiv	vibration mode
J	\equiv	function minimized in optimization algorithm
j	\equiv	complex variable
K_i	\equiv	mode specific parameter for optimization of experimental data
L	\equiv	arbitrary specimen length
$M(x,t)$	\equiv	laminare bending moment
M	\equiv	beam element bending moment
m	\equiv	beam mass
m_e	\equiv	beam element mass
P_i	\equiv	modal participation of $q_i(t)$

p_i	\equiv	parameters in the modal response equation
$Q_i(s)$	\equiv	Laplace transform of the mode participation parameter
$q_i(t)$	\equiv	mode participation parameter
s	\equiv	complex frequency variable
$T_i(s)$	\equiv	beam response function
t_1	\equiv	laminae thickness
$U(s)$	\equiv	Laplace transform of the input variable
$u(t)$	\equiv	generalized description of beam input
$V(x,t)$	\equiv	beam element shear force
$W(x)$	\equiv	variable for separation of variable method
W_{pot}	\equiv	potential energy
W_{dis}	\equiv	dissipated energy
x	\equiv	independent spatial variable
$Y(1,s)$	\equiv	Laplace transform of the specimen free end displacement
$y(x,t)$	\equiv	neutral axis vertical displacement
y_l	\equiv	laser displacement measurements
y_k	\equiv	eddy current displacement measurements
y_m	\equiv	measured free end displacement
y_p	\equiv	predicted free end displacement
y_t	\equiv	beam element vertical velocity
y_v	\equiv	beam element vertical displacement
$z(x,t)$	\equiv	transformed displacement term

Greek Letters

Δf	\equiv	half-power bandwidth
Δx	\equiv	differential beam element length
∂t	\equiv	time partial derivative

∂_x \equiv spatial partial derivative

λ_i \equiv eigenvalue

ρ \equiv specimen density

$\Phi_i(x)$ \equiv eigenfunction solution

ξ \equiv dimensionless damping ratio

Subscripts

t \equiv time derivative

x \equiv spatial derivative

Superscripts

$(\)'$ \equiv spatial derivative

$(\)\dot{}$ \equiv time derivative

1.0 INTRODUCTION

Performance requirements for many components in the aerospace and automotive industries require the combination of high stiffness and damping characteristics in one material. A need exists for a material capable of enduring large applied loads while possessing the ability to dissipate vibrational energies. Historically, monolithic materials have been utilized to meet these requirements, but of late their dominance has been challenged with the introduction of composite materials. The term “composite materials” is used here in its broad definition in that it describes the integration of two or more dissimilar constituent materials into one material of superior mechanical properties and thus improved performance.

Enhancement of a material’s ability to dissipate energy via damping can be advantageous to the system in which it resides. This is true whether the system is a commercial aircraft or the extremity of a robot. In an environment where acoustic energy is unwanted, dissipation within structural materials results in less noise in areas where it is undesirable. This benefit of energy dissipation within the material can eliminate secondary manufacturing operations traditionally designed to minimize noise levels. Increased material damping can also reduce the physical motion of a system. Reduction of internal vibration within structural members can reduce unwanted oscillatory motions during starting and stopping. An example of this phenomena is the replacement of an aluminum robot arm with a composite arm by Magolan [1]. A reduction in the amount of internal vibrations can result in less physical motion of the system and thus an increase in the fatigue life of the structure.

Numerous attempts have been made to improve the damping of structural composite materials. In general, fiber/epoxy composite materials have better damping than metallic monolithic materials. Rivin [2] constructed thin-layer rubber-metal composite materials such that impact loads were better cushioned and a reduction in peak sound pressure levels was attained.

The type of composite material focused upon in this study is composed of carbon reinforcing fibers embedded in an epoxy matrix. Carbon/epoxy composite materials are furnished with the means for internal dissipation of vibrational energy. In general, it is assumed that energy is removed at three locations within a composite laminate. Vibration losses occur in the reinforcing fibers, within the matrix, and at the interface common to the fibers and matrix. The damping characteristic of single carbon fibers is quantified by Adams [3].

Desired mechanical and aesthetic performance levels of a composite material are determined by the selection of the constituent fibers and matrix, and their volumetric percentages. The size, type, and orientation of reinforcing fibers can determine the damping properties of the laminate. Comparisons between continuous and discontinuous reinforcing fibers indicates that material damping is larger for discontinuous fiber composites than continuous fiber laminates [4, 5]. Another methodology to improve laminate damping is via optimization of fiber orientation and ply thickness [6, 7]. Liao et al developed an algorithm that determines a maximum specific damping capacity when provided values for ply thickness and fiber orientation [8].

Further attempts to improve material damping have explored the addition of a constrained viscoelastic layer within the composite material. The exclusive purpose of this layer is the dissipation of energy. Basic versions of this constrained layer ideology consider three ply laminates in which the middle ply is responsible for damping and the outer two layers are responsible for stiffness and constraining [9, 10]. Finite element models have been designed for the three ply, constrained layer laminates that predict strategies of minimal natural frequency and maximum modal damping [11]. Lall et al used the Rayleigh-Ritz method to assess damping and modal loss factors of a simply supported plate with a partial layer of constrained viscoelastic material. Results indicate that a decrease in the shear modulus of the viscoelastic layer produces an increase in the laminate loss factor and lower resonant frequencies [12]. Beam specimens equipped with a constrained layer of

viscoelastic material along the length axis have been the focus of studies [13-15]. Maximum material damping has been acknowledged via both optimal placement of damping strips along the specimen and optimal ratio of damping strip length to beam length.

Many authors have performed the task of modeling the damping proficiency of composite laminates [16-19]. A common approach used when analyzing damping properties is to compute values for the material's specific damping capacity and loss factor; these quantities are typically determined for quasi-static conditions. Algorithms used to compute dynamic characteristics typically originate as the classical laminate theory. Investigators have modified these algorithm's such that the predicted values for dynamic properties include hygrothermal effects and allow for consideration of hybrid composite laminates [20, 21]. An experimental observation worthy of note evaluated the dynamic properties of S-2 glass/epoxy unidirectional, cantilever specimens excited over a 30 Hz to 1000 Hz band. Loss factors spanning 5×10^{-3} to 10×10^{-3} were measured using the half power bandwidth method [22].

The current study will identify and assess the ability to modify the damping properties of carbon/epoxy composite laminates. Specimens used to generate experimental data represent three damping strategies including carbon/epoxy laminate, carbon/epoxy laminate with a general damping enhancement, and a carbon/epoxy laminate with optimal enhancing of its damping mechanisms. Each strategy is applied to a unidirectional and crossply layup geometry. The transfer function of an unloaded Bernoulli-Euler clamped-free beam considering viscous damping is developed; this relation is used to construct a modal response equation. The modal response relation is used in conjunction with experimental data to acquire values for the dimensionless damping parameter and the natural frequency. Specimen modal damping values are indicative of their material damping measured in a dynamic environment. Specimen modal damping values are compared. Deviations and regularities of damping parameter magnitudes are addressed as well as inconsistencies between experimental data and predicted results.

2.0 DAMPING IN COMPOSITE LAMINATES

A composite laminate is produced by stacking a desired number of prepreg layers upon one another. The number of prepreg layers and the orientation of their fiber angles dictate the material properties of the laminate. A prepreg layer, also termed a lamina, is a thin sheet of continuous, unidirectional fibers embedded in an epoxy matrix. The thickness of an uncured prepreg layer is unchanged during the autoclave cure cycle. An autoclave cure cycle uses elevated pressure and temperature to harden the prepreg layers to their end consistency. The fibers typically provide a laminate with its strength and structural integrity while the epoxy matrix protects the reinforcing fibers from damage due to the surroundings and provides the means to transfer applied forces within the laminate. Fibers are generally composed of carbon, glass, or an organic substance termed Kevlar. As mentioned above, the angle of a ply's reinforcing fibers, termed ply orientation, will dictate the material properties and dynamic response of a laminate. Desired material properties and dynamic response can be achieved by altering the number of lamina and/or the ply orientations. The presence of an interface region where the fibers and matrix bind together provides a laminate with an internal means to dissipate energy; vibrational energy is lost across the fiber/epoxy interface. Such a mode of energy dissipation within the internal structural system offers composite laminates a distinct advantage over monolithic materials in the realm of energy dissipation.

2.1 Laminate Methods of Internal Energy Dissipation

The main source of internal material damping in a composite laminate is due to the viscoelastic phenomenon of the relative slipping between the matrix and fibers. The amount of energy dissipated internally, and thus the amount of damping, is dependent upon the following factors:

- 1) fiber volume fraction
- 2) fiber diameter
- 3) matrix properties

- 4) thermoelastic damping
- 5) fiber orientation within the laminate
- 6) fiber surface treatment
- 7) presence of debonds, inclusions and voids

The initial four modes of internal energy dissipation listed above are specific to the component fiber and matrix materials selected, while the latter three means of energy dissipation arise as a product of the fabrication process and the design ideals when developing the manufactured item [23]. Factors 1 and 2 indicate that the amount of energy dissipated corresponds to the amount of fiber/matrix interface area present within the laminate. Increasing the fiber volume fraction or fiber diameter allows more interfacial area in which energy dissipation can occur. The properties of the matrix relate to the amount of friction between a sliding fiber and the stationary matrix. Thermoelastic damping is due to the different thermal coefficients of expansion between the fiber and matrix.

Fibers oriented in the direction of an applied load will have a higher degree of mobility, and thus exhibit more dissipation of energy to friction, than fibers oriented perpendicular to the direction of an applied load. Fiber surface coatings regulate interface friction and bonding strength which effects the amount of material damping. Lastly, the presence of fabrication defects, voids, debonds, or delamination offer regions for additional energy dissipation which are specific to the quality of fabrication and not the abilities of the material.

2.2 Laminate Shear Analysis

In the fabrication of a composite laminate, the process of stacking and curing prepreg layers introduces a distribution of shear through the laminate's thickness. Transverse shear deformation within a laminate will influence certain static and dynamic properties including lateral deformation, bucking loads, and natural frequencies.

Transverse shear is the means by which a laminate internally dissipates energy due to its motions. The amount of energy removed from a laminate can be further increased with the

addition of an energy absorbing material at laminae interfaces. Inclusion of a secondary material provides an auxiliary means by which vibrational energies are internally dissipated as a function of shear. Addition of an object foreign to the laminate at an interface will cause a reduction in overall laminate strength due to the interruption of the interfacial surface area. Interfacial surface area is the means by which a laminate distributes loads across its thickness and is the plane of failure when a laminate's maximum load is exceeded. Thus a trade off is recognized, positioning damping material at a laminae interface increases laminate damping with an associated strength reduction penalty. It is desirable to position the energy absorbing material at height positions corresponding to high shear values to best utilize its damping abilities.

2.3 Damping Strategies

Three damping strategies varying in the amount and placement of viscoelastic damping material will be combined with two layup geometries, crossply and unidirectional. The three methodologies include no viscoelastic damping material, a general arrangement of viscoelastic damping material, and optimally positioned damping material to dissipate energies of the first and second vibration modes.

Damping strips are located about the laminate midplane because this is the region where the largest shear values exist. Therefore, a maximum damping benefit is achieved while the associated laminate strength reduction penalties are minimized. In the spirit of maintaining a midplane symmetric laminate of eight plies, damping material may be added at one, three, five or seven ply interfaces. The interruption of five or seven interfaces with the damping material would offer increased damping at the expense of major strength reductions because nearly all the planes of load transition, ply interfaces, are made weaker by the presence of the damping material. Placing the strips of the viscoelastic material only at the midplane interface would retain the laminate strength, but not produce notable increases in laminate damping. Thus it was decided to employ the damping material at the three interfaces about

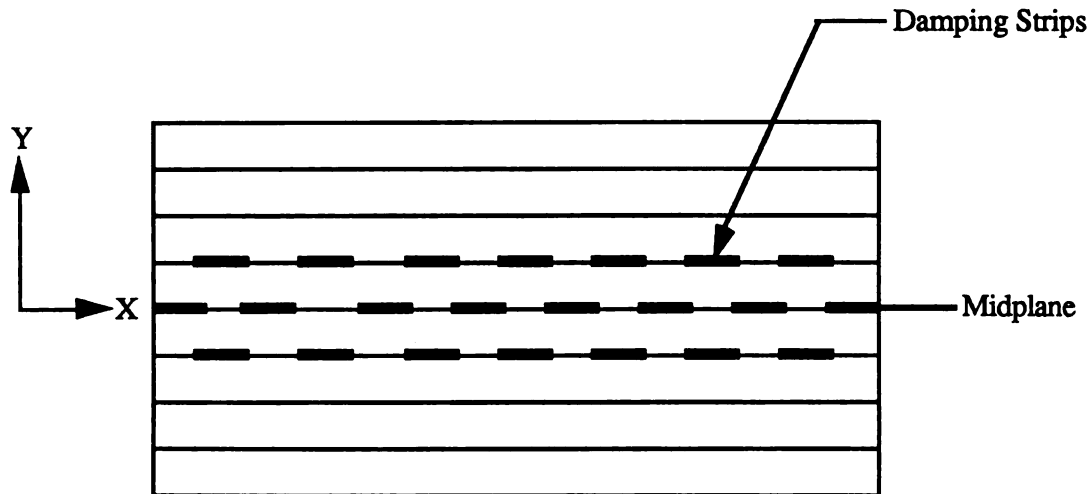


Figure 2-1 Laminate side view of a generally damped specimen.

the midplane to achieve a desirable amount of damping without major strength reduction penalties as shown in Figure 2-1. Strips of viscoelastic damping material were one-half inch in width were laid perpendicular to the beam's longitudinal axis. The one-half inch damping strip width was selected to combine ease of fabrication with strips that were not excessively wide yielding large segments of non-contact at laminae interfaces thereby reducing laminate strength.

2.3.1 Undamped Specimens

Specimens without viscoelastic material were constructed to determine the damping characteristics of the carbon/epoxy material. Undamped specimens allow for comparison of the effect of different ply orientations on internal damping. The crossply laminate should experience greater amounts of internal energy dissipation than the unidirectional laminate. Furthermore, because these specimens do not have the viscoelastic material interrupting their ply interfaces, they should have higher laminate strength properties than both the generally damped and optimally damped specimens.

2.3.2 Generally Damped Specimens

The generally damped strategy equips laminates with strips of damping material located at the three ply interfaces symmetric about the laminate midplane. The viscoelastic material

was dispersed with one-half inch spacing between the strips in a checkerboard pattern through the laminate height as displayed in Figure 2-1. Spacing between damping strips allows for both damping enhancement and lamina interaction to occur simultaneously at an interface; ideally this method will achieve the desired improvements in damping with only a minimal reduction in laminate strength.

2.3.3 Optimally Damped Specimens

In the design of the optimally damped specimens, internal energies were removed according to the mode of vibration with which they were associated. For the clamped-free arrangement, the percentage of total system energy associated with a mode generally decreases as the mode number increases. This energy per mode relation mandates that the energy dissipation associated with the first two modes is of larger magnitude than the dissipation of the higher modes. Optimally damped specimens were equipped with damping material at selected positions along their length axes to facilitate the dissipation of energies associated with the first two modes of vibration. The optimally positioned viscoelastic material also serves to dissipate the energies of higher vibration modes.

These “best” locations of the viscoelastic strips were determined by observing the methods in which energy is stored and dissipated within a Bernoulli-Euler beam model. The amount of vertical displacement is essential to the beam model’s internal energy storage mechanism due to the shear distribution along its length. Distribution of shear along the beam specimen will determine the amount of work that can be performed as the system transitions from an initial, deformed configuration to a final undeformed position as displayed in Figure 2-2. The beam specimen is geometrically designated using the variables $x \equiv$ independent spatial variable, $y \equiv$ neutral axis vertical displacement, and $b \equiv$ beam width.

A free-body diagram for a beam element, of mass m_e and length Δx , is shown in Figure 2-3 with the associated shear forces, V , and bending moments, M . It is assumed that the

shear forces acting within the beam have a much greater effect upon the system dynamics than the bending moments. This allows the bending moments to be neglected in the determination of the internal energies.

It is desirable to determine the energy dissipated within a beam specimen for a selected mode of vibration. Energy lost within a non-conservative beam system is accounted for via shear forces acting upon an arbitrary beam element in motion.

As the beam oscillates through its range of motion, the balance of energy is determined by investigating the kinetic, potential and dissipative energy mechanisms within the beam. The potential energy stored, W_{pot} , is computed as the product of a vertical displacement, y_v , and the beam element shear force summation. A vertical displacement accounts for the difference in position of the beam element for the two beam positions in question. This displacement is independent of the path the beam element travels to arrive at the new position. The rate of energy dissipation, \dot{W}_{dis} , is a product of the shear forces on the beam element and a vertical velocity, y_t , of the beam element. Equations (2-1) and (2-2) are expressions for the potential energy stored and the rate energy is dissipated in a beam element respectively. Note the displacement and velocity terms in the energy equations are negative, this is a result of the direction of deformation arbitrarily selected in Figure 2-2 and

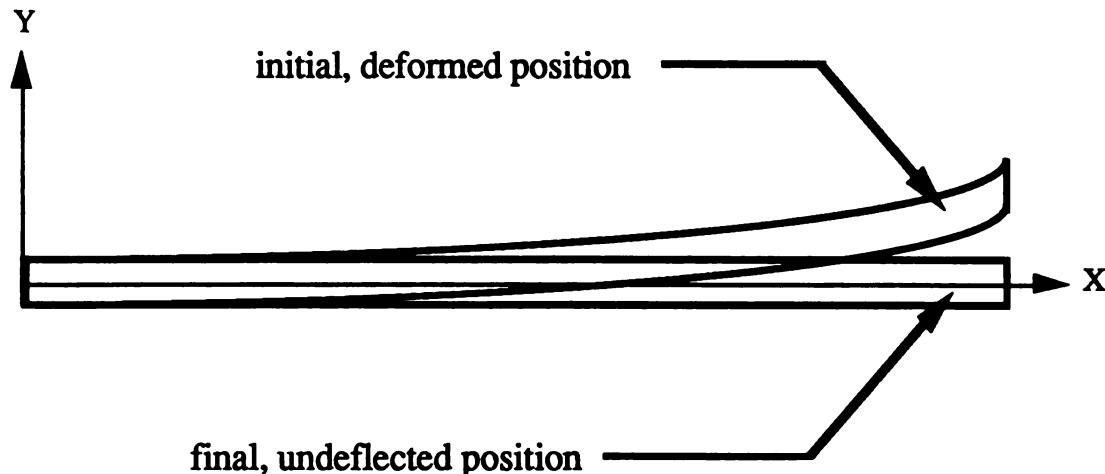


Figure 2-2 Beam configurations for energy analysis.

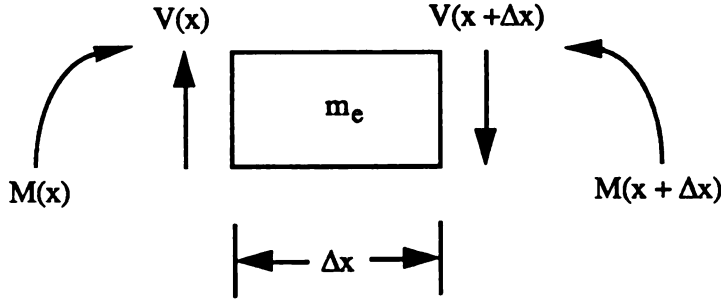


Figure 2-3: Beam Element Free Body Diagram

assigning the y -axis as positive in the upward direction.

$$[V(x) - V(x + \Delta x)] \cdot (-y_v) = \Delta W_{\text{pot}} \quad (2-1)$$

$$[V(x) - V(x + \Delta x)] \cdot (-y_t) = \Delta \dot{W}_{\text{dis}} \quad (2-2)$$

Dividing both energy equations by the length of the beam element and taking the limit as the beam element becomes infinitesimally small we obtain differential equations relating the change in shear to the differential energy components.

$$\frac{\partial V(x)}{\partial x} \cdot (y_v) = \frac{\partial W_{\text{pot}}}{\partial x} \quad (2-3)$$

$$\frac{\partial V(x)}{\partial x} \cdot (y_t) = \frac{\partial \dot{W}_{\text{dis}}}{\partial x} \quad (2-4)$$

The subscripts v and t , indicative of the virtual displacement and virtual velocity respectively, will be removed to simplify the notation of subsequent equations.

Recall that the shear force, in general, is composed of two components. One component is related to the stiffness of the beam and is proportional to the third spatial derivative of the displacement term. This component is indicative of the potential energy stored in the beam element. The other component is related to the damping of the beam and is proportional to the time rate of change of the third spatial derivative. This component is indicative of the

rate at which energy is being dissipated within the beam element. The expressions that result are:

$$EI y_{xxxx} y \, dx = dW_{pot} \quad (2-5)$$

$$BI y_{xxxx} y_t \, dx = d\dot{W}_{dis} \quad (2-6)$$

Two integrations by parts on the left hand sides of the fourth order equations above produce the energy equations, integrated along the beam of arbitrary length, L , which account for the energy stored via potential energy, (2-7), and the rate of energy dissipation, (2-8).

$$W_{pot} = EI \left\{ \left[y_{xxx} \cdot y \right]_0^L + \left[y_x \cdot y_{xx} \right]_0^L + \int_0^L (y_{xx})^2 \, dx \right\} \quad (2-7)$$

$$\dot{W}_{dis} = BI \left\{ \left[y_{xxx} \cdot y_t \right]_0^L + \left[y_{xt} \cdot y_{xxt} \right]_0^L + \int_0^L (y_{xxt})^2 \, dx \right\} \quad (2-8)$$

The first two terms on the right hand sides of the above equations represent the boundary conditions for the beam specimen. End conditions for the clamped-free beam arrangement are listed in (2-9). The clamped-free boundary conditions cause the first two terms on the right hand sides of the above equations to be zero producing the desired integral relations, (2-10) and (2-11), which indicate the amount of energy stored internally within a clamped-free beam as potential energy and the rate of energy dissipation, respectively.

The damping material was placed at locations where the bending moments of the first

Clamped end:

$$y(0) = 0$$

$$y_x(0) = 0$$

Free end:

$$y_{xx}(L) = 0$$

$$y_{xxx}(L) = 0$$

(2-9)

$$W_{pot} = EI \int_0^L (y_{xx})^2 \, dx \quad (2-10)$$

$$\dot{W}_{dis} = EI \int_0^L (y_{xxt})^2 \, dx \quad (2-11)$$

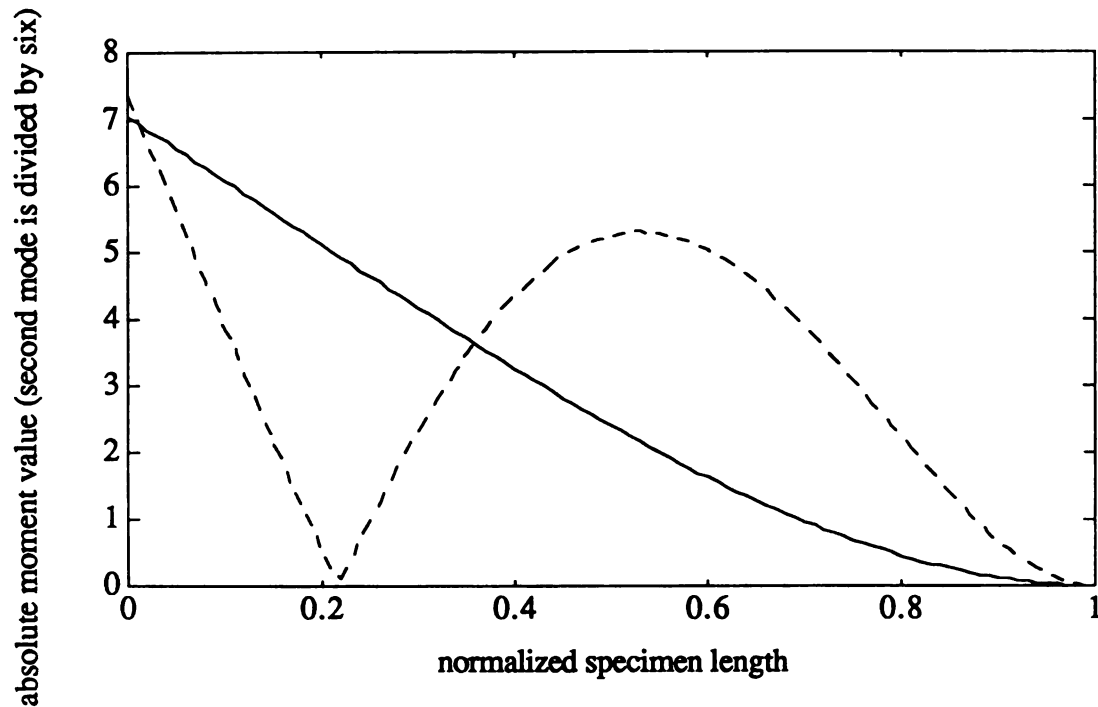


Figure 2-4 Optimal Damping Strategy.

two modes of vibration are at maximum levels. Such placement of the damping material at positions along the specimen having large moments allows the strips to maximize their internal damping capabilities with minimal strength reduction penalties. A plot of the bending moment versus the normalized beam length was generated to assist the determination of regions where large moments exist. Moment values were obtained by evaluating the second spatial derivative of the equivalent eigenfunction solution, $\Phi_i(x)$; the equivalent eigenfunction solution is developed in the following chapter.

Figure 2-4 displays the absolute moment magnitude versus normalized beam length for the first and second modes of vibration. Moment values for the first mode are significantly lower in magnitude than those of the second mode. To aid the comparison of mode participation, the imbalance in magnitude was offset by dividing the second mode magnitudes by a factor of six. Scaling of the second mode is used to interpret the general trends associated with the moment values and normalized beam length positions. Inspection

<u>Normalized Position</u>	<u>Mode Damped</u>
$0.325 \leq x \leq 0.350$	1 st
$0.450 \leq x \leq 0.475$	2 nd
$0.525 \leq x \leq 0.550$	2 nd
$0.650 \leq x \leq 0.675$	1 st

Table 2-1: Position of optimal damping strips.

of the traces indicated positions of large moments for the second mode correspond to minimum moment locations for the first mode. This may be attributed to the orthogonality condition discussed latter. This poses the problem that a strip of damping material may be designated to dissipate the energies of either the first or second mode, but not both. Results of Figure 2-4 indicate first mode damping is best attained by positioning viscoelastic material near the clamped end and second mode damping is achieved by locating the viscoelastic material at the specimen mid-length. These predictions are verified in Sun et al [24].

To preserve laminate strength properties, a minimal number of damping strips were used in the optimally damped specimens. Two strips were allotted for both the first and second modes. The four strips were positioned symmetric to the specimen mid-length. Damping material was not positioned at the specimens ends because maximum laminate strength is needed in this region to support the substantial moments a clamped-free specimen experiences during static loading. These regions, termed “end regions”, were designated in the normalized length units as: $0 \leq x \leq 0.25$ and $0.75 \leq x \leq 1.0$. Locations chosen for the damping material and the mode from which they dissipate energy are listed in Table 2-1. Selection of the optimal damping strip locations was determined using a trace that was not an exact representation of clamped-free beam dynamics.

The rate of energy dissipation per damping strip for a given mode is quantified via the equation listed below. Equation (2-12) is integrated across the damping strip’s normalized width. The viscoelastic damping term is assigned a large value, corresponding to the

dimensionless damping of 0.025, when equation (2-12) is used to quantify the energy dissipation associated with the strips of viscoelastic material.

$$\dot{W}_{dis} = BI \int_x^{x+\Delta x} (\Phi_{i,xx})^2 dx \quad (2-12)$$

3.0 DEVELOPMENT OF THE CANTILEVER BEAM MODEL

A Bernoulli-Euler beam model was used to predict the dynamic response of a clamped-free composite beam. The generic Bernoulli-Euler beam equation was derived such that a frequency domain transfer function relating the displacement of the clamped end to the free end could be developed. Damping parameter values were assigned to correspond to the three methods of internal damping and the two layup geometries.

3.1 Bernoulli-Euler Model

Certain assumptions and constraints must be applied to the beam system to assure the validity of the Bernoulli-Euler beam model. It is assumed that both the radius of curvature of the deflected beam is large relative to its thickness and that beam cross sections, which are oriented perpendicular to the neutral axis prior to bending, remain plane during flexure. Since the Bernoulli-Euler model is most accurate at low excitation frequencies, the experimental work was performed using a random excitation signal between 0 Hz and 800 Hz. This excitation bandwidth contains the first four natural frequencies for the eight ply, clamped-free laminate specimens.

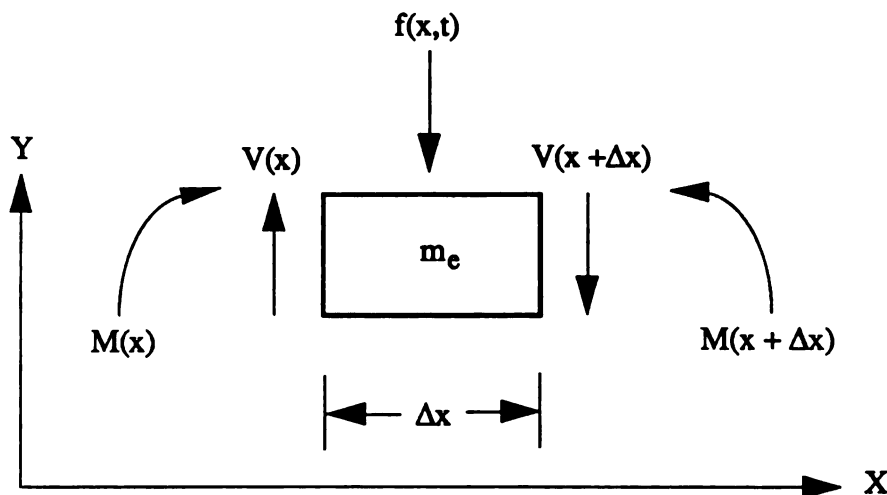


Figure 3-1: Differential Beam Element

The differential beam element free body diagram of Figure 3-1 is used to display the bending moments, shear forces, and applied loadings. The bending moment and shear force relations are applied to establish equations (3-1) and (3-2). These initial equations are combined to produce the shear-moment relation of equation (3-3).

$$M(x,t) = EIy_{xx} + BIy_{xxt} \quad (3-1)$$

$$V(x,t) = \frac{-\partial M(x,t)}{\partial x} \quad (3-2)$$

$$V(x,t) = -[EIy_{xxx} + BIy_{xxtt}] \quad (3-3)$$

Evaluation of the shear forces acting upon the differential beam element yields equation (3-4) and a force summation leads to equation (3-5). Equation (3-5) contains the specimen density, ρ , and the specimen cross sectional area, a .

$$V(x + \Delta x, t) = V(x, t) + \frac{\partial V}{\partial x} \cdot \Delta x + 0(\Delta x^2) \quad (3-4)$$

$$\left[\frac{\partial V(x,t)}{\partial x} \cdot \Delta x + V(x,t) \right] - V(x,t) + f(x,t) \cdot \Delta x = -(\rho a)y_{tt} \Delta x \quad (3-5)$$

Addition of the two shear force terms on the left hand side of equation (3-5) reduces it to a three-term equation (when higher order terms are neglected) in which each term includes the differential beam element length. Dividing by the element length and taking the limit as $\Delta x \rightarrow 0$ produces the general Bernoulli-Euler equation of motion presented in equation (3-6). According to the sign convention shown in Figure 3-1, beam displacement is positive in the upward direction. The force summation assumes downward forces are positive. The externally applied distributed load, $f(x,t)$, is in the positive force direction and will result in a negative vertical displacement of the differential beam element and thus a negative beam element acceleration. This negative acceleration is accounted for on the right hand side of equation (3-5).

$$[EIy_{xxxx} + BIy_{xxxx}] + f(x,t) = -(\rho a)y_{xx} \quad (3-6)$$

The equation of motion for the unloaded Bernoulli-Euler beam model is therefore given by equation (3-7).

$$[EIy_{xxxx} + BIy_{xxxx}] + (\rho a)y_{xx} = 0 \quad (3-7)$$

3.2 Boundary Conditions

The experimental procedure introduced a random wide band displacement input into the clamped-free specimen via a vibration exciter. This system driving input located at the clamped end was characterized by the general time function, $u(t)$, and is represented by the clamped-free time varying boundary conditions.

<u>Clamped:</u> $y(0,t) = u(t)$ $y_x(0,t) = 0$	<u>Free:</u> $y_{xx}(1,t) = 0$ $y_{xxx}(1,t) = 0$	(3-8)
--	---	-------

Note that henceforth x is considered to be the dimensionless length variable and the requisite scaling is applied.

The random input motion at the clamped end causes the boundary conditions to become non-homogeneous. A variable transformation, (3-9), is used to obtain a partial differential equation with homogeneous boundary conditions, equation (3-10).

$$y(x,t) = z(x,t) + u(t) \quad (3-9)$$

$$\frac{1}{L^4} [EIz_{xxxx} + BIz_{xxxx}] + (\rho a) [z_{xx}(x,t) + \ddot{u}(t)] = 0 \quad (3-10)$$

3.3 Eigenfunction Solution

The separation of variables technique is used to develop an eigenfunction solution describing the displacement of the resulting beam model. The transformed displacement

term, $z(x,t)$, is separated into its spatial and time domain components according to equation (3-11).

$$z(x,t) = W(x) \cdot e^{st} \quad (3-11)$$

The eigenfunction solution is obtained by solving the homogeneous portion of the system governing equation. The homogeneous solution is acquired by equating the force input $u(t)$ to zero. The spatial and time derivatives of the variable separation equation are incorporated into the now homogeneous equation resulting in equation (3-12).

$$EI \cdot W_{xxxx} e^{st} + BI \cdot W_{xxx} s e^{st} + (\rho a) L^4 W(x) s^2 e^{st} = 0 \quad (3-12)$$

Dividing out the time domain exponential terms and consolidating the terms associated with the fourth spatial derivative of the separated displacement variable, $W_{xxxx}(x)$, one obtains a simplified form of the above relation, the general displacement solution, in equation (3-13).

$$W_{xxxx} - \lambda^4 W(x) = 0 \quad (3-13)$$

$$\lambda^4 = - \left[\frac{\rho a L^4 s^2}{EI + BIs} \right] \quad (3-14)$$

The general displacement written below is the solution of a homogeneous, fourth order differential equation. Expressions will be determined to obtain values for the constants C_i .

$$W(x) = C_1 e^{\lambda x} + C_2 e^{-\lambda x} + C_3 e^{j\lambda x} + C_4 e^{-j\lambda x} \quad (3-15)$$

The first three spatial derivatives of the general displacement solution yield three new relations. The transformed boundary conditions are then applied to the spatial derivative relations to obtain homogeneous equations in terms of the constants C_i . These homogeneous equations have been consolidated into a concise matrix form and displayed in equation (3-16).

$$\begin{bmatrix} 1 & 1 & 1 & 1 \\ \lambda & -\lambda & j\lambda & -j\lambda \\ \lambda^2 e^\lambda & \lambda^2 e^{-\lambda} & -\lambda^2 e^{j\lambda} & -\lambda^2 e^{-j\lambda} \\ \lambda^3 e^\lambda & -\lambda^3 e^{-\lambda} & -j\lambda^3 e^{j\lambda} & j\lambda^3 e^{-j\lambda} \end{bmatrix} \cdot \begin{bmatrix} C_1 \\ C_2 \\ C_3 \\ C_4 \end{bmatrix} = 0 \quad (3-16)$$

The above homogeneous matrix relation is rewritten in the abbreviated form to simplify the ensuing discussion.

$$[F][C_i] = 0 \quad (3-17)$$

When establishing values for the constants C_i , one wants to avoid the undesirable, trivial case when the constants are all equal to zero. This is precluded by stipulating that the determinant of matrix F be equated to zero. This requirement is given by

$$Det.[F] = 4 + e^{-(1+j)\lambda} + e^{(-1+j)\lambda} + e^{(1-j)\lambda} + e^{(1+j)\lambda} = 0 \quad (3-18)$$

Algebraic manipulation of (3-18) produces the general eigensolution from which an infinite number of mode specific eigenvalues, λ_i , can be obtained. The mathematical development to obtain the general eigensolution is shown in detail in Appendix A.

$$\cos(\lambda_i) \cdot \cosh(\lambda_i) = -1 \quad (3-19)$$

3.4 Eigenfunction Selection and Normalization of Constants

Eigenvalues are mode specific numbers used to represent the system's dynamics. The eigenvalues for the first five modes of vibration were computed by using the general eigensolution and the symbolic manipulation software package "Mathematica". Eigenvalues, truncated to the sixth decimal position, are listed in Table 3-1.

Determination of the eigenvalues became cumbersome as we moved away from the fundamental mode, ten or more decimal positions were not sufficient to obtain the eigenvalues for modes five through ten. Initially the eigenvalues were computed by using only four decimal positions for accuracy, this resulted in unacceptable errors of 7% for the

third mode and 121% for the fourth mode. The numerical precision was then increased to six decimal positions, with a large increase in computational time, which produced minimal truncation errors in the first four vibration modes as listed in Table 3-1. The resulting truncation error percentage is computed via the equation below. The “actual” term in the error equation is the value obtained when the truncated eigenvalue was substituted directly into the general eigensolution.

$$\% \text{ error} = \frac{-1 - (\text{actual})}{-1} \times 100 \quad (3-20)$$

An eigenfunction solution form that is equivalent to the general displacement solution is established next. This solution form is used to generate values for the constants C_i . An equivalent eigenfunction expansion is given below. It may be shown that the eigenfunctions are orthogonal, normal, and complete.

$$\Phi_i(x) = C_1 \cos(\lambda_i x) + C_2 \sin(\lambda_i x) + C_3 \cosh(\lambda_i x) + C_4 \sinh(\lambda_i x) \quad (3-21)$$

The transformed, homogeneous clamped-free boundary conditions written below are substituted in equation (3-21) to solve for the unknown constants. Note that spatial derivatives are signified with a prime.

<u>Homogeneous clamped:</u> $\Phi_i(0) = 0$ $\Phi'_i(0) = 0$	<u>Homogeneous free:</u> $\Phi''_i(1) = 0$ $\Phi'''_i(1) = 0$	(3-22)
--	---	--------

i	<u>truncated λ_i</u>	<u>actual</u>	<u>% error</u>
1	1.875000	-0.999983	0.0017
2	4.694096	-0.999739	0.0261
3	7.854760	-1.003305	0.3305
4	10.995541	-0.992099	0.7901
5	14.137169	-1.420000	41.9999

Table 3-1: Eigenvalues and truncation errors.

The combination of the homogeneous boundary conditions with the equivalent eigenfunction solution are listed below. The equivalent eigenfunction solution and its first derivative establish relationships which eliminate the constants C_3 and C_4 .

$$\Phi_{i(0)} = 0 = C_1 + 0 + C_3 + 0 \quad (3-23a)$$

$$\Phi'_{i(0)} = 0 = \lambda_i [0 + C_2 + 0 + C_4] \quad (3-23b)$$

$$\Phi''_{i(1)} = 0 = \lambda_i^2 [-C_1 \cos(\lambda_i) - C_2 \sin(\lambda_i) + C_3 \cosh(\lambda_i) + C_4 \sinh(\lambda_i)] \quad (3-23c)$$

$$\Phi'''_{i(1)} = 0 = \lambda_i^3 [C_1 \sin(\lambda_i) - C_2 \cos(\lambda_i) + C_3 \sinh(\lambda_i) + C_4 \cosh(\lambda_i)] \quad (3-23d)$$

Elimination of two constants simplifies equation (3-23) to a two-equation, two-unknown situation. The eigenvalue outside the brackets on the right hand side of the two remaining equations is divided out allowing the trigonometric terms to be equated to zero. This division of the eigenvalue shows the assumption that the eigenvalue does not equal zero and is greater than zero for all vibration modes. The remaining trigonometric expressions are consolidated into the following matrix form. Equating the determinant of the two by two matrix to zero confirms the previously stated eigensolution.

$$\begin{bmatrix} \cos(\lambda_i) + \cosh(\lambda_i) & \sin(\lambda_i) - \sinh(\lambda_i) \\ \sin(\lambda_i) - \sinh(\lambda_i) & \cos(\lambda_i) + \cosh(\lambda_i) \end{bmatrix} \cdot \begin{bmatrix} C_1 \\ C_2 \end{bmatrix} = 0 \quad (3-24)$$

The equivalent eigenfunction solution is used to select arbitrary values for the constants. Manipulation of equation (3-24) produces a relation from which mode specific, non-normalized values for the two remaining constants are obtained.

$$C_2 = -C_1 \left[\frac{\cos(\lambda_i) + \cosh(\lambda_i)}{\sin(\lambda_i) + \sinh(\lambda_i)} \right] \quad (3-25)$$

Non-normalized values for the constants are acquired by arbitrarily fixing the value of one constant and computing the value of the second constant. Non-normalized values for

C_2 over the first five modes were computed by fixing $C_1 = 1.0$ and substituting the eigenvalues into equation (3-25).

Normalization of constants consists of integrating the square of the equivalent function solution over the generalized beam length, $0 \leq x \leq 1$, as displayed in equation (3-26). Normalized values for C_1 and C_2 for each vibration mode are computed by using equation (3-27) and are listed in Appendix B.

$$\text{normal} = \int_0^1 \Phi_i(x) \cdot \Phi_i(x) dx \quad (3-26)$$

$$C_{1in} = \frac{C_{1i}}{\sqrt{\text{normal}}} \quad C_{2in} = \frac{C_{2i}}{\sqrt{\text{normal}}} \quad (3-27)$$

3.5 Solving for $z(x,t)$

Having specified the constants in the equivalent eigenfunction solution, one can now obtain a mode specific solution for the transformed beam displacement. The equivalent eigenfunction solution, $\Phi_i(x)$, can replace the general displacement solution, $W(x)$, in the variable separation. Since the equivalent eigenfunction solution is dependent upon the vibration mode in question, the exponential time domain term in the variable separation will be replaced by the mode participation term, $q_i(t)$. These substitutions are displayed below. The presence of the summation sign represents the most general form of any solution.

$$z(x,t) = \sum_i \Phi_i(x) \cdot q_i(t) \quad (3-28)$$

To make use of the beam transfer function model, information at both ends of the clamped-free beam must be specified. The clamped end displacement is provided via the system input term, whereas the free end data is obtained from the transformed displacement term that is measured at the free end's normalized position, $x=1$. The mode participation term is the only parameter that has yet to be specified.

The general equation of motion with the beam displacement described in the z-coordinate system is repeated below.

$$EIz_{xxxx} + BIz_{xxxx} + (\rho a)L^4[z_u(x, t) + \ddot{u}(t)] = 0 \quad (3-29)$$

Separation of the spatial and time domains of equation (3-28) are employed in the general equation of motion to transform it into a more usable form. It is evident in the variable description that q_i is a function of time and Φ_i is a spatial function. Thus their respective arguments, (t) and (x) will be neglected in the following derivation. Also, the subscript derivative notations t and x will be changed to the derivative descriptions $\frac{d}{dt}$ and $\frac{d}{dx}$ respectively.

$$EI \cdot \frac{\partial^4}{\partial x^4} \left[\sum_i \ddot{q}_i(t) \Phi_i(x) \right] + BI \cdot \frac{\partial^5}{\partial t \partial x^4} \left[\sum_i \ddot{q}_i(t) \Phi_i(x) \right] + (\rho a)L^4 \cdot \frac{\partial^2}{\partial t^2} \left[\sum_i \ddot{q}_i(t) \Phi_i(x) \right] + (\rho a)L^4 \ddot{u} = 0 \quad (3-30)$$

Enclosing the summation terms in the brackets and consolidating the partial derivatives with respect to x and t produces equation (3-31) shown below.

$$\sum_i \left[\left(EI q_i + BI \frac{dq_i}{dt} \right) \cdot \left(\frac{d^4 \Phi_i}{dx^4} \right) + (\rho a)L^4 \Phi_i \frac{d^2 q_i}{dt^2} \right] + (\rho a)L^4 \ddot{u} = 0 \quad (3-31)$$

Recalling that the eigenfunctions are a sum of sine, cosine, hyperbolic sine, and hyperbolic cosine, one will note the validity of equation (3-32) which is used to produce equation (3-33).

$$\frac{d^4 \Phi_i}{dx^4} - \lambda_i^4 \Phi_i(x) = 0 \quad [3-32]$$

$$\sum_i \left\{ \left[\lambda_i^4 \cdot \left(EI \cdot q_i + BI \cdot \frac{dq_i}{dt} \right) + \rho a L^4 \frac{d^2 q_i}{dt^2} \right] \Phi_i(x) \right\} + \rho a L^4 \ddot{u} = 0 \quad [3-33]$$

Recall that the notations d/dt and $(\dot{})$ both signify time derivatives. The different notations are used to facilitate the reader's understanding of the origin of that derivative. The d/dt derivative is for the mode participation parameter and the $(\dot{})$ is for the input description.

Eigenfunctions are selected as normal with a 2-norm of one. Orthogonality and completeness of the eigenfunction is stated in the condition of equation (3-34). Multiplication of equation (3-33) by the equivalent eigenfunction $\Phi_j(x)$ and integration over the length of the beam leads to equation (3-35).

$$\int_0^1 \Phi_i(x) \cdot \Phi_j(x) \cdot dx = \begin{cases} 0 & \text{for } i \neq j \\ 1 & \text{for } i = j \end{cases} \quad (3-34)$$

$$\lambda_i^4 \cdot \left(EI \cdot q_i + BI \cdot \frac{dq_i}{dt} \right) + \rho a L^4 \frac{d^2 q_i}{dt^2} + \rho a L^4 \ddot{u} \int_0^1 \Phi_i(x) dx = 0 \quad (3-35)$$

The $\Phi_i(x)$ term inside the integral is equivalent to the $\Phi_j(x)$ according to (3-34). A notation simplifying relation is substituted into equation (3-35) to obtain equation (3-37).

$$-P_i = \int_0^1 \Phi_i(x) dx \quad (3-36)$$

$$\ddot{u} = \frac{1}{\rho a L^4 P_i} \left[q_i (\lambda_i^4 EI) + \frac{dq_i}{dt} (\lambda_i^4 BI) + \rho a L^4 \frac{d^2 q_i}{dt^2} \right] \quad (3-37)$$

In the development of the transfer function in the following section, a relation for the mode participation parameter in the frequency domain is needed. This requirement is fulfilled by taking the Laplace transform of (3-37) and consolidating the resulting $Q(s)$ terms to produce equation (3-38).

$$Q_i(s) = \frac{s^2 \cdot P_i \cdot \rho a L^4 \cdot U(s)}{[(\lambda_i^4 EI) + s \cdot (\lambda_i^4 BI) + s^2 \cdot \rho a L^4]} \quad (3-38)$$

3.6 Transfer Function Solution Process

The transfer function relating the displacement of the clamped end to the free end is now developed. A complete and accurate transfer function includes an infinite summation of the individual transfer functions for each mode of vibration. The analysis at hand will determine an approximate transfer function based upon the first four modes of vibration since this is the range over which the eigenvalues were most accurately computed.

The relationship in the frequency domain between the mode participation factor, $Q_i(s)$, and the system input, $U(s)$, are necessary in developing the transfer function. This relationship is termed the beam response function, $T_i(s)$. This relation provides the beam's response at the free end due to a given input for a selected mode.

$$T_i(s) = \frac{Q_i(s)}{U(s)} \quad (3-39)$$

The relation of the free end displacement (output) to the clamped end displacement (input) in the Laplace domain is:

$$Y(1,s) = \sum_i [\Phi_i(1) \cdot Q_i(s)] + U(s) \quad (3-40)$$

Substitution of $Q_i(s)$ and moving the $U(s)$ term to the left hand side of the equation produces a transfer function, $H(s)$.

$$H(s) = \frac{Y(1,s)}{U(s)} = \sum_i [\Phi_i(1) \cdot T_i(s)] + 1 \quad (3-41)$$

The $T_i(s)$ term is expanded using equations (3-38) and (3-39) to obtain the form of the following transfer function equation, which is used to generate the theoretical magnitude and phase angle plots and define the modal response relation.

$$H_i(s) = \frac{\Phi_i(1) \cdot P_i \cdot (\rho a L^4) s^2}{[(\lambda_i^4 EI) + s \cdot (\lambda_i^4 BI) + s^2 \cdot \rho a L^4]} \quad (3-42)$$

3.7 Modal Parameter Values

Material properties and beam dimensions need to be established so magnitude and phase angle plots for select damping values can be generated as well as a definition of the modal damping relation. Material properties of the 3M graphite/epoxy “Scotchply” material will be used. Specimen beam dimensions are assigned as 28cm x 2.54cm x 0.112cm. Pertinent material properties and specimen geometry values are listed in Appendix B. Values for the damping parameter were selected to correspond to the dimensionless damping ratio, ξ , typical of carbon/epoxy composite laminates. Appendix C shows the development of the dimensionless damping ratio.

The transfer function equation was combined with the material properties to produce the analytical frequency response for clamped-free laminates. Calculations were performed in using the MATLAB software package. Transfer function responses were developed for five damping values. Magnitude versus frequency and phase angle versus frequency plots were also generated. Magnitude and phase angle responses were evaluated across the frequency band spanning 1×10^{-3} Hz to 1×10^8 Hz, dynamic activity was noted in the 1 Hz to 1000 Hz frequency band. This was consistent with experimental observations.

3.8 Analysis of Results

Plots comparing the one mode, two mode, three mode, and four mode magnitude and phase angle approximations of the transfer function for varying values of the dimensionless

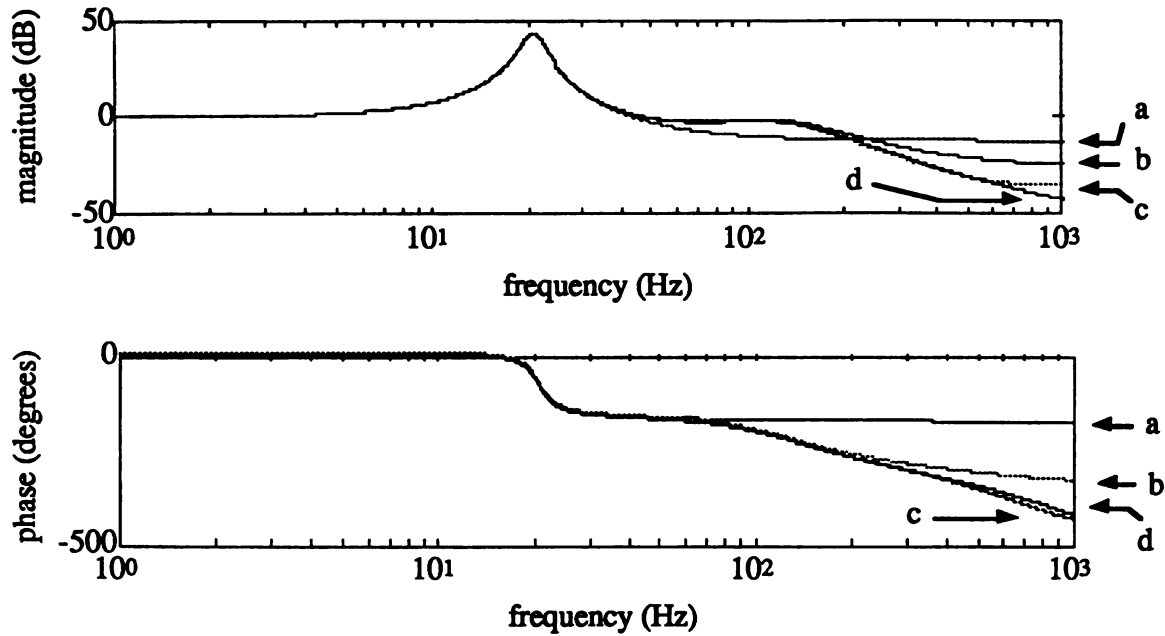


Figure 3-2: Magnitude and phase angle approximations for the transfer function and dimensionless damping equal to 0.025. In the traces, 'a' indicates the one mode approximation, 'b' indicates the two mode approximation, 'c' indicates the three mode approximation, and 'd' indicates the four mode approximation.

damping parameter are located in Appendix D. Magnitude and phase angles for a dimensionless damping parameter equal to 0.025 are displayed in Figure 3-2. Magnitude plots for varying dimensionless damping parameters exhibit an overall decrease in magnitude for increased damping.

4.0 EXPERIMENTAL MATERIALS

4.1 Experimental Materials

The crossply and unidirectional beam specimens were fabricated using materials donated by the 3M Corporation. Beam laminates were constructed from aerospace grade carbon/epoxy prepreg. This continuous filament prepreg is termed “Scotchply” SP-319 by its producers. When properly cured, this thermoset material has a fiber volume fraction of 55%, a tensile strength of 245 kpsi and a density of 1.55 g/cc. The internal damping of the carbon/epoxy laminates was enhanced via the introduction of strips of viscoelastic damping material laid at the interface region between the laminate’s plys as shown in Chapter 2. The viscoelastic material was designed to suppress internal laminate vibrations by dissipation of mechanical energies. This viscoelastic material, also donated by the 3M Corporation, is assigned the reference number SJ 2015X type 1202 and referenced by the trade name “Scotchdamp”.

4.1.1 Material Aging

In handling prepreg materials one must consider their individualized storage temperatures and shelf lives. The shelf life of the Scotchdamp viscoelastic material is of minimal concern since it is a stable thermoplastic. Thermoplastic materials are composites that can be repeatedly heated, formed, and cooled without significant losses to their mechanical properties. On the other hand, the carbon/epoxy prepreg is a thermoset material whose shelf life and storage temperature is of paramount concern. A thermoset prepreg becomes a laminate after being exposed to the elevated heat and pressure of the cure cycle. A laminate will meet its stated mechanical properties if the cure process is performed within the designated shelf life provided the prepreg has been stored below its specified storage temperature. A thermoset material will “age” quicker when stored at temperatures that exceed their individualized storage temperature. An aged prepreg will suffer a lack of

tackiness during fabrication and produce a laminate possessing reduced mechanical properties.

Estimation of a prepreg's useful shelf life, or time during which it retains its tackiness, is essential to both fabrication and research. A prepreg is a single layer of fibers embedded in a solution of partially cured monomers. Polymers are dissolved into solvents forming solutions. Storing polymers in the solution form is essential to the prepreg fabrication process in that the polymer evaporation rate decreases, the polymer solubility is improved, and the polymer is stored and processed in a less volatile state [25]. Below a temperature unique to a monomer, termed the storage temperature, monomers are prevented from reacting with one another. This absence of monomer interaction disrupts the solvent integrity and causes a reduction in prepreg tackiness. This stabilizing temperature is provided by the prepreg supplier. The amount of time a prepreg is stored at temperatures exceeding its stabilizing temperature, termed "out time", will cause the prepreg to lose its tackiness, and material aging will occur. Loss of tackiness creates difficulties in the layup of laminae during fabrication in that prepreg plies do not readily adhere to one another. Sanjana [26] cited the loss of prepreg tackiness as the critical parameter in determining the aging of prepreg.

Akay [27] performed an assortment of mechanical property tests on unidirectional, 63% fiber volume fraction carbon/epoxy specimens having out times ranging from 100 hours to 930 hours. The battery of tests, which included interlaminar shear and flexural modulus, do not show a degradation of mechanical properties over the range of out times studied. The same analysis was performed using specimens immersed in 70°C water for twenty one days to evaluate the combination of out time and hygrothermal effects. In addition to the expected reduction in mechanical properties for the wetted specimens, the test results showed that out time did not have an effect upon lowering the mechanical properties for a hygrothermally treated specimen. As noted by Akay, the only effect out time had upon mechanical

properties was an increase in the glass transition temperature by approximately 5°C for out times of forty days.

4.1.2 Aging Effects Upon Specimens

The aerospace grade SP-319 carbon/epoxy prepreg must be stored at temperatures below 40°F to prevent aging and retain material tackiness. The thermoset prepreg used in this study was packaged in solid carbon dioxide to assure its material temperature remained below its storage temperature during shipping; transportation delays caused the dry ice to sublimate, exposing the prepreg to approximately 75°F temperatures for a period of time not exceeding three days. According to the results stated in the Akay study, a prepreg out time of three days will not affect the mechanical properties of the carbon/epoxy laminate used to produce the beam specimens.

4.2 Specimen Fabrication

Unidirectional and crossply beam laminates were fabricated with the assistance of the Composite Materials and Structures Center at Michigan State University. The carbon/epoxy prepreg layup was autoclave cured according to the cure methods outlined by the material supplier. Viscoelastic damping material used in the general and optimally damped specimens was added at the prepreg interfaces during the lay-up process and subjected to the elevated pressures and temperatures of the curing cycle.

4.2.1 Lay-up Orientations and Damping Material Locations

Tests were performed on six laminates that varied in the amount of viscoelastic damping material and orientation of reinforcing fibers as discussed in Chapter 2. Specimens 2.54 cm in width and 28 cm in length were cut from laminates approximately 5.25 inches by 12 inches in size using a diamond blade circular saw. They were cut from the middle portion of the plates to reduce the effects of edge discontinuities that arise in fabrication.

The decision to enhance material damping by placing discontinuous strips of viscoelastic material at ply interfaces distinguishes this study from its predecessors. Previous studies

have considered continuous layers of viscoelastic material covering interface surface areas. A continuous layer of viscoelastic material at an interface will undoubtedly produce large amounts of material damping but at the expense of reductions in laminate strength. Laminate strength is reduced when intimate attachment between neighboring plies is prohibited by the inclusion of damping material.

An arrangement strategy for the viscoelastic damping strips that received consideration for the current study specified two-quarter-inch wide strips of damping material be laid parallel along the length of the beam specimen. This strip arrangement may be advantageous in the analysis of experimental data because the material damping property is continuous along the length of the specimen. Continuous damping is desirable for analysis since the damping characteristic is assumed to be constant throughout the specimen. This arrangement was not used due to the difficulties associated in fabricating specimens of repeatable quality. A large potential for error exists when attempting to accurately position quarter inch wide strips in a parallel fashion across a one foot laminate and machining inch wide beam specimens with consistent damping strip orientation. Although the parallel arrangement of the damping strips may be desirable from an analytical standpoint, the associated fabrication limitations were deemed too severe.

The damping strip arrangement used for the optimal and general damping strategies has one-half-inch-wide viscoelastic strips positioned perpendicular to the length axis. This ensures a simple and highly repeatable specimen fabrication process. The discontinuous damping arrangement at the interior interfaces is not consistent with the analytical model that was constructed under the assumption of constant damping throughout the material. However, one may think of the resulting analytical model of the dynamics as the result of applying the method of assumed modes. Although this discontinuous arrangement of the damping strips has shortcomings, the ability to sustain the production of specimens with consistent location of the damping material was considered to be of greater importance.

4.2.2 Fabrication Equipment

The prepreg laminates were cured under elevated temperature, 120°C, and pressure, 620 kPa, in an autoclave. A concern arose that the elevated temperature and pressure of the cure cycle would have an adverse effect upon the viscoelastic property of the Scotchdamp material causing a reduction in its energy dissipation capabilities. Consultation with a 3M representative provided assurance that the Scotchdamp would not suffer permanent material property degradation. The material retains its viscoelastic damping capabilities to a temperature of 180°C. The 3M representative advised that Scotchdamp will become less viscous at the temperatures and pressures of the cure cycle and will slowly flow within the laminate [28]. Upon laminate cooling, the viscoelastic material will solidify and return to its original position. Such flow of the viscoelastic material during the cure cycle initiated a concern that the desired damping strategies could be altered. Upon visual inspection of the laminate surfaces it was noted that the position of the damping strips remained unchanged. This inspection was performed visually because the damping strips "read through" to the laminate's surface.

4.2.3 Fabrication Methods

The unidirectional, continuous roll of prepreg was wound on a spool and stored in a freezer to guard against material aging. The five and a quarter inch wide prepreg roll was cut to make the unidirectional and crossply laminates. Unidirectional laminates were created by stacking eight layers of prepreg upon one another; extreme care was used to ensure that the fibers of adjoining plies were oriented parallel to one another so as to maintain the integrity of the unidirectional laminate. Crossply specimens required four plies sized 5.25 in by 12 in to produce the 0° layers and twelve 5.25 in square plies to make the four 90° layers. Three square plies were needed to compose each 90° ply. Proper positioning of the Scotchdamp material was assured by employing a wooden, rectangular fixture.

Two layers of prepreg were rolled after stacking to improve the degree of interfacial contact and to remove air trapped at the interface. The direction of rolling was consistent with the fiber orientation of the top prepreg layer to avoid fiber damage by exerting lateral loads upon the fibers. Latex gloves were worn during the layup process to prevent body contact with the carbon/epoxy prepreg or the viscoelastic damping material. Gloves are essential in protecting the prepreg from body oils and perspiration, which produce voids and delamination in a laminate. The necessity of wearing gloves is paramount in the process of positioning the damping strips on the prepreg. Force is exerted upon the strips with one's fingers to remove entrapped air and to improve the contact between the prepreg and viscoelastic materials. If gloves were not worn, one's fingers would come into contact with the exposed surface of the carbon/epoxy prepreg. Prior to the laying out of the damping strips (when the interface surface is contacted by the latex gloves) the fingertip areas of the gloves were rinsed with acetone to remove unwanted foreign particles that might have settled there during the fabrication process.

4.2.4 Problems Unique To Fabrication

The viscoelastic damping material is adhered to a backing that improves its handling. This backing material was removed after the damping strips were laid out at the laminate interface. Ideally the backing peels away from the damping material without incident. Occasionally fragments of the backing remain adhered to the damping material and/or the prepreg. Although very small in size, these remnants must be removed otherwise a void or delamination may occur in the laminate. Backing remnants are best removed via light scraping of the prepreg with a scalpel. Such scraping can induce local disruptions of fiber orientation or sever previously continuous carbon fibers. Disorientation and cutting of fibers are undesirable occurrences, but necessary to elude the possibility of voids and delamination since the presence of the latter has a more pronounced effect upon enhancing laminate damping characteristics.

5.0 EXPERIMENTAL PROCESS

The forced vibration method was selected as the experimental means to compare the damping characteristics of the composite specimens. To assure that the measured damping was only indicative of material damping, the response of the specimen was measured with apparatus selected and positioned so as not to violate the assumptions of the Bernoulli-Euler beam model. Linearity of the laminate specimens and the sensors was verified experimentally for the operating conditions of interest.

5.1 Experimental Set-up

The experimental equipment was arranged as depicted in Figure 5-1. The forcing signal driving the clamped-free specimen originated as a random voltage output with specified frequency content from a programmable source on a Hewlett-Packard (HP) signal analyzer. This voltage signal was amplified using the Brüel & Kjær (B&K) power amplifier prior to introduction into the B&K Vibration Exciter. The exciter transformed the current signal into a vertical displacement. Random displacement of the clamped end was used to stimulate the dynamics of the beam specimen over the specified frequency range. Measurements of the vertical displacement at the free end were made using a B&K Laser Displacement/Velocity Transducer. The clamped end vertical displacement was measured by using a non-contacting Kaman Measuring Systems (KMS) eddy current sensor. Measured displacement data were collected using a National Instruments data acquisition board and a Macintosh IIfx computer. The software package LabVIEW was used to create a virtual instrument to aid in this task. Both the rate of data collection and the number of samples collected were controlled, and the measurements were automatically stored in a file for subsequent processing.

5.2 Equipment descriptions

Random displacement at the clamped end was generated by using the programmable source from a HP 35660A Dynamic Signal Analyzer and amplified by means of a B&K

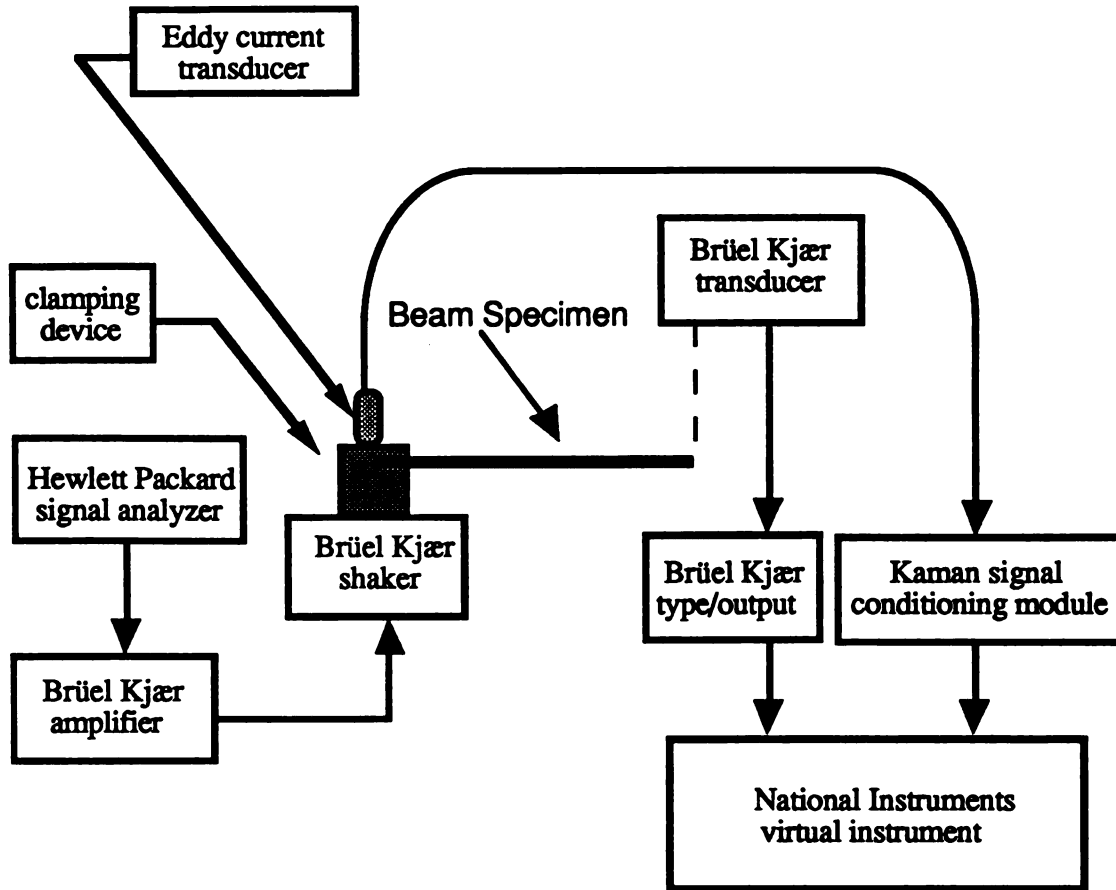


Figure 5-2: Experimental Set-up

Power Amplifier Type 2706. When using the HP analyzer as a signal generator, the type, magnitude level, and frequency span of the source output are selected by the user. The amplifier is beneficial in the start-up experimental process in that it allows for simple and instantaneous changes of the input signal magnitude, which alters the peak to peak free end displacement. The ability to change and monitor the free end displacement is important when aerodynamic damping is considered and a minimum free end amplitude with acceptable dynamic stimulation is sought.

The amplified signal was introduced into a B&K Type 4809 Vibration Exciter. This vibration exciter transfers the current input signal into a vertical displacement. Beam specimens are rigidly mounted onto the shaker device via an aluminum clamping

mechanism. The aluminum clamping device was designed to distribute an equal force across the laminate while maintaining a minimal weight so as not to impede the performance of the shaker device. The vibration exciter has a bare table frequency range to 20 kHz. The acceleration capabilities of the vibration exciter are dependant upon the payload weight it is required to displace. The clamping device and specimen weigh approximately 130 g which equates to maximum acceleration levels of 246 m/g^2 (25 g), as stated in the B&K Vibration Exciter manual.

Displacements of the clamped end are measured using a non-contact proximity measuring device developed by KMS. The eddy current measuring system mensurates changes in displacement of the aluminum clamping device that is rigidly attached to the laminate specimen.

The B&K Type 3544 Laser Transducer is non-contacting and quantifies displacement with an accuracy to $10 \text{ }\mu\text{m}$ over a frequency span of 0.3 Hz to 20 kHz. The transducer uses a Helium-Neon laser to measure the velocity of a target surface; displacement values are obtained through an integration of the velocity signal. Velocity values are acquired by splitting the laser light into two beams: one of which is directed at the external target, and the other remains within the unit to serve as a reference beam. Integration of a velocity measurement of zero frequency yields a bias component in the displacement measurement. Removal of this displacement bias is addressed in the Data Manipulation section. Small pieces of retroreflective tape are adhered on the target surface to reflect the light beam back into the transducer where it heterodynes with the reference beam. Movement of the target induces a Doppler Frequency shift between the two light beams. This shift is converted into a voltage signal which is proportional to the velocity of the target.

The experiment was arranged such that the laser was positioned 25 cm above the retroreflective tape. This separation guaranteed that the laser was within its optimum operating distance.

A virtual instrument was designed to collect and organize voltage displacement signals on a Macintosh IIfx using the National Instruments LabVIEW 2.0 scientific software package. The data sampling rate and number of data sets sampled per test run were specified by modifying the front panel of the virtual instrument.

5.3 Excitation Method

Specimen excitation must stimulate the vibration modes under evaluation as well as provide meaningful displacement information. The forced vibration method was selected over the free vibration method for its wide band frequency input capabilities and the ease in control of the magnitude of the input signal, which is essential in regulating the free end displacement.

When used on a cantilever beam the forced vibration method has advantages over the free vibration method in that it allows for convenient adjustment of a specimen's dynamic response via selection of beam length as well as the input signal magnitude and frequency content. Further, the input signal magnitude is effortlessly varied allowing for direct control of the free end displacement in the clamped-free test arrangement. Ready regulation of the free end displacement is a necessity when one wishes to avoid system damping. The frequency span of the input signal is easily modified in the forced vibration method, which allows for control of the frequency content that excites the specimen. This is of importance when attempting to excite selected vibration modes.

In an attempt to excite the third and fourth vibration modes, the input band was centered about the natural frequency of the fourth mode. Such input should adequately stimulate the mode at the input frequency as well as all lower vibration modes.

5.4 Specimen Linearity

For small vibration displacements within undamaged polymer laminates, one can assume that the dynamic response is linear if the stiffness and damping are independent of

the displacement amplitude [29]. This statement regarding linearity of polymer laminates is verified by using a process in which peak to peak free end displacements are monitored for various known sinusoidal excitation signals. As shown in Table 5-1, peak to peak displacement vary by the same factor as input signal levels thus indicating the polymer composite laminates have a basically linear response. Data in Table 5-1 represents a sinusoidal input of 18 Hz, the fundamental natural frequency for the crossply-generally damped laminate used to perform the specimen linearity check. The linearity between specimen input and peak to peak free end displacement is also valid when the system sinusoidal excitation signals are increased to the natural frequencies of the second and third modes. System excitation of frequencies of the second and third modes revealed a weak coupling between the first two modes and between the first and third modes respectively.

5.5 System Damping

During evaluation of a specimen's damping capabilities it is essential to assure that the recorded damping values are only indicative of the energies dissipated by the material. Extraneous energy can be lost to the experimental apparatus and surroundings. This undesirable energy loss, termed "parasitic damping", inflates material damping values. Energy dissipated to the experimental equipment is termed "apparatus damping" while the energy lost to the surroundings as a result of the oscillatory beam motion is termed "aerodynamic damping". Parasitic damping is recognizable because it typically is non-linear. This non-linear characteristic of parasitic damping distinguishes it from the generally linear damping of an undamaged composite laminate.

<u>Input Level</u>	<u>Peak to Peak Displacement</u>
50 mV	0.4 mm
100 mV	0.8 mm
150 mV	1.2 mm
200 mV	1.6 mm
250 mV	1.9 mm

Table 5-1: Specimen Linearity

5.5.1 Apparatus Damping

Apparatus damping accounts for the energy lost to the constraining devices, motion sensing devices, and lead wire that may contact the specimen during testing. Energy loss associated with mounting accelerometers or strain gauges on the beam specimen was avoided through the use of non-contact displacement measuring transducers. Frictional damping accounts for energy lost at the interface between the clamping device and specimen. Clamping devices that have smaller stiffness values than that of the specimen will experience deformation in testing resulting in extraneous energy loss. Deformation losses increase with greater free end displacement.

5.5.2 Aerodynamic Damping

Aerodynamic damping accounts for vibrational energy losses from the specimen to the surrounding air. Aerodynamic damping is dependent upon specimen geometry and the free end displacement. The larger the free end displacement and beam surface area hindering the path of motion, the greater the amount of air the specimen is required to move as it oscillates. In general, the energy required to remove air from the specimen's path is the energy dissipated due to aerodynamic damping.

Aerodynamic damping is dependent upon the amplitude of the vibrating beam and the pressure of the ambient air. For a unidirectional carbon fiber reinforced plastic Adams and Bacon found that a linear relationship existed between aerodynamic damping and beam amplitude [30]. Results from Gibson and Plunkett indicate that the loss factor increases with increases in ambient pressure and beam amplitude [31].

Performing forced vibration cantilever beam experiments in a vacuum is one method that allows the assumption of negligible aerodynamic damping. A second method to minimize the effects of aerodynamic damping is to restrict free end peak to peak displacements to be less than the specimen thickness. Gibson stated that imposing such a constraint allows the assumption of negligible aerodynamic damping [29].

5.6 Input Displacement Content

The dynamic response for the clamped-free specimens was approximated using a four mode model. In order to evaluate the dynamic response associated with a vibration mode, that vibration mode needs to be adequately excited by the system input. Modes are activated when the frequency content of the displacement input has a noticeable magnitude at a mode's natural frequency. A noticeable magnitude is one which is distinguishable from the magnitude of the background noise.

The voltage output signal from the source on the signal analyzer was adjusted such that a desirable frequency band was attained. The natural frequencies for the first four vibration modes of the clamped-free specimens are less than 800 Hz. In an initial observation it was assumed that an excitation signal of 0 - 800 Hz would be sufficient to excite the first four modes. It was later noted that the dynamics of the B&K amplifier and vibration exciter have a 20 dB per decade roll-off and this signal roll-off results in only adequate stimulation of the first two modes. Input levels at the third and fourth mode natural frequencies were indistinguishable from that of the background noise.

Damping parameter values for the one mode, two mode-one damping parameter, and two mode-two damping parameter approximations were obtained using the aforesaid excitation signal. Experimental results indicated that modal damping did a better job predicting free end displacements than the assumed Bernoulli-Euler beam model. Henceforth we will be concerned predominantly with models assuming modal damping. Since the third and fourth vibration modes were not adequately stimulated, accurate assessments of the associated damping parameters was not obtained.

A second acquisition of experimental data was conducted from two specimens indicative of extremes in damping for structural materials. The pair of specimens were excited over a frequency band of ± 100 Hz about the natural frequency of their fourth vibration mode. Specimen excitation about the natural frequency of the highest mode of interest was

necessary to provide stimulation of the lower modes to be investigated. Values for damping parameters were computed for approximations including one, two, three, and four modes. Multiple parameters were used to numerate the damping value in the multi-mode approximations, for example three damping parameters were used in the three mode approximation. The specimen representing the highest damping was the crossply laminate equipped with the general damping strategy. Data for this specimen was compared to a representative monolithic material, aluminum 6061, machined to geometric dimensions identical to those of the composite specimens.

5.7 Specimen Quality

In experimental determination of material damping values, it is of paramount concern that specimens are not excited to a level that exceeds their maximum strain amplitude. When this limiting strain level is surpassed, permanent strain induced internal damage occurs within the laminate. This microscopic damage will produce significant increases in material damping values without noticeable losses in stiffness properties [32]. Internal strain damage was avoided by maintaining an excitation signal small enough so that the minimal free end amplitudes occurred. Also, specimens were only excited in the experimental set-up when calibration and test measurements were being recorded. System set-up and trial scenarios were preformed using laminates other than the experimental beam specimens.

6.0 EXPERIMENTAL RESULTS

6.1 Data Collection

Displacement information was collected using a virtual instrument as described above. A total of six data sets were accumulated for each test specimen. Three data sets comprised the calibration data group, used for scaling subsequent data, and three data sets constituted the actual test data group. A data set consisted of displacement measurements for both the laser and eddy current systems recorded over one second.

6.1.1 Sampling Rate

Two considerations influenced the rate at which the displacement information was sampled by the virtual instrument. The first concern applied to the accurate reproduction of the system's dynamics and the second to the ensuing mathematical post-processing of data sets. Dynamics of a system are best captured when data is sampled at a rate that is at least ten times faster than the highest frequency of concern. For an eight-ply clamped-free specimen this frequency of concern is the natural frequency of the fourth mode, approximately 550 Hz. Upon the completion of the collection process, data sets were mathematically processed to extract meaningful information regarding the dimensionless damping and natural frequency characteristics. In light of these concerns and recognizing the memory capacity and processing rates of a Macintosh IIfx, the system used to manipulate the data sets, displacement values were sampled at a rate of 4096 Hz for one second. This sampling rate was a minimum of seven times the rate of the largest frequency of concern. Test and calibration data consisted of two sets of 4096 entries; data was written and stored in two columns. A sampling period of one second was sufficient to capture the random dynamic trends of the cantilever specimens considered.

6.1.2 Sampling Process

As stated previously, clamped-end displacements were measured using a KMS eddy current sensor. In order to observe the full range of motion of the clamped end, the KMS

potentiometer gain was increased to levels that introduced a bias into its output signal. When a test specimen was clamped into the experimental set-up, three sets of displacement measurements were sampled for calibration purposes. The setup for this data set consisted of positioning both the B&K laser transducer and the eddy current sensor at the clamped end to measure the motion of the aluminum clamping device under random excitation. After gathering this data, the laser transducer was repositioned at the free end at which time three specimen test data sets were collected.

Since the gain for the Kaman system is highly sensitive, it was of great concern that the testing equipment not be disturbed (for example by bumping the table) during the sampling of calibration data and test data or during movement of the laser transducer.

6.2 Data Manipulation

In an effort to ascertain physically meaningful information from the displacement information, manipulation of the data sets was required. Post processing of data allowed for recognition and removal of bias components from both the laser and eddy current measuring systems and identification and optimization of parameters that yielded values for specimen damping and stiffness terms.

6.2.1 Laser Calibration

The HP Laser Velocity-transducer displacement measurements were afflicted with a DC bias. This bias signal occurred because the laser transducer recognizes and measures motion as a velocity, then integrates this velocity value to obtain a displacement measurement. The laser bias was removed by subtracting an average value from individual laser measurements; this average value was computed for each calibration data group or test data group.

6.2.2 Kaman Calibration

A calibration group consisting of three data sets was recorded each time a new specimen was clamped into the experimental set-up. Calibration data sets consisted of laser and eddy

current displacements measured at the clamped end. This data was used to compute scale factors that convert the eddy position change information into a displacement signal measured in millimeters.

The virtual instrument was arranged such that displacement signals were sampled in an alternating order separated by equal intervals of time. To accurately compute scale factors, laser and eddy current data points need to occur at identical times. The linear interpolation of laser displacement values in equation (6-1) was performed on the two laser measurements that sandwich an eddy current data point to obtain a locally averaged laser displacement measurement that occur simultaneously in time with the eddy current measurement. The process of aligning the time locations of the data values eliminated one measurement from the calibration data set. Scale factors, a_0 and a_1 were computed for each calibration data set according to the equation below. Factors for the three calibration sets were averaged to obtain the scale factors for a test group.

$$y(k) = \frac{y(k) + y(k-1)}{2} \quad (6-1)$$

$$y_l = a_0 + a_1 y_k \quad (6-2)$$

The laser and eddy current displacement measurements are denoted by using y_l and y_k respectively. The factor a_1 represents the Kaman system's "guage" factor.

6.3 Parameter Identification

Specimen dimensionless damping and natural frequency values were obtained via optimization of the modal response equation. A modal response equation is an approximate function whose exactness is improved by increasing the number of vibration modes included in its representation. New modes are added to the modal response equation in a block like fashion through the addition of general forms, equation (6-3), of the previously developed transfer function. A general form of the transfer function was attained by dividing the density-cross sectional area term, $\rho A L^4$, from the numerator and denominator

on the right hand side of the transfer function and substitution of three parameters as detailed below.

$$T_i(s) = \frac{K_i}{s^2 + p_1 s + p_2} \quad (6-3)$$

$$\left. \begin{aligned} K_i &\equiv \Phi_i(1) \int_0^1 \Phi_i(x) dx \\ p_1 &\equiv \frac{B_1 I}{\rho a L^4} \\ p_2 &\equiv \frac{B_2 I}{\rho a L^4} \\ p_3 &\equiv \frac{EI}{\rho a L^4} \end{aligned} \right\} \quad (6-4)$$

A value was calculated from the modal information and assigned to parameter K_i for each mode. This value decreases as the mode number increases indicating that higher modes have a smaller impact upon system dynamics than lower frequency modes. Parameters $p_{1,2}$ and p_3 are proportional to the modal dimensionless damping and the natural frequency terms respectively. These parameters were found using the optimization algorithm and were used to generate approximate solutions for the modal response equation.

In the development of the modal response equation, the resulting degree of accuracy is determined by the number of modes used in its construction. Inclusion of more modes improves the modal response approximation at the expense of computation time. The modal response relation can be amended to evaluate an additional mode by including the right hand side of equation (6-3) into the existing modal approximation. A steady state component indicative of the zeroth mode was included in the modal response. This component has a value of one. Equation (6-5) denotes the form of the one mode and two mode approximations.

$$\left. \begin{aligned}
 \text{One Mode Approximation: } T_i(s) &= 1 + \left[\frac{K_1}{s^2 + p_1 \lambda_1^4 s + p_3 \lambda_1^4} \right] \\
 \text{Two Mode - One Damp: } T_i(s) &= 1 + \left[\frac{K_1}{s^2 + p_1 \lambda_1^4 s + p_3 \lambda_1^4} \right] + \left[\frac{K_2}{s^2 + p_1 \lambda_2^4 s + p_3 \lambda_2^4} \right] \\
 \text{Two Mode - Two Damp: } T_i(s) &= 1 + \left[\frac{K_1}{s^2 + p_1 \lambda_1^4 s + p_3 \lambda_1^4} \right] + \left[\frac{K_2}{s^2 + p_2 \lambda_2^4 s + p_3 \lambda_2^4} \right]
 \end{aligned} \right\} \quad (6-5)$$

Addition of a mode to the modal response relation increases the number of parameters the optimization routine must determine. An increase in the number of parameters reduces the function approximation error with an increase in computation time. Modes are accompanied by two initial condition parameters. The damping term may be easily represented using one damping parameter as shown in the “Two Mode-One Damp” approximation of equation (6-5). A more exact method of representing material damping for modes other than the fundamental is to assign a damping parameter to each mode as shown in the “Two Mode-Two Damp” approximation of equation (6-5). A single natural frequency parameter was defined for the system and remained constant regardless of the number of modes included in the approximation.

The optimization algorithm used to generate parameter values is in the MATLAB Optimization Toolbox distributed by The MATH WORKS, Inc. The routine employs the Sequential Quadratic Programming method to determine the minimum of a non-linear function and allows constraints to be imposed upon parameters. Since the damping and frequency parameters represent non-negative physical quantities, their associated parameters were constrained to be equal to or greater than zero. Limitations of the optimization routine require the function and constraints to be continuous and no assurance is provided that the final parameter values represent the desired global extremum; they may instead represent

local extrema. The function to be minimized, J , is the time integral of the square of the difference between the measured free end displacement, y_m , and the predicted free end displacement, y_p , as shown below.

$$J = \int_0^1 |y_m - y_p|^2 dt \quad (6-6)$$

Converging upon local minimums was avoided by careful selection of initial parameter values. Values determined during the minimization of experimental data included: dimensionless damping parameters, the natural frequency, and the initial conditions. The dimensionless damping and natural frequency parameters were of the greatest interest, their initial values were selected using apriori information in an effort to guard against the convergence to false minimums.

Since the initial conditions were small in magnitude compared to the damping and frequency parameters, their initial values were prescribed to be zero for each new data set. Initial values for the damping and frequency parameters for the one mode approximation were selected to be close to their analytically predicted values. The initial damping parameter was chosen as zero and the frequency parameter was specified as one thousand. Initial parameter values for modes other than the fundamental were specified by using the final parameters of the next lowest mode.

6.4 Results

Parameter values were used to predict the motion of the specimen's free end. For each test case, predicted traces were superimposed onto the corresponding experimental data. Plots corresponding to excitation signals of 0 - 800 Hz are located in Appendix E. Appendix F includes the plots for the 6061 Aluminum and crossply-generally damped specimens with excitation signals having a 200 Hz band centered about the fourth mode resonant frequency.

Scaled free end displacements of the crossply specimens exhibited a beat phenomena within their generally oscillatory motion. The beat pulse occurred at approximately two Hertz. Beat effects were not present in traces of the unidirectional specimen's free end displacements. The beat motion is best displayed in the crossply-undamped test case 'B' and the crossply-generally damped test case 'A'.

6.4.1 Parameter Values

Dimensionless damping parameter values and the natural frequencies for specimens excited over the 0 - 800 Hz band are located in Tables 6-1 through 6-6. Similar results for specimens excited about their fourth mode natural frequency are listed in Table 6-8 through 6-15. A value of "0" indicates the minimization algorithm predicts zero dimensionless damping for the specimen. Values of "0.0000" indicates an amount dimensionless damping is specified by the minimization algorithm, but the non-zero parameter digits are lost to truncation.

	One mode approx.			two mode-one damp. approx.			two mode-two damp. approx.		
<u>Case</u>	<u>mode 1</u>	<u>freq.</u>		<u>mode 1</u>	<u>mode 2</u>	<u>freq.</u>	<u>mode 1</u>	<u>mode 2</u>	<u>freq.</u>
test A:	0.0082	31.67		0.0079	0.0493	31.67	0.0082	0.0115	31.65
test B:	0.0076	31.70		0.0072	0.0452	31.70	0.0076	0.0115	31.69
test C:	0.0083	31.69		0.0081	0.0508	31.69	0.0083	0.0113	31.69
Total:	0.0080	31.69		0.0077	0.0485	31.69	0.0080	0.0118	31.69

Table 6-1: Crossply-generally damped dimensionless damping parameter and natural frequency values values.

	One mode approx.			two mode-one damp. approx.			two mode-two damp. approx.		
<u>Case</u>	<u>mode 1</u>	<u>freq.</u>		<u>mode 1</u>	<u>mode 2</u>	<u>freq.</u>	<u>mode 1</u>	<u>mode 2</u>	<u>freq.</u>
test A:	0.0016	37.52		0.0023	0.0142	37.51	0.0016	0.0143	37.51
test B:	0.0025	37.56		0.0027	0.0171	37.56	0.0025	0.0319	37.56
test C:	0.0032	37.43		0.0043	0.0269	37.40	0.0034	0.0324	37.42
Total:	0.0021	37.54		0.0029	0.0181	37.56	0.0021	0.0353	37.54

Table 6-2: Unidirectional-generally damped dimensionless damping parameter and natural frequency values values.

	One mode approx.			two mode-one damp. approx.			two mode-two damp. approx.		
<u>Case</u>	<u>mode 1</u>	<u>freq.</u>		<u>mode 1</u>	<u>mode 2</u>	<u>freq.</u>	<u>mode 1</u>	<u>mode 2</u>	<u>freq.</u>
test A:	0.0031	31.84		0.0009	0.0057	31.84	0.0009	0.0057	31.84
test B:	0	31.89		0.0005	0.0029	31.87	0	0.0030	31.87
test C:	0.0008	31.95		0.0007	0.0041	31.94	0.0008	0.0040	31.94
Total:	0.0013	31.91		0.0007	0.0041	31.89	0.0013	0.0083	31.89

Table 6-3: Crossply-optimally damped dimensionless damping parameter and natural frequency values values.

	One mode approx.		two mode-one damp. approx.			two mode-two damp. approx.		
<u>Case</u>	<u>mode 1</u>	<u>freq.</u>	<u>mode 1</u>	<u>mode 2</u>	<u>freq.</u>	<u>mode 1</u>	<u>mode 2</u>	<u>freq.</u>
test A:	0	37.89	0	0	37.89	0.0011	0.0028	37.89
test B:	0.0000	37.93	0.0008	0.0050	37.95	0.0000	0.0050	37.95
test C:	0.0009	37.82	0.0011	0.0068	37.82	0.0010	0.0150	37.82
Total:	0.0000	37.88	0.0007	0.0043	37.88	0.0000	0.0103	37.88

Table 6-4: Unidirectional-optimally damped dimensionless damping parameter and natural frequency values values.

	One mode approx.		two mode-one damp. approx.			two mode-two damp. approx.		
<u>Case</u>	<u>mode 1</u>	<u>freq.</u>	<u>mode 1</u>	<u>mode 2</u>	<u>freq.</u>	<u>mode 1</u>	<u>mode 2</u>	<u>freq.</u>
test A:	0.0015	30.53	0.0003	0.0021	30.52	0.0015	0.0007	30.52
test B:	0.0006	30.52	0.0003	0.0017	30.52	0.0006	0.0017	30.52
test C:	0.0006	30.55	0.0003	0.0019	30.54	0.0006	0.0017	30.54
Total:	0.0010	30.54	0.0003	0.0018	30.52	0.0010	0.0014	30.53

Table 6-5: Crossply-undamped damped dimensionless damping parameter and natural frequency values values.

	One mode approx.		two mode-one damp. approx.			two mode-two damp. approx.		
<u>Case</u>	<u>mode 1</u>	<u>freq.</u>	<u>mode 1</u>	<u>mode 2</u>	<u>freq.</u>	<u>mode 1</u>	<u>mode 2</u>	<u>freq.</u>
test A:	0.0012	36.73	0.0013	0.0079	36.73	0.0012	0.0088	36.73
test B:	0.0005	36.74	0.0011	0.0067	36.74	0.0005	0.0090	36.74
test C:	0.0007	36.76	0.0012	0.0076	36.74	0.0007	0.0089	36.74
Total:	0.0011	36.73	0.0012	0.0076	36.73	0.0010	0.0089	36.73

Table 6-6: Unidirectional-undamped damped dimensionless damping parameter and natural frequency values values.

In general, the computed natural frequency values were very consistent for both excitation methods. The largest standard deviation of the 0 - 800 Hz specimens was 0.0057 for the two mode-one damping parameter approximation of the unidirectional-generally damped specimen. The crossply specimens had larger natural frequencies than unidirectional specimens for the three damping strategies considered and the all carbon/epoxy specimens had larger natural frequency values than the aluminum 6061 specimen.

The dimensionless damping parameter values of the optimally damped specimens were not consistent in value. This lack of commonality was noted for the unidirectional-optimally damped dimensionless damping parameters that vary by two orders of magnitude for different test samples of a damping strategy, and optimally damped parameter values of zero which indicate the physically impossible condition of no material damping. The inconsistent

dimensionless damping parameter values for the optimally damped strategy may be attributed to modelling a discontinuous arrangement of damping strips using a model which assumes damping is continuous along the length of the specimen. Since the dimensionless damping parameter values for the optimally damped strategy were scattered, they will not be considered in the ensuing discussion of experimental results.

Comparison of generally damped and undamped specimen's dimensionless damping parameter values indicates the first mode damping of the two mode-two damping parameter approximation is nearly equal to the dimensionless damping parameter value of the one mode approximation; these similar values are different from the dimensionless damping parameter value of the two mode-one damping parameter approximation. This difference is anticipated since the two mode-one damping parameter approximation accounts for the effects of the first and second mode damping whereas the other parameters exclusively consider only the damping of the fundamental. Unidirectional second mode dimensionless damping parameter of the two mode-two damping parameter approximation had larger values than the corresponding parameter for the crossply specimens.

An increase in the dimensionless damping parameter value was recognized between the undamped specimens and the generally damped specimens. This enhancement of material damping was noted for each test of a specimen and the consistency of damping improvement is displayed in Table 6-7. The damping enhancement ratios listed are the quotient of dividing the average generally damped value by an average undamped value. Average values are the mean of the three test sets and the total case for each damping strategy. Dimensionless damping parameters of the crossply laminates achieved a factor of eight improvement while the unidirectional laminates recognized approximately a 2.75 factor of improvement.

	one mode approx. <u>first mode</u>	two mode approx. <u>first mode</u>	<u>second mode</u>
Crossply:	8.63	8.66	8.47
Unidirectional:	2.65	2.84	3.20

Table 6-7: Damping enhancement ratios.

Specimens excited about their fourth mode natural frequencies in general had consistent dimensionless damping parameter values for the one, two, and three mode approximations. Values corresponding to fourth mode damping of the four mode approximation were scattered for aluminum and larger than anticipated for the crossply-generally damped specimen. The inconsistency of the fourth mode values may be attributed to mathematical difficulties the minimization algorithm encounter during the optimization process or an insufficient amount of input energy occurs at that frequency. Dimensionless damping parameter results for the one mode and two mode approximations for the composite specimen are close in value to the values obtained when the same specimen was excited using the 0 - 800 Hz band. The first mode dimensionless damping parameter values for the aluminum specimen were scattered, this scatter may result from their small magnitudes.

<u>Approximation</u>	<u>mode 1 damp</u>	<u>mode 2 damp</u>	<u>mode 3 damp</u>	<u>mode 4 damp</u>	<u>frequency</u>
One Mode	0.0000	-	-	-	27.25
Two Mode	0.0001	0.00376	-	-	27.21
Three Mode	0.0001	0.00401	0.00045	-	27.22
Four Mode	0.0000	0.00401	0.00046	2.7280	27.22

Table 6-8: Aluminum 6061 modal dimensionless damping parameter values and natural frequency values for one, two three, and four mode approximations; test case A.

<u>Approximation</u>	<u>mode 1 damp</u>	<u>mode 2 damp</u>	<u>mode 3 damp</u>	<u>mode 4 damp</u>	<u>frequency</u>
One Mode	0.0005	-	-	-	27.24
Two Mode	0.0007	0.0041	-	-	27.20
Three Mode	0.0007	0.0041	0.0039	-	27.20
Four Mode	0.0006	0.0041	0.0039	21.295	27.20

Table 6-9: Aluminum 6061 modal dimensionless damping parameter values and natural frequency values for one, two three, and four mode approximations; test case B.

<u>Approximation</u>	<u>mode 1 damp</u>	<u>mode 2 damp</u>	<u>mode 3 damp</u>	<u>mode 4 damp</u>	<u>frequency</u>
One Mode	0	-	-	-	27.30
Two Mode	0	0.0008	-	-	27.30
Three Mode	0	0.0037	0.0017	-	27.30
Four Mode	0.0000	0.0040	0.0019	0.1326	27.27

Table 6-10: Aluminum 6061 modal dimensionless damping parameter values and natural frequency values for one, two three, and four mode approximations; test case C.

<u>Approximation</u>	<u>mode 1 damp</u>	<u>mode 2 damp</u>	<u>mode 3 damp</u>	<u>mode 4 damp</u>	<u>frequency</u>
One Mode	0.0000	-	-	-	27.25
Two Mode	0.0000	0.0040	-	-	27.21
Three Mode	0.0003	0.0040	0.0020	-	27.22
Four Mode	0.0002	0.0040	0.0021	0.0061	27.23

Table 6-11: Aluminum 6061 modal dimensionless damping parameter values and natural frequency values for one, two three, and four mode approximations; total test case.

<u>Approximation</u>	<u>mode 1 damp</u>	<u>mode 2 damp</u>	<u>mode 3 damp</u>	<u>mode 4 damp</u>	<u>frequency</u>
One Mode	0.0082	-	-	-	31.66
Two Mode	0.0082	0.0124	-	-	31.64
Three Mode	0.0073	0.0145	0.0044	-	31.82
Four Mode	0.0073	0.0145	0.0044	0.2526	31.81

Table 6-12: Crossply-generally damped modal dimensionless damping parameter values and natural frequency values for one, two three, and four mode approximations; test Case A.

<u>Approximation</u>	<u>mode 1 damp</u>	<u>mode 2 damp</u>	<u>mode 3 damp</u>	<u>mode 4 damp</u>	<u>frequency</u>
One Mode	0.0073	-	-	-	31.69
Two Mode	0.0073	0.0123	-	-	31.68
Three Mode	0.0073	0.0169	0.0044	-	31.81
Four Mode	0.0073	0.0169	0.0044	0.2526	31.81

Table 6-13: Crossply-generally damped modal dimensionless damping parameter values and natural frequency values for one, two three, and four mode approximations; test Case B

<u>Approximation</u>	<u>mode 1 damp</u>	<u>mode 2 damp</u>	<u>mode 3 damp</u>	<u>mode 4 damp</u>	<u>frequency</u>
One Mode	0.0081	-	-	-	31.69
Two Mode	0.0081	0.0120	-	-	31.68
Three Mode	0.0079	0.0112	0.0044	-	31.76
Four Mode	0.0079	0.0112	0.0044	0.2526	31.76

Table 6-14: Crossply-generally damped modal dimensionless damping parameter values and natural frequency values for one, two three, and four mode approximations; test Case C.

<u>Approximation</u>	<u>mode 1 damp</u>	<u>mode 2 damp</u>	<u>mode 3 damp</u>	<u>mode 4 damp</u>	<u>frequency</u>
One Mode	0.0079	-	-	-	31.68
Two Mode	0.0079	0.0122	-	-	31.67
Three Mode	0.0075	0.0143	0.0044	-	31.79
Four Mode	0.0075	0.0143	0.0045	0.1902	31.79

Table 6-15: Crossply-generally damped modal dimensionless damping parameter values and natural frequency values for one, two three, and four mode approximations; total test case.

6.4.2 Parameter Magnitude

The optimization algorithm is designed to obtain a minimum for the modal approximation relation by perturbing the parameters such that the modal approximation error is reduced. The algorithm's ability to correctly identify parameter values is related to the

magnitude of the individual parameter. It was observed the larger the damping parameter's magnitude the less effect a perturbation, necessary to reduce modal approximation error values, had upon the time response. This is evident when comparing the damping parameter values listed in Tables 6-8 through 6-15 for the crossply-generally damped and aluminum 6061 specimens excited about their fourth modes. The crossply-generally damped damping parameters are typically two orders of magnitude larger than those for aluminum. Damping parameters for the crossply-generally damped specimens have consistent magnitudes whereas the aluminum damping parameter magnitudes are quite scattered. This trend of better consistency in identification of damping parameter values for specimens having larger parameter magnitudes is also demonstrated in the six specimens excited over the 0-800 Hz band.

6.4.3 Analysis of Time Responses

Minimal deviation between the measured and predicted traces creates difficulty in discerning the quality of the predicted responses. Qualification of predicted traces is measured via computation of the square of the 2-norm of the difference between the measured and predicted data, E_e , for the modal approximations. These values were computed via integration over the normalized beam length according to the equations below.

$$E_e = \int_0^1 |y_m - y_p|^2 dt \quad (6-7)$$

$$E_{ym} = \int_0^1 |(y_m)|^2 dt \quad (6-8)$$

The values recorded in Tables 6-16 through 6-19 correspond to the specimens excited over the 0 - 800 Hz input band. The 2-norm of the error for the two mode approximations defined with two damping parameters was always less than the norm of the error for the two mode-one damping parameter approximations excluding the total cases of specimens:

crossply-generally damped, unidirectional-generally-damped, and crossply-optimally damped. The smaller error magnitudes for the two mode-two damping parameter case indicates specimen damping is best modeled using modal damping. It is also an indication that the presumed damping mechanism used in the transfer function derivation is not very representative for multimode approximations. For the multimode models an independent damping parameter was determined for each mode and excellent agreement with the experimental measurements was observed. In general, error signal magnitudes are approximately 3% of the total measured signal.

<u>Specimen</u>	<u>test A</u>	<u>test B</u>	<u>test C</u>	<u>Total</u>
Crossply-general damp.	0.2793	0.3507	0.4133	1.0433
Unidirect-general damp.	0.3696	0.4153	0.0861	0.8710
Crossply-optimal damp	0.7240	0.3553	1.1397	2.2190
Unidirect-optimal damp.	0.5895	0.4570	0.5441	1.5906
Crossply-undamped	1.5818	0.5925	1.5865	3.7608
Unidirect-undamped	0.6063	0.2101	0.3141	1.5906

Table 6-16: 2-norm of measured displacement signal.

<u>Specimen</u>	<u>test A</u>	<u>test B</u>	<u>test C</u>	<u>Total</u>
Crossply-general damp.	0.0049	0.0049	0.0043	0.0143
Unidirect-general damp.	0.0051	0.0031	0.0066	0.0158
Crossply-optimal damp.	0.0192	0.0216	0.0184	0.0642
Unidirect-optimal damp	0.0075	0.0034	0.0149	0.0297
Crossply-undamped	0.0251	0.0262	0.0496	0.1018
Unidirect-undamped	0.0051	0.0045	0.0064	0.0164

Table 6-17: 2-norm of one mode approximation error signal.

<u>Specimen</u>	<u>test A</u>	<u>test B</u>	<u>test C</u>	<u>Total</u>
Crossply-general damp.	0.0029	0.0026	0.0027	0.0082
Unidirect-general damp.	0.0048	0.0025	0.0053	0.0151
Crossply-optimal damp.	0.0056	0.0106	0.0057	0.0251
Unidirect-optimal damp	0.0066	0.0020	0.0142	0.0269
Crossply-undamped	0.0059	0.0036	0.0275	0.0378
Unidirect-undamped	0.0021	0.0030	0.0017	0.0069

Table 6-18: 2-norm of two mode-one damping parameter approximation error signal.

<u>Specimen</u>	<u>test A</u>	<u>test B</u>	<u>test C</u>	<u>Total</u>
Crossply-general damp.	0.0013	0.0011	0.0016	0.2178
Unidirect-general damp.	0.0045	0.0022	0.0052	0.0125
Crossply-optimal damp	0.0056	0.0105	0.0057	0.0243
Unidirect-optimal damp.	0.0066	0.0016	0.0141	0.0252
Crossply-undamped	0.0035	0.0036	0.0274	0.0358
Unidirect-undamped	0.0021	0.0029	0.0015	0.0474

Table 6-19: 2-norm of two mode-two damping parameter approximation error signal.

The values recorded in Tables 6-20 and 6-21 are the 2-norm of the measured free end displacement and the error between the predicted and measured displacements for the specimens excited about their fourth mode natural frequencies. The 2-norm magnitudes for the crossply-generally damped specimens have a consistently larger measured signal than the aluminum specimens; these greater magnitude values are consistent with the larger peak to peak displacements on the crossply-generally damped traces of Appendix F.

The 2-norm error between the measured and predicted signals for the two mode, three mode, and four mode approximations of the crossply-generally damped specimen were all less than 1% of the measured free end displacement. The small error percentages indicate the modal approximations predicted the free end displacement with a high degree of accuracy. One mode approximations for the crossply-generally damped specimen had 2-norm error values that were approximately 65% of the measured free end signal. These large error signal percentages were evident in the traces for the one mode approximation. The inability of the one mode approximation to predict free end displacement may be the result of insufficient stimulation of the fundamental. The aluminum specimen also experienced large 2-norm error values for the one mode approximation. The percentage of error was approximately 20% of the measured free end displacement.

	Approximation Error (Predicted - Measured)				measured signal
	<u>one mode</u>	<u>two mode</u>	<u>three mode</u>	<u>four mode</u>	
test A:	0.03430	0.00048	0.00048	0.00048	0.05343
test B:	0.05733	0.00038	0.00039	0.00038	0.08472
test C:	0.06566	0.00078	0.00077	0.00077	0.09101

Table 6-20: 2-norm of measured free end displacement and the error between predicted free end displacements and measured free end displacements, crossply-generally damped specimen.

	Approximation Error (Predicted - Measured)				measured signal
	<u>one mode</u>	<u>two mode</u>	<u>three mode</u>	<u>four mode</u>	
test A:	0.00100	0.00021	0.00028	0.00033	0.00869
test B:	0.00176	0.00049	0.00051	0.00051	0.00902
test C:	0.00136	0.00071	0.00072	0.00105	0.00553

Table 6-21: 2-norm of measured free end displacement and the error between predicted free end displacements and measured free end displacements, aluminum 6061 specimen.

6.4.4 Damping Parameter Convergence To Zero

The damping parameter converged to a value of zero for two test cases. The physical impossibility of damping parameters being equal to zero indicates either an error in the minimization process or a problem with the data set. Successive iterations of these test cases with varying initial conditions each converged to damping parameter values of zero. Both test cases afflicted with this condition were optimally damped specimens. The discontinuous nature of the optimal damping strategy may cause the laminate damping to vary greatly from the continuous material damping assumption of the modal response equation. Zero values were converged upon for test case 'B' of the crossply-optimally damped specimen and test case 'A' of the unidirectional-optimally damped specimen. Damping parameters for the two mode crossply-optimally damped approximations did not converge to zero.

Traces of scaled free end displacements for the two specimens having zero valued damping parameters were evaluated. Displacements for the unidirectional-optimally damped specimen appear to be consistent for its three test cases. Displacements had similar peak to peak displacements and minimal visual variations in their higher mode effects. Analysis of the three crossply-optimally damped data sets exhibited a unique tendency for the test case whose first mode damping value converged to zero. Data sets 'A' and 'C' had approximately one half of their displacement signals dominated by the oscillatory motion of the fundamental mode. Data set 'B' did not have a region of large first mode oscillations. This lack of first mode oscillation may have caused the first mode damping parameter value for test data set 'B' to converge to zero while both of its two mode approximations had positive damping parameters.

7.0 CONCLUSIONS and RECOMMENDATIONS

7.1 Conclusions

1) A general arrangement of viscoelastic material at three ply interfaces symmetric to the midplane increases the dimensionless damping parameter values of a carbon/epoxy laminate by a factor of eight for a crossply layup and an approximate factor of three for a unidirectional layup.

2) Crossply carbon/epoxy laminates exhibit larger dimensionless damping parameter values than unidirectional carbon/epoxy laminates of similar geometric dimensions.

3) Prediction consistency of dimensionless damping parameter can be improved by increasing the number of modes included in the modal response relation.

4) Prediction of damping characteristic is improved by using multiple damping parameters to define modal damping for modes other than the fundamental mode.

5) Parameter values for the optimally damped strategy were not consistent in magnitude, this may be a result of the discontinuous arrangement of their damping material and the use of a model that assumes continuous damping.

7.2 Recommendations

The study at hand serves as only an introduction into the realm of enhancing the internal damping characteristics of composite laminates. It can also serve as a springboard from which numerous areas of study may be explored. Additional areas of study can expand upon the amount and placement of the viscoelastic damping material, variation in the type or thickness of the damping material, combination of different ply layup orientations to determine the maximum damping associated with a ply layup strategy.

Additionally, investigation of the laminate mechanical properties of toughness, tensile strength, and fatigue life as a function of the amount and location of viscoelastic material at ply interfaces would provide information crucial for determining the practical utility of this model.

Ultrasonic analysis of laminates can be performed to determine if voids, inclusions or delamination occur within a laminate; such fabrication induced items increase material dimensionless damping parameter value. Ultrasonic analysis was not performed on the specimens used in this experimental analysis. Laminates can also be fabricated with voids or regions of delamination purposely included to quantify their effects upon laminate damping and strength properties.

REFERENCES

- 1: Magolan, A.M., "An Investigation on the Retrofitment of an Industrial Robot Manipulator with a Composite Arm: Design, Analysis and Fabrication", Master of Science Thesis, Department of Mechanical Engineering, Michigan State University, East Lansing, MI, 1989.
- 2: Rivin, E.I., "A Laminated Material for Impact Noise Abatement and its Applications", Proceedings of the Sixth Annual ASM/ESD Advanced Composites Conference, Detroit, Mi, October 8-11, 1990, pp. 491-495.
- 3: Adams, R.D., "The Dynamic Longitudinal Shear Modulus and Damping of Carbon Fibers", Journal of Physics D: Applied Physics, **8**, pp. 738-748 (1975).
- 4: Suarez, S., Gibson, R., Sun, C. and Chaturvedi, S., "The Influence of Fiber Length and Fiber Orientation On Damping and Stiffness of Polymer Composite Materials", Experimental Mechanics, **26** (2), pp. 175-184 (1986).
- 5: Way, S., Ashton, J.N. and El-Sobky, H., "An investigation of the Influence of Anisotropy and Frequency on Damping in Short Glass Fibre Reinforced Polypropylene", Composite Structures, **15** (1), pp. 43-60 (1990).
- 6: Adams, R.D. and Bacon, D.G., "Effect of Fibre Orientation and Laminate Geometry on the Dynamic Properties of CFRP", Journal of Composite Materials, **7** (10), pp. 402-428 (1973).
- 7: Andersen, S.M., Jackson, G B. and Vinson, J.R., "Effects of Fiber Orientation on Material Damping In Beams of Composite Materials", Proceedings of the Sixth Annual ASM/ESD Advanced Composites Conference, Detroit, Mi, October 8-11, 1990, pp. 471-475.
- 8: Liao, D.X., Sung, C.K. and Thompson, B.S., "The Optimal Design of Symmetric Laminated Beams Considering Damping", Journal of Composite Materials, **20** (9), pp. 485-500 (1986).
- 9: Moser, K. and Lunassegger, M., "Increasing the Damping of Flexural Vibrations of Laminated FPC Structures by Incorporation of Soft Intermediate Plies with Minimum Reduction of Stiffness", Composite Structures, **10** (4), pp. 321-334 (1985).

10: Sun, C.T., Sankar, B.V. and Roa, V.S., "Damping and Vibration Control of Unidirectional Composite Laminates Using Add-on Viscoelastic Materials", Journal of Sound and Vibration, **139** (2), pp. 277-287 (1990).

11: Lifshitz, J. and Leibowitz, M., "Optimal Sandwich Beam Design for Maximum Viscoelastic Damping", International Journal of Solids and Structures, **23** (7), pp. 1027-1034 (1987).

12: Lall, A.K., Asnani, N.T. and Nakra, B.C., "Vibration and Damping Analysis of Rectangular Plate With Partially Covered Constrained Viscoelastic Layer", Journal of Vibration, Acoustics, Stress and Reliability in Design, **109** (7), pp. 241-247 (1987).

13: Mantena, P.R. and Gibson, R.F., "Constrained Layer Damping Treatments for Vibration Control of Composite Structural Elements", Proceedings of the Sixth Annual ASM/ESD Advanced Composites Conference, Detroit, Mi, October 8-11, 1990, pp. 3-14.

14: Plunkett, R. and Lee, C.T., "Length Optimization for Constrained Viscoelastic Layer Damping", Journal of Acoustical Society of America, **48**, pp. 150-161 (1970).

15: Q: Sun, C.T., Sankar, B.V. and Rao, V.S., "Damping and Vibration Control of Unidirectional Composite Laminates Using Add-On Viscoelastic Materials", Journal of Sound and Vibration, **139** (2), pp. 277-287 (1990).

16: Sun, C., Wu, J. and Gibson, R., "Prediction of Material Damping of Laminated Polymer Composites", Journal of Materials Science, **22**, pp. 1006-1012 (1987).

17: Lin, D.X., Ni, R.G. and Adams, R.D., "Predictions and Measurement of the Vibrational Damping Parameters of Carbon and Glass Fibre-Reinforced Plastics Plates", Journal of Composite Materials, **18** (3), pp. 132-152 (1984).

18: Ni, R. and Adams, R., "A Rational Method for Obtaining the Dynamic Mechanical Properties of Laminae for Predicting the Stiffness and Damping of Laminated Plates and Beams", Composites, **15** (3), pp. 193-199 (1984).

19: Ni, R. and Adams, R., "The Damping and Dynamic Moduli of Symmetric Laminated Composite Beams-Theoretical and Experimental Results", Journal of Composite Materials, **18** (3), pp. 104-121 (1984).

20: Lee, C.Y., Pfeifer, M., Thompson, B. and Gandhi, M., "The Characterization of Elastic Moduli and Damping Capacities of Graphite /epoxy Composite Laminated Beams in Hygrothermal Environments", Journal of Composite Materials, 23 (8), pp. 819-845 (1989).

21: Ni, R.G., Lin, D.X. and Adams, R.D., "The Dynamic Properties of Carbon/Glass Fibre Sandwich-Laminated Composites: Theoretical, Experimental and Economic Considerations", Composites, 15 (4), pp. 297-304 (1984).

22: Crane, R.M. and Gillespie Jr., J.W., "Effect of Vibration Amplitude and Frequency on the Vibration Damping Loss Factor of Glass/Epoxy Composites", Proceedings of the Sixth Annual ASM/ESD Advanced Composites Conference, Detroit, Mi, October 8-11, 1990, pp.461-470.

23: Adams, R.D., "Damping Properties Analysis of Composites", ASM International Engineered Materials Handbook Volume 1-Composites, pp.206-217, 1988.

24: Sun, C.T., Sankar, B.V. and Rao, V.S., "Damping and Vibration Control of Unidirectional Composite Laminates Using Add-On Viscoelastic Materials", Journal of Sound and Vibration, 139(2) pp. 277-287 (1990).

25: Rudin, A., The Elements of Polymer Science and Engineering: An Introductory Text for Engineers and Chemists, Academic Press, Inc., 1982.

26: Sanjana, S.N., "Average Indications for Prepreg Products", SAMPE Journal, 25(1), pp. 5 - 11 (1980).

27: Akay, M., "Effects of Prepreg Ageing and Post Cure Hygrothermal Conditioning on Mechanical Behaviour of Carbon-Fiber/Epoxy Laminates", Composite Science and Technology, 38(4), pp. 359-370 (1990).

28: Johnson, R., 3M Corporation, telephone conversation June 28, 1990.

29: Gibson, Ronald F., "Damping Characteristics of Composite Materials and Structures", Proceedings of the Sixth Annual ASM/ESD Advanced Composites Conference, Detroit, Mi, October 8-11, 1990, pp. 441-449.

30: Adams, R.D. and Bacon, D.C ., "Measurement of the flexural damping capacity and dynamic Young's modulus of metals and reinforced plastics", Journal of Physics D: Applied Physics, **6**, pp. 27-41 (1972).

31: Gibson, R.F. and Plunkett, R., "A Forced-vibration Technique for Measurement of Material Damping", Experimental Mechanics, **17**(8) pp. 297-302 (1977).

32: Gibson, R., "Dynamic Mechanical Behavior of Fiber-Reinforced Composites: Measurement and Analysis", Journal of Composite Materials, **10** (10), pp. 325-341 (1976).

Appendix A

General eigensolution matrix.

The following two relations will be used to solve (3-19).

$$e^{a+jb} = e^a(\cos b + j\sin b) \quad \text{and} \quad e^{a-jb} = e^a(\cos b - j\sin b) \quad (\text{A-1})$$

Rewrite (3-18):

$$\text{Det [F]} = 0 = 4 + e^{-(1+j)\lambda} + e^{-(1-j)\lambda} + e^{(1-j)\lambda} + e^{(1+j)\lambda} \quad (\text{A-2})$$

Combination of (A-1) and (A-2) produce:

$$4 + e^{-a}(\cos(-b) + j\sin(-b)) + e^{-a}(\cos(b) - j\sin(b)) + \quad (\text{A-3})$$

$$e^a(\cos(-b) - j\sin(-b)) + e^a(\cos(b) + j\sin(b)) = 0$$

$$\text{note: } \sin(b) = -\sin(-b) \quad \text{and} \quad \cos(b) = \cos(-b) \quad (\text{A-4})$$

Equation (A-4) allows consolidation of (A-3) as follows:

$$4 + e^{-a}(2\cos b) + e^a(2\cos b) = 0 \quad (\text{A-5})$$

$$4 + 2\cos b [e^{-a} + e^a] = 0$$

$$\text{recall: } \frac{e^{-a} + e^a}{2} = \cosh a$$

$$4 + 4\cos b \cosh a = 0$$

$$\text{recall: } a = b = \lambda$$

$$4 + 4\cos \lambda \cosh \lambda = 0$$

$$\text{Thus: } \cos \lambda_i \cosh \lambda_i = -1$$

Appendix B

Values of variables used in chapters are listed below:

CONSTANT VALUES

specimen length	$\equiv l = 28 \text{ cm}$
specimen base	$\equiv b = 2.54 \text{ cm}$
specimen height	$\equiv h = 8 * t_l = 8 * (0.014 \text{ cm}) = 0.112 \text{ cm}$
material density	$\equiv \rho = 1.55 \text{ g/cm}^3$
laminae thickness	$\equiv t_l = 0.014 \text{ cm}$
Young's modulus	$\equiv E = 1.2609 \times 10^{+11} \text{ kg/s}^2\text{m}$
area moment of inertia	$\equiv I = 2.9738 \times 10^{-12} \text{ m}^4$
specimen mass	$\equiv m = \rho(w \cdot h) l = 1.232 \times 10^{-2} \text{ kg}$

PER MODE VALUES

<u>mode number</u>	<u>eigen- value</u>	<u>normalized</u>		<u>$\Phi_i(1)$</u>	<u>P_i</u>	<u>K_i</u>
		<u>C_1</u>	<u>C_2</u>			
1	1.875100	1.000007	-0.734105	-1.960669	0.765639	-1.501166
2	4.694090	0.999985	-1.018454	+1.863479	0.468193	+0.872468
3	7.854760	0.999959	-0.999183	-1.776306	0.230822	-0.410010
4	10.995541	1.023346	-1.023349	+0.927019	0.289813	+0.268662

Appendix C

Solving for the non-dimensional damping parameter in terms of material and geometric properties.

Compare the following two equations:

$$\ddot{q} + p_{1,2}\lambda_i^4\dot{q} + p_3\lambda_i^4q = 0 \quad (C-1)$$

$$\ddot{y} + (2\xi w_n)\dot{y} + (w_n^2)y = 0 \quad (C-2)$$

Relations (C-3a) and (C-3b) can be obtained from (C-1) and (C-2) by equating the coefficients for the terms with similar derivatives.

$$2\xi w_n = p_{1,2}\lambda_i^4 \quad (a) \qquad w_n^2 = p_3\lambda_i^4 \quad (b) \quad (C-3)$$

Substitute [H-3b] into [H-3a]:

$$2\xi\sqrt{p_3\lambda_i^4} = p_{1,2}\lambda_i^4 \quad (C-4)$$

We will solve (C-4) to obtain a relation for the damping ratio, ξ , based upon the known values: eigenvalue, λ_i , Young's modulus, E , area moment of inertia, I , laminate density, ρ , and specimen cross sectional area, a .

$$\xi_i = \frac{p_{1,2}\lambda_i^2}{2\sqrt{p_3}} \quad (C-5)$$

Appendix D

Magnitude and Phase angle plots for varying values of the dimensionless damping parameter.

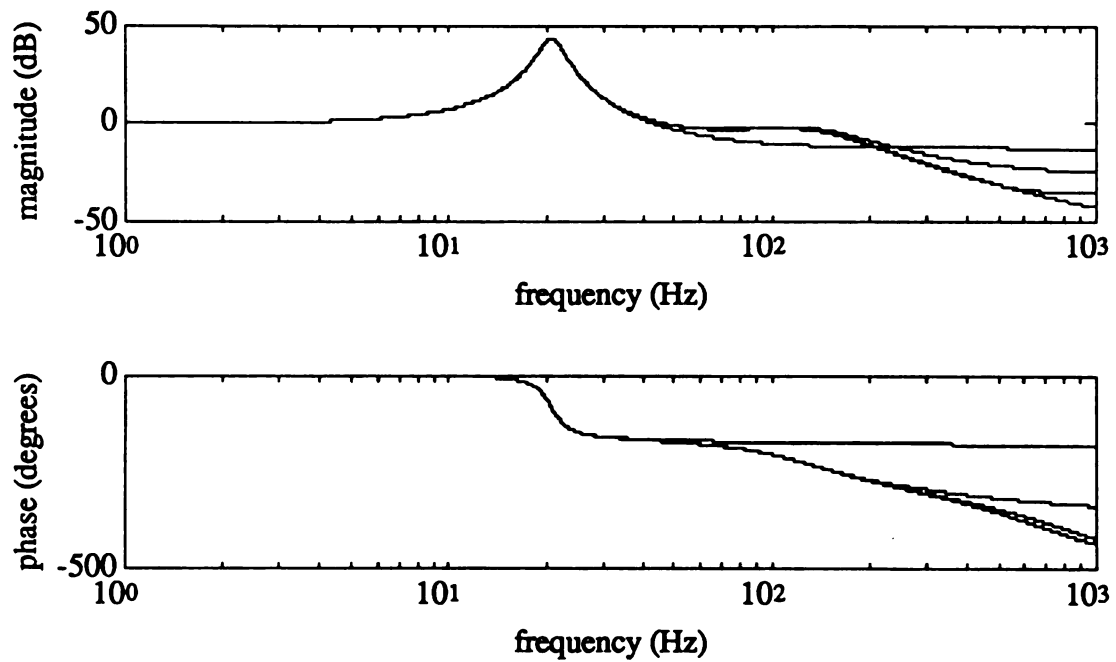


Figure D-1: Dimensionless damping parameter of the first mode = 0.025.

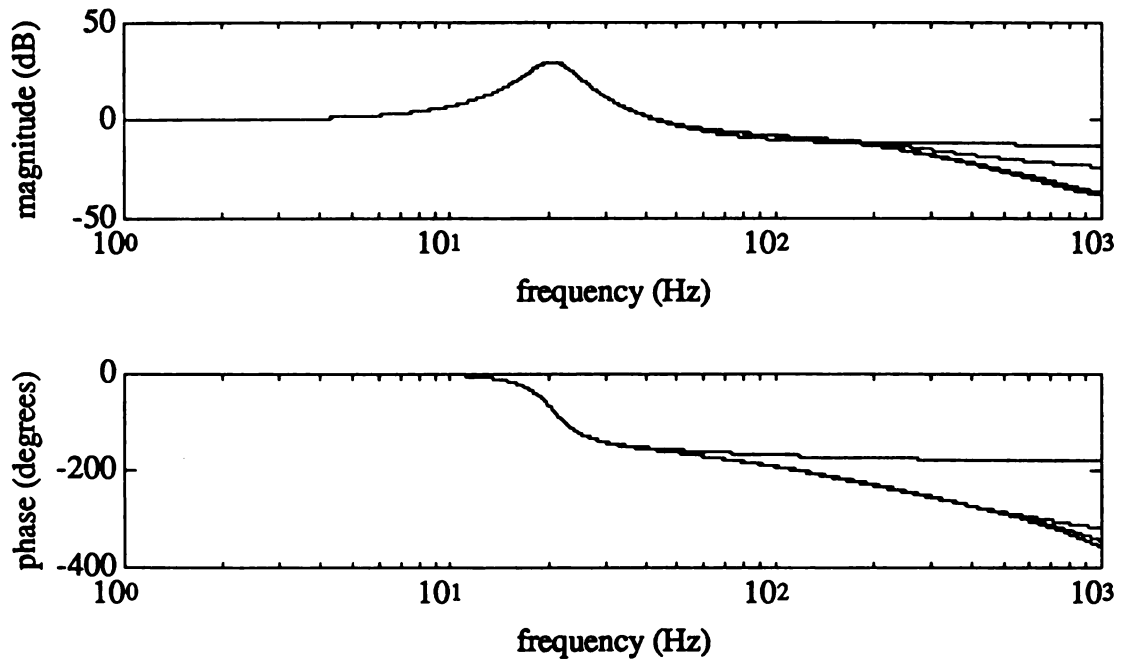


Figure D-2: Dimensionless damping parameter of the first mode = 0.050:

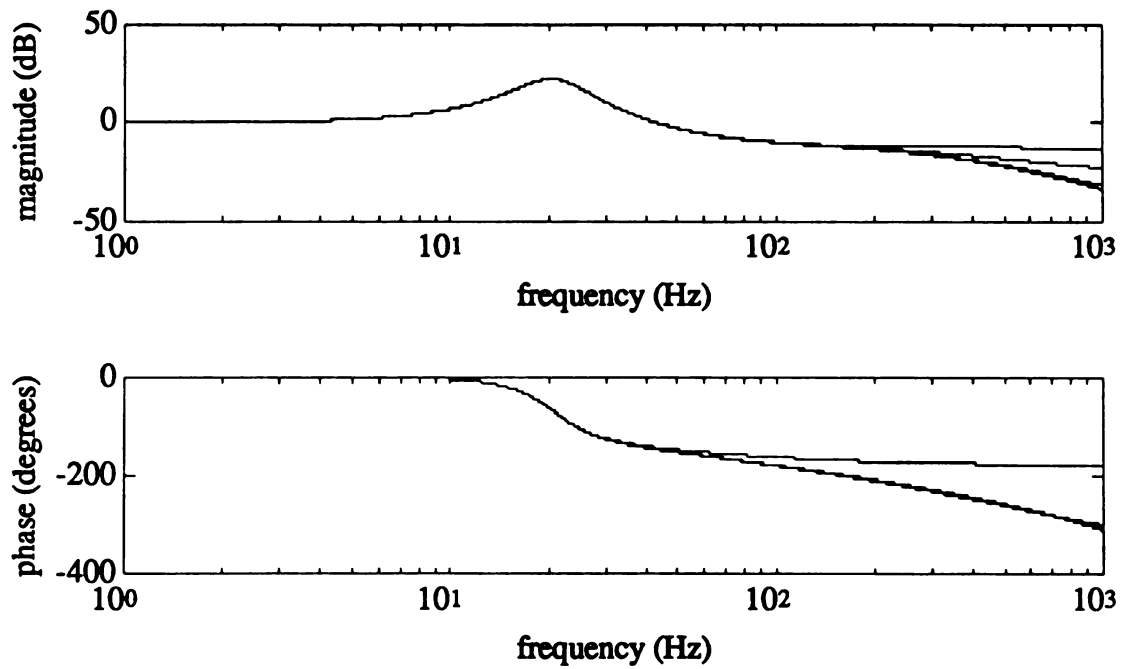


Figure D-3: Dimensionless damping parameter of the first mode = 0.075.

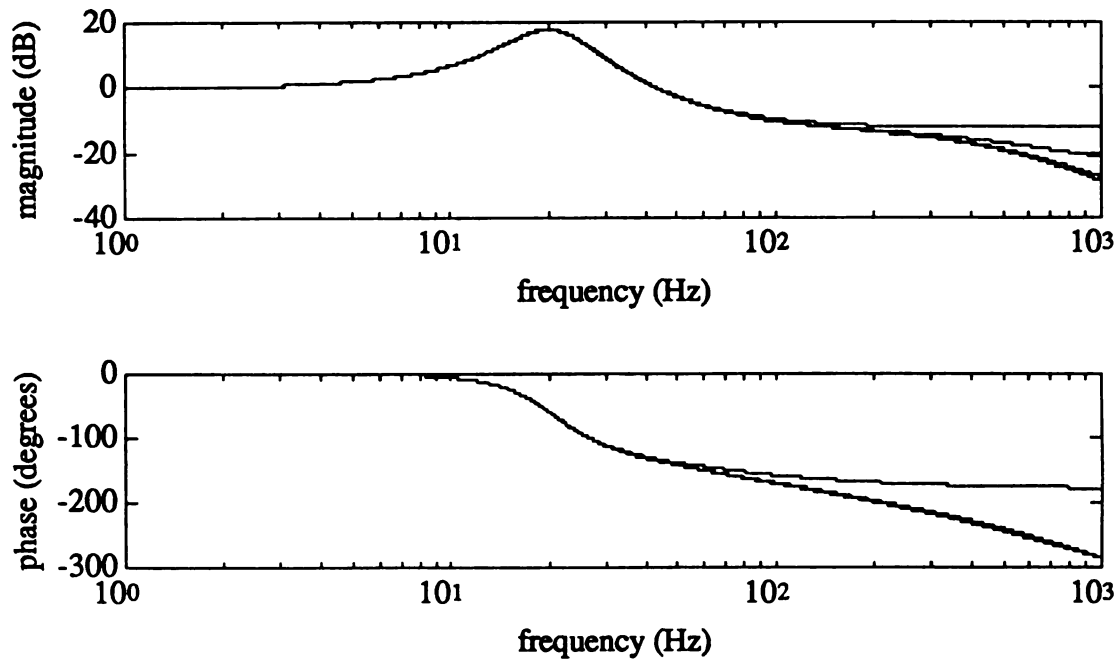


Figure D-4: Dimensionless damping parameter of the first mode = 0.100.

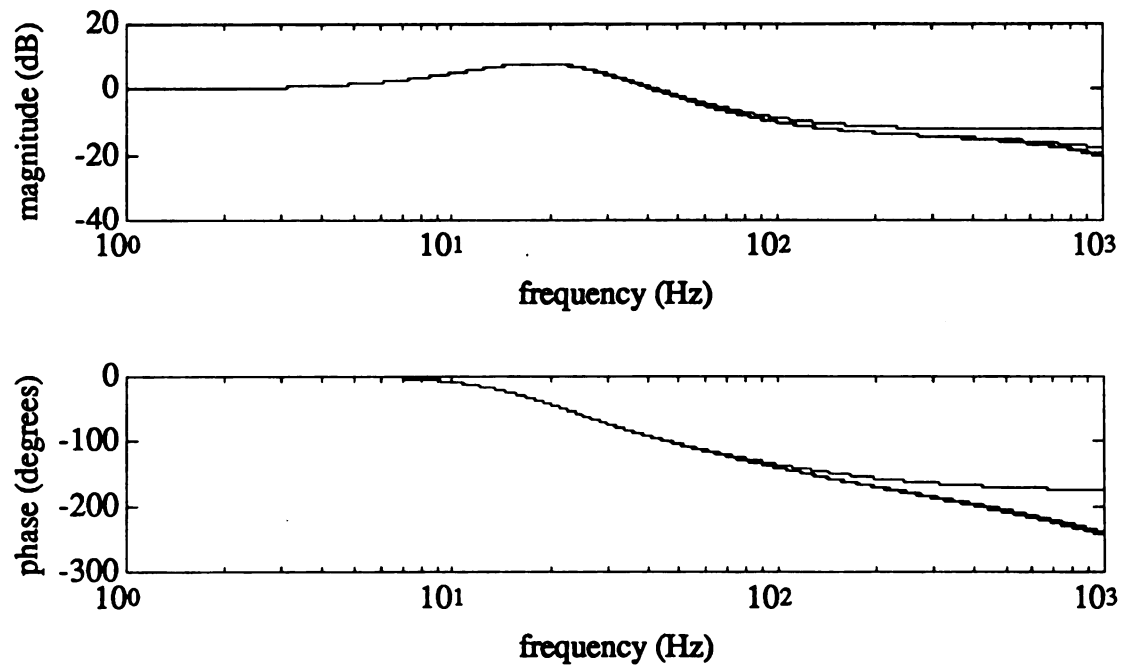
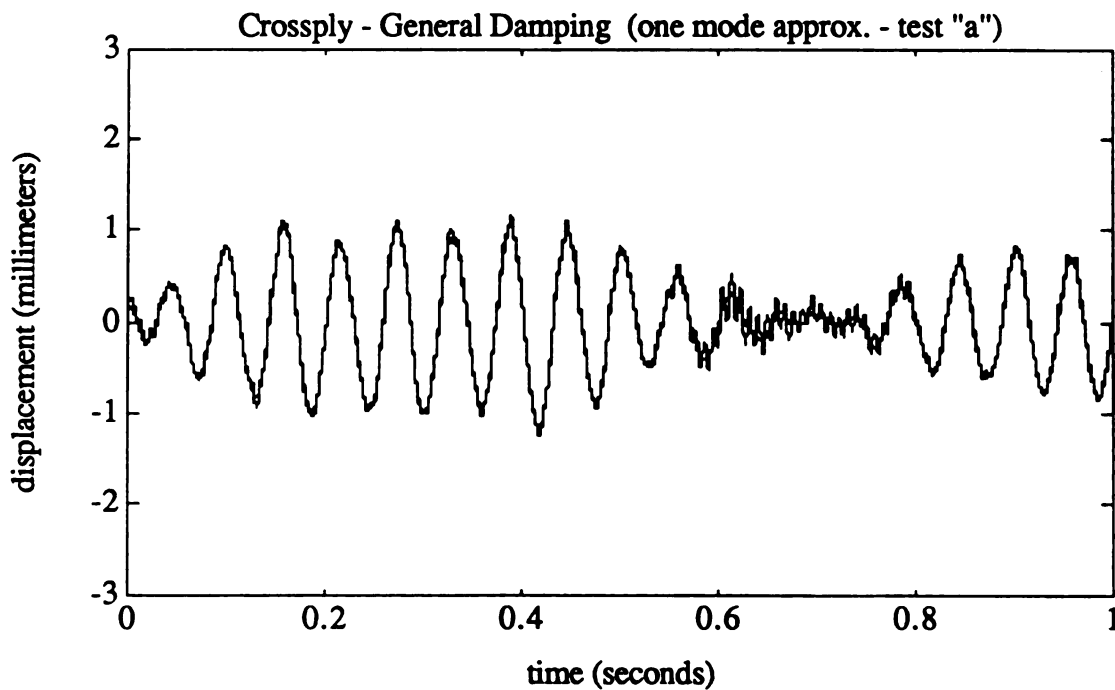
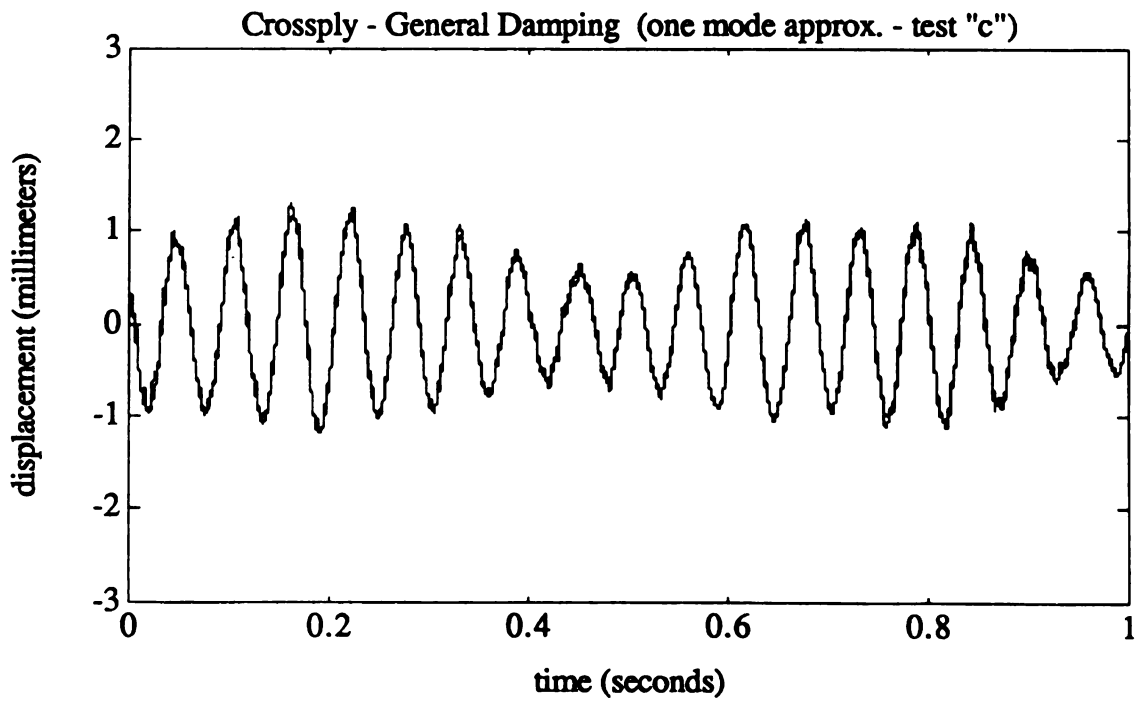
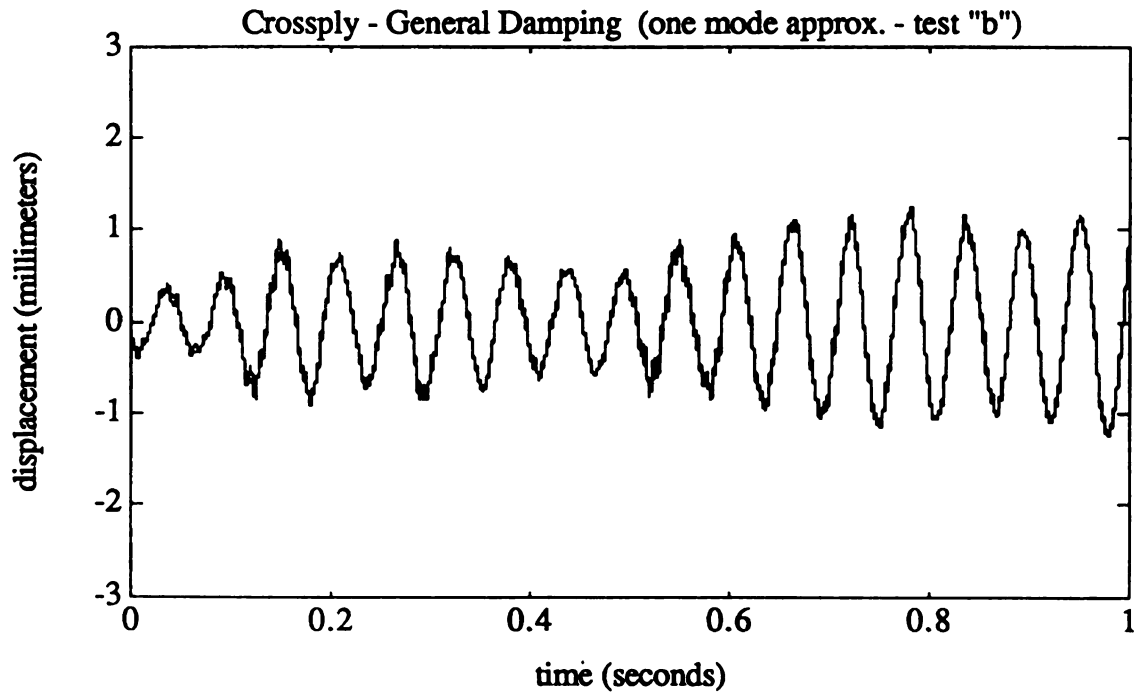


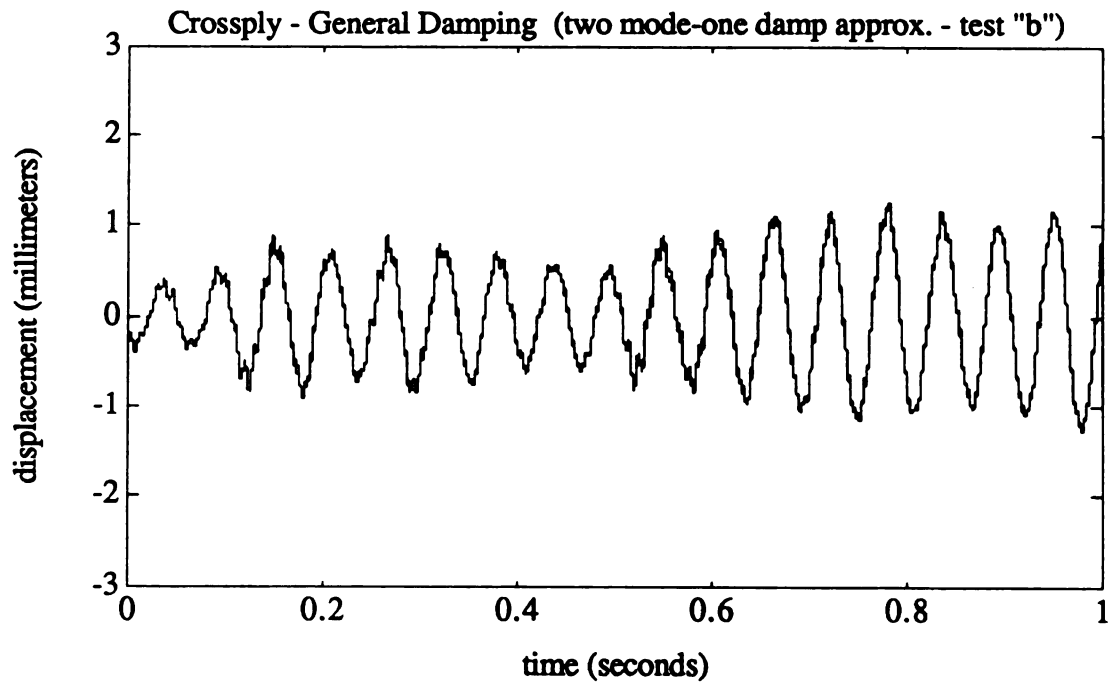
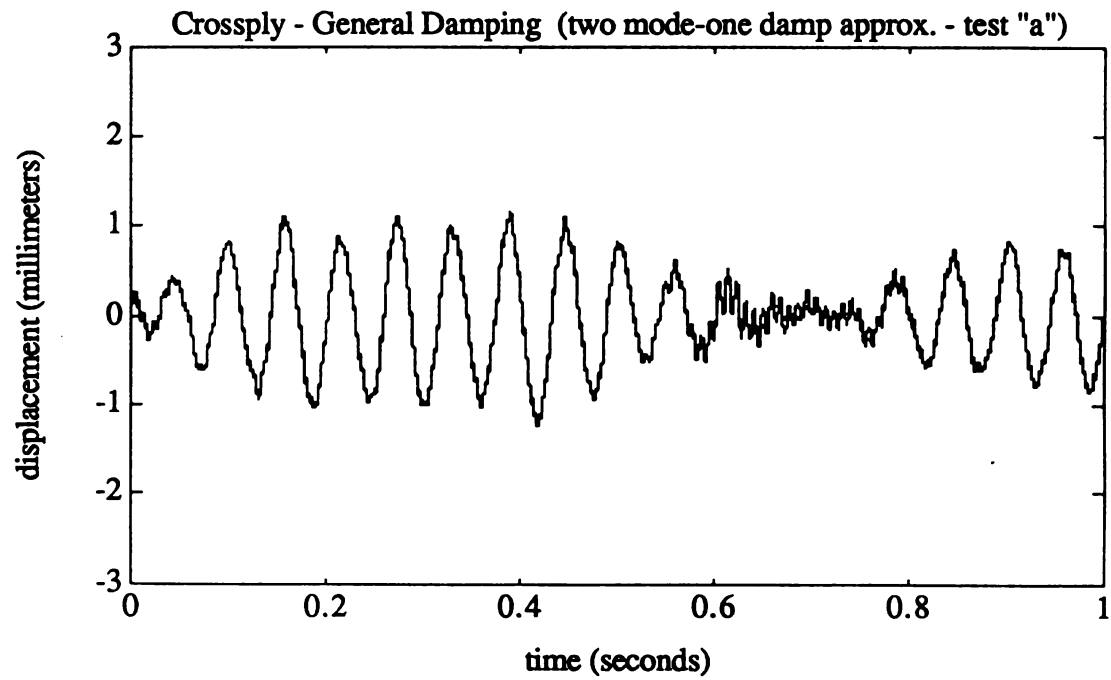
Figure D-5: Dimensionless damping parameter of the first mode = 0.200.

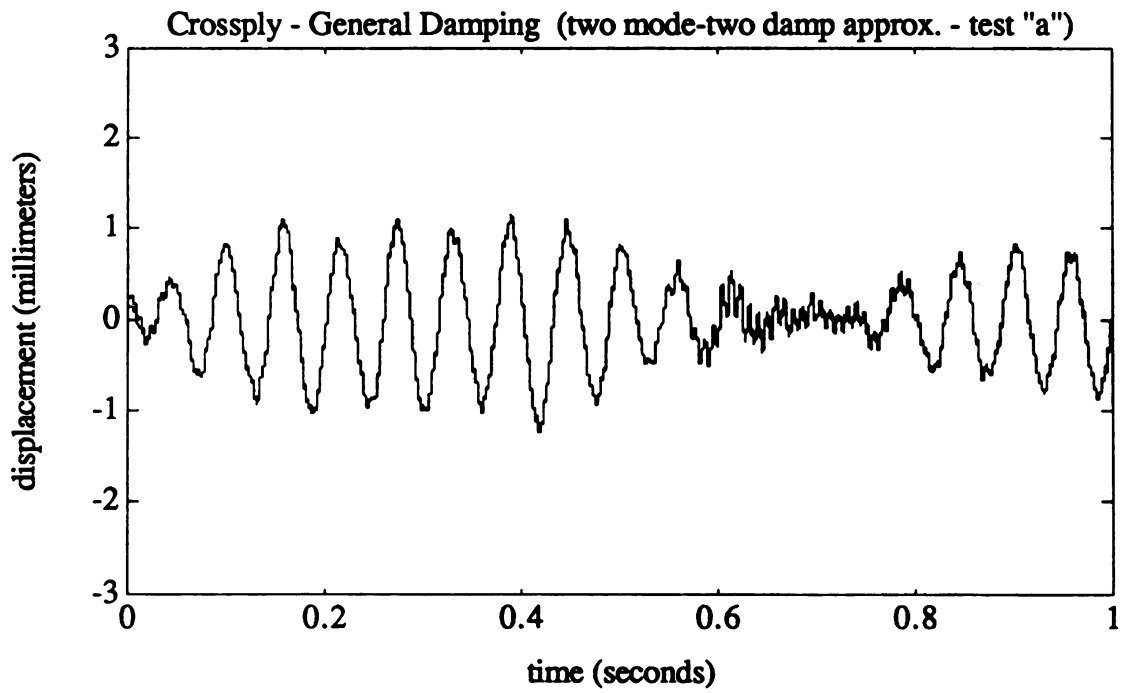
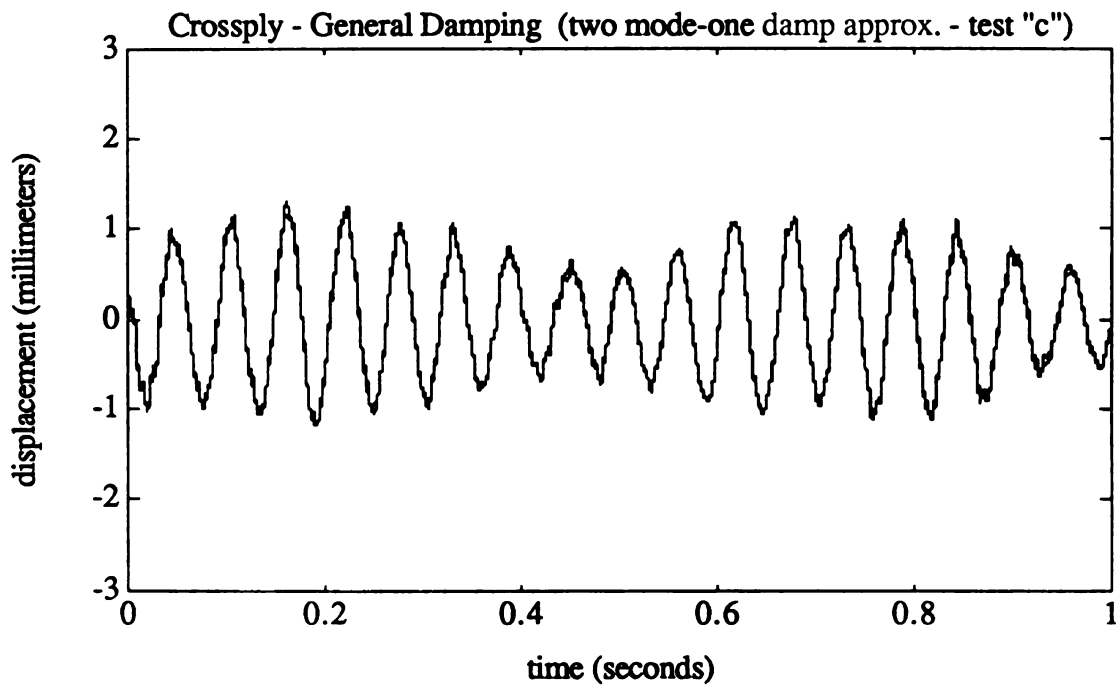
Appendix E

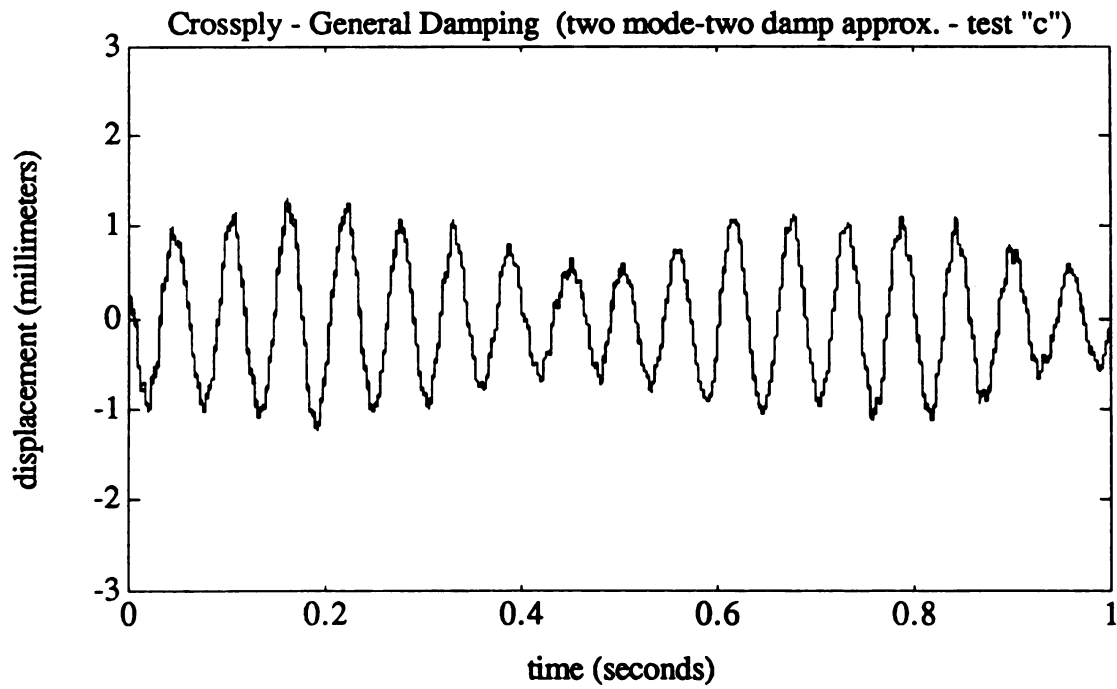
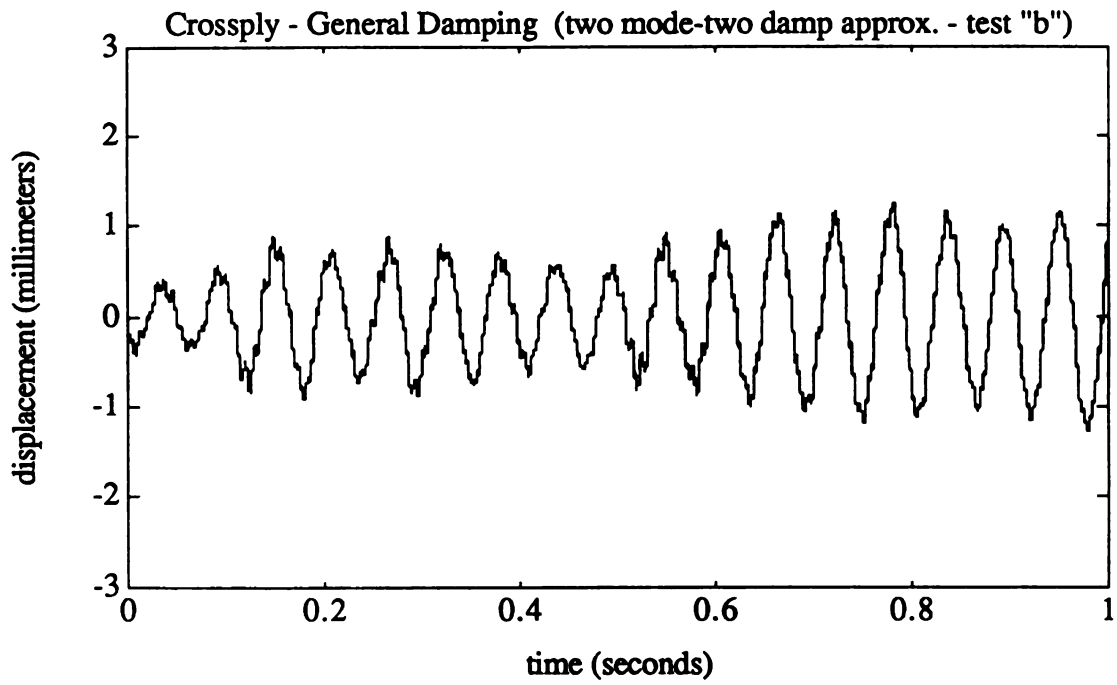
Traces of predicted and measured free end displacement for the six clamped-free specimens for the one mode approximation, the two mode-one damping parameter approximation and the two mode-two damping parameter approximation. All data is for the 0 - 800 Hz band of random excitation at the clamped end.

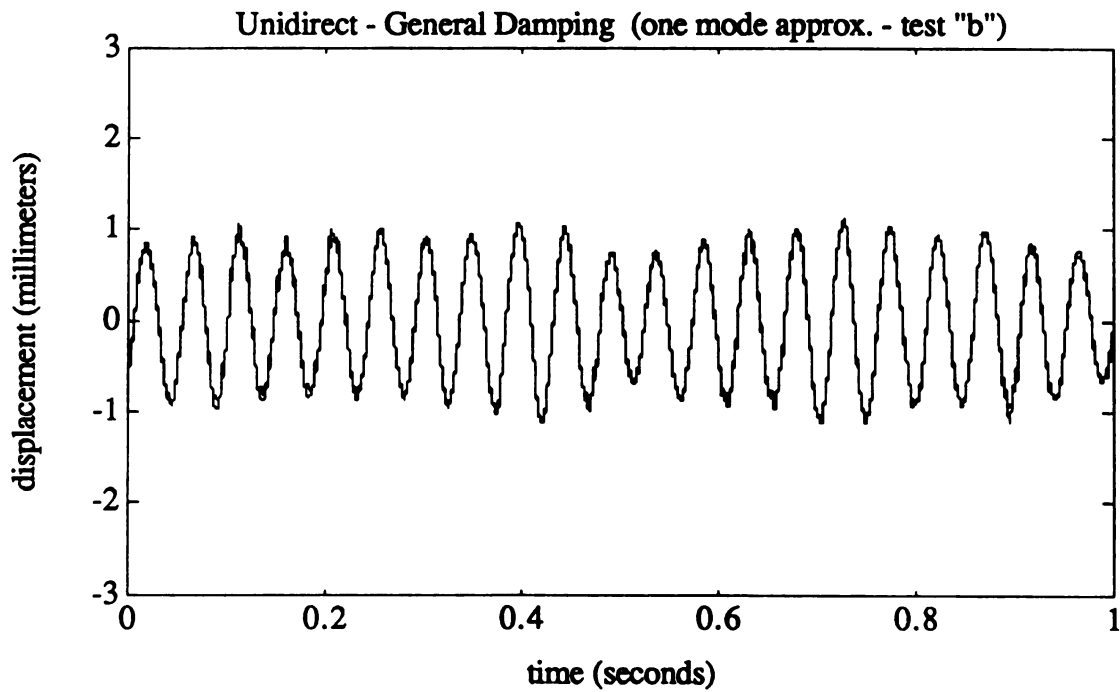
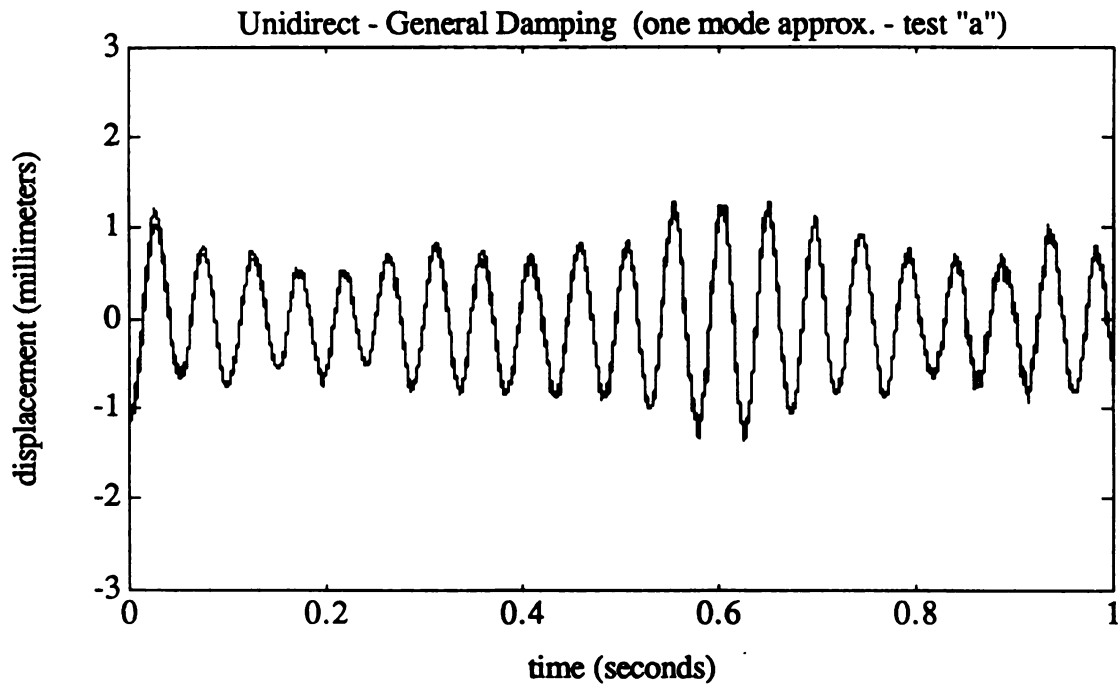


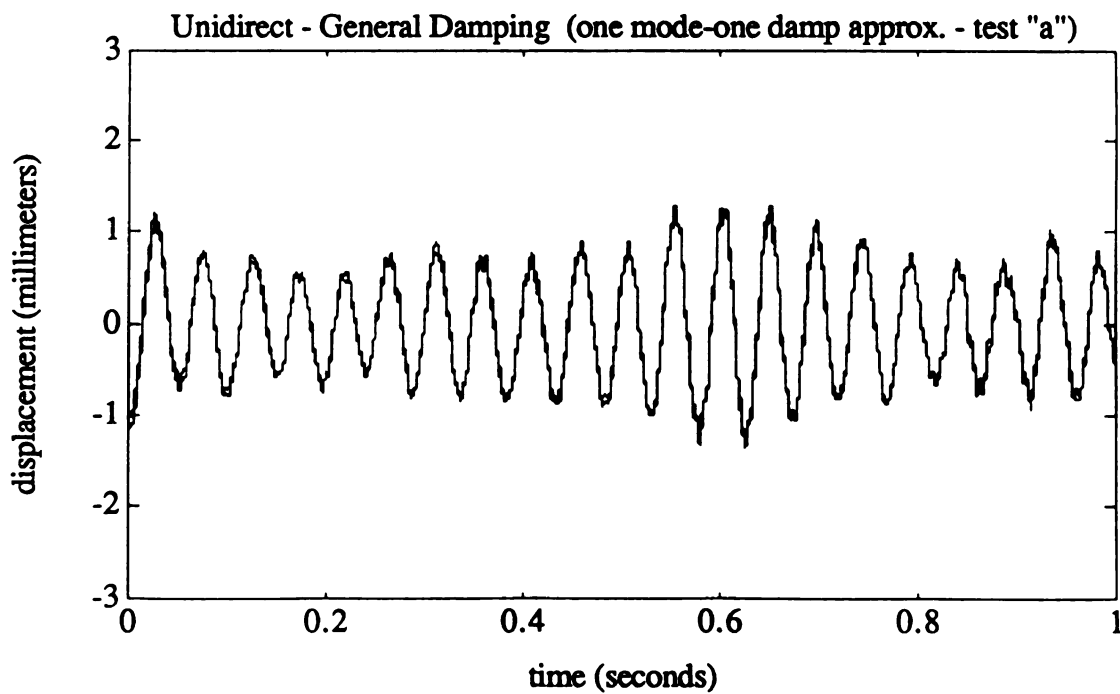
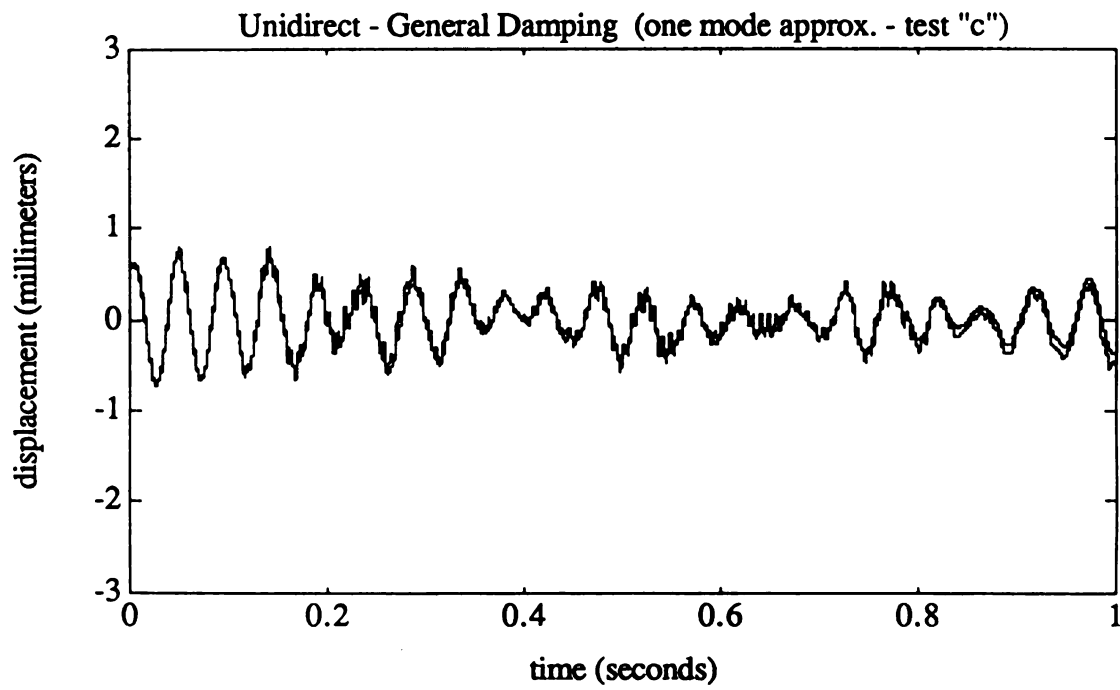


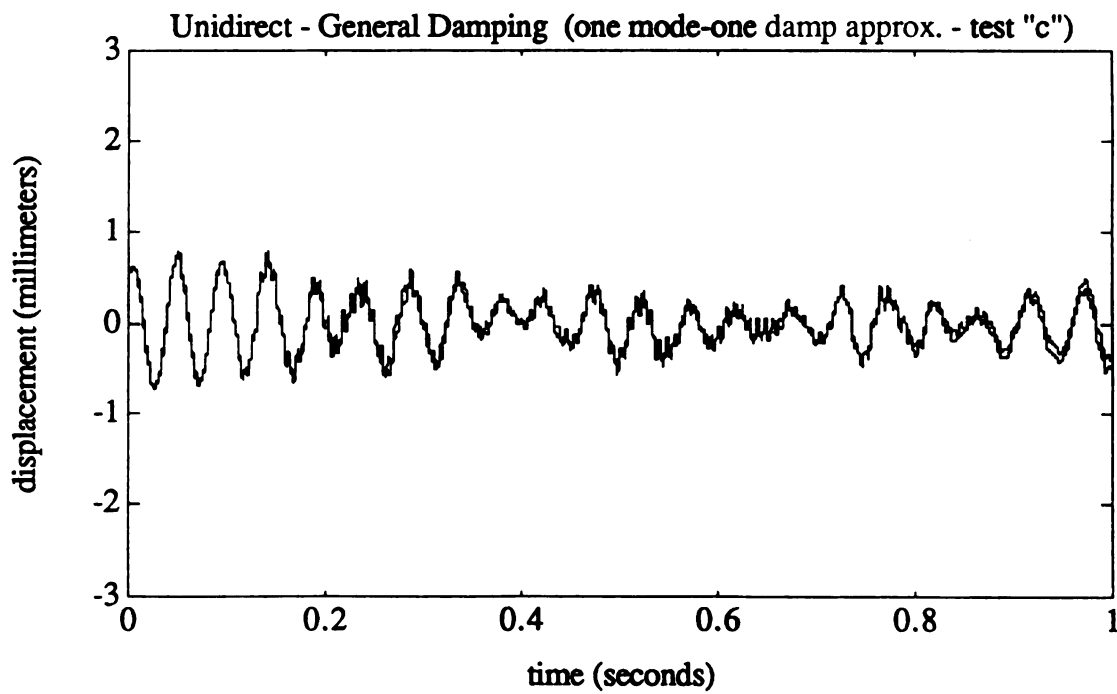
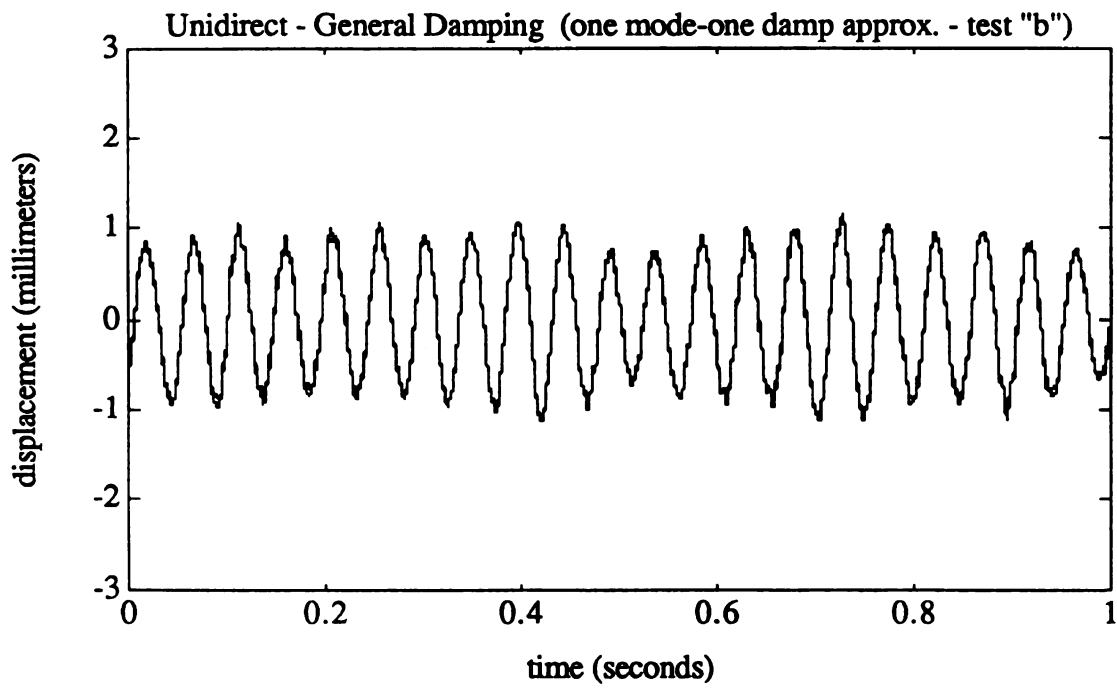


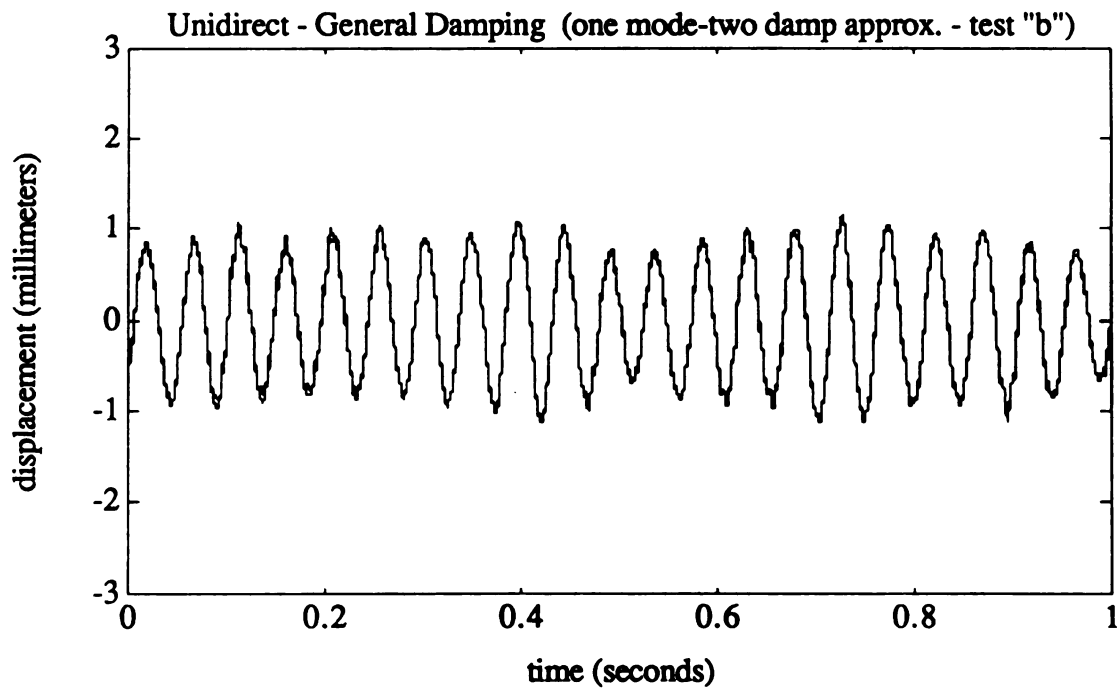
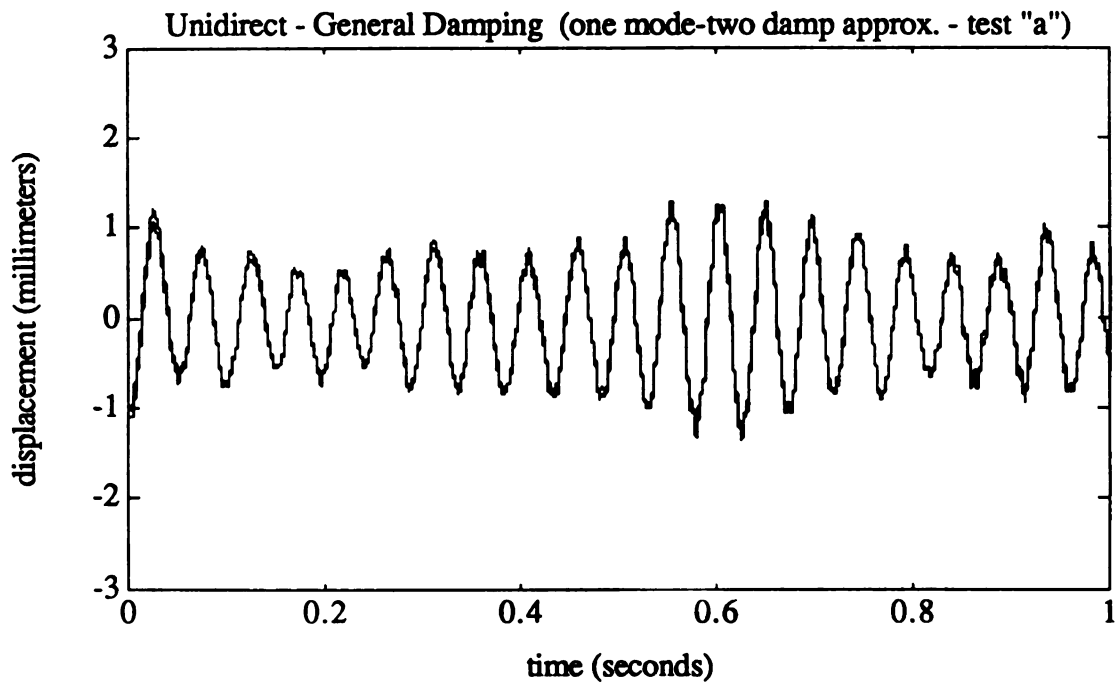


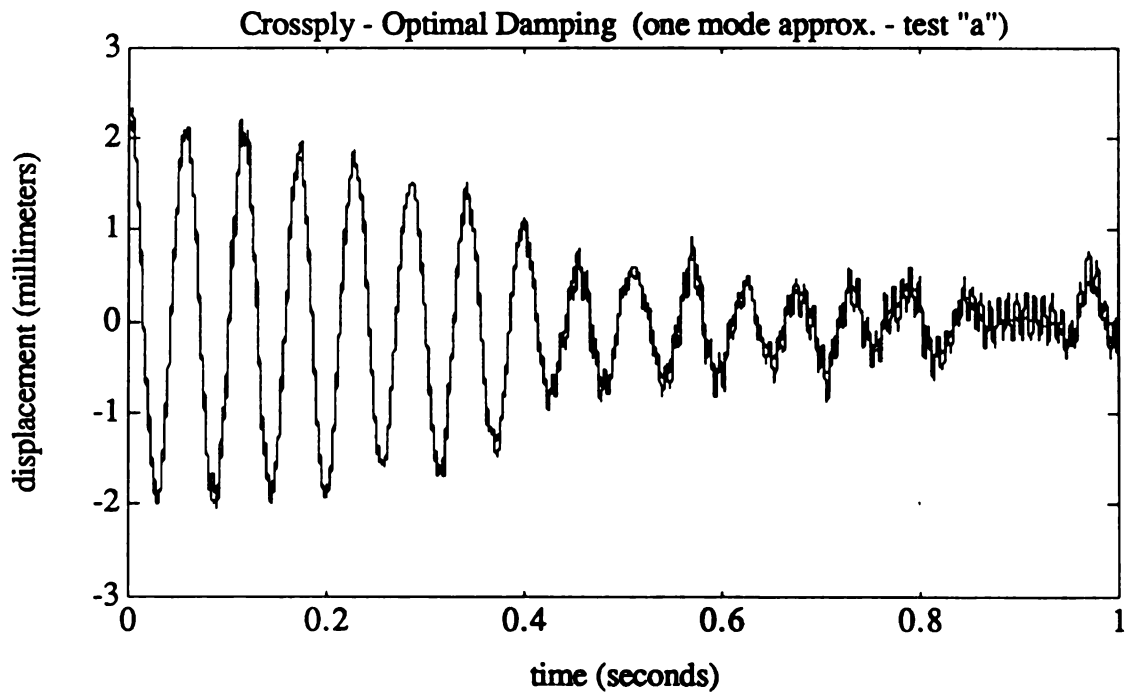
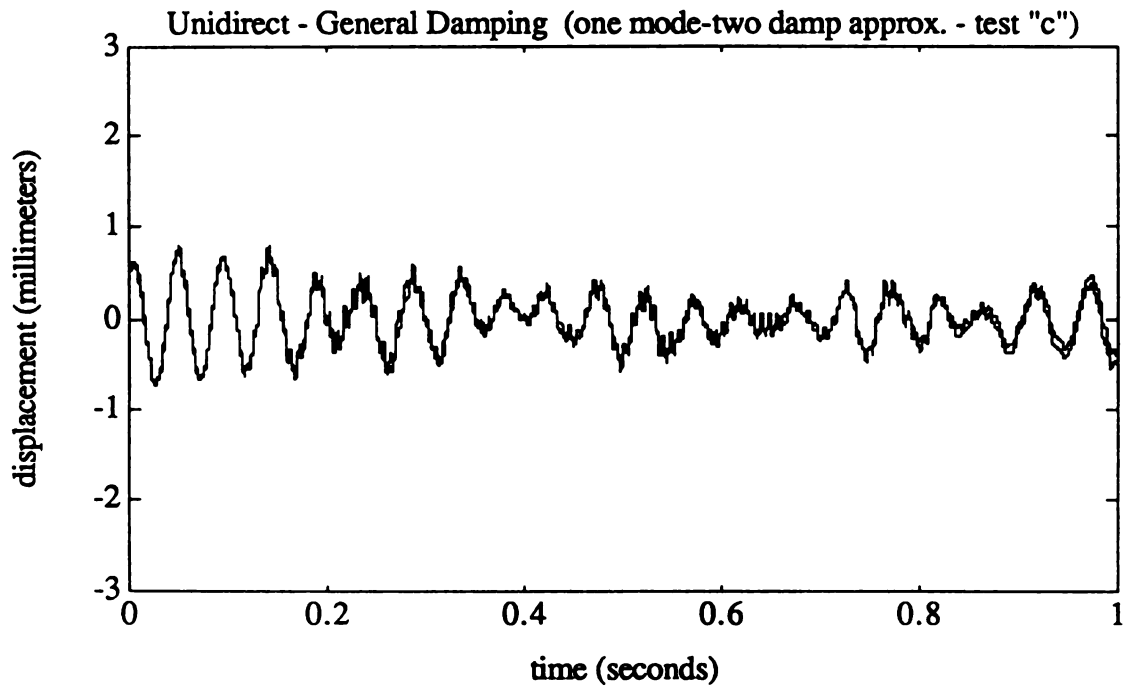


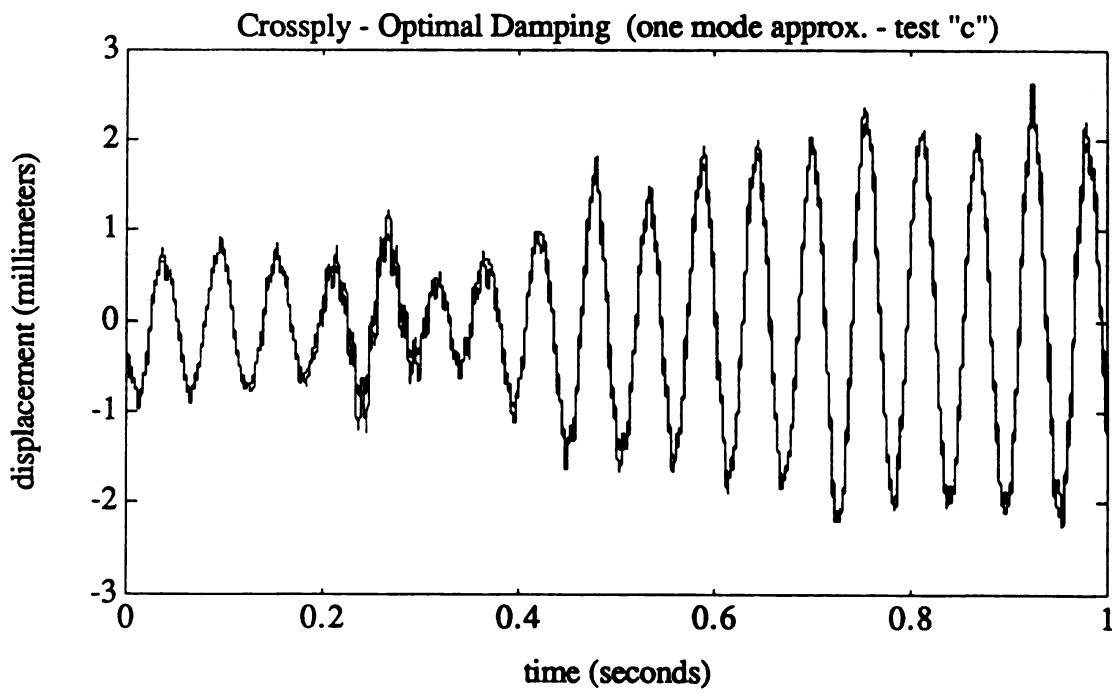
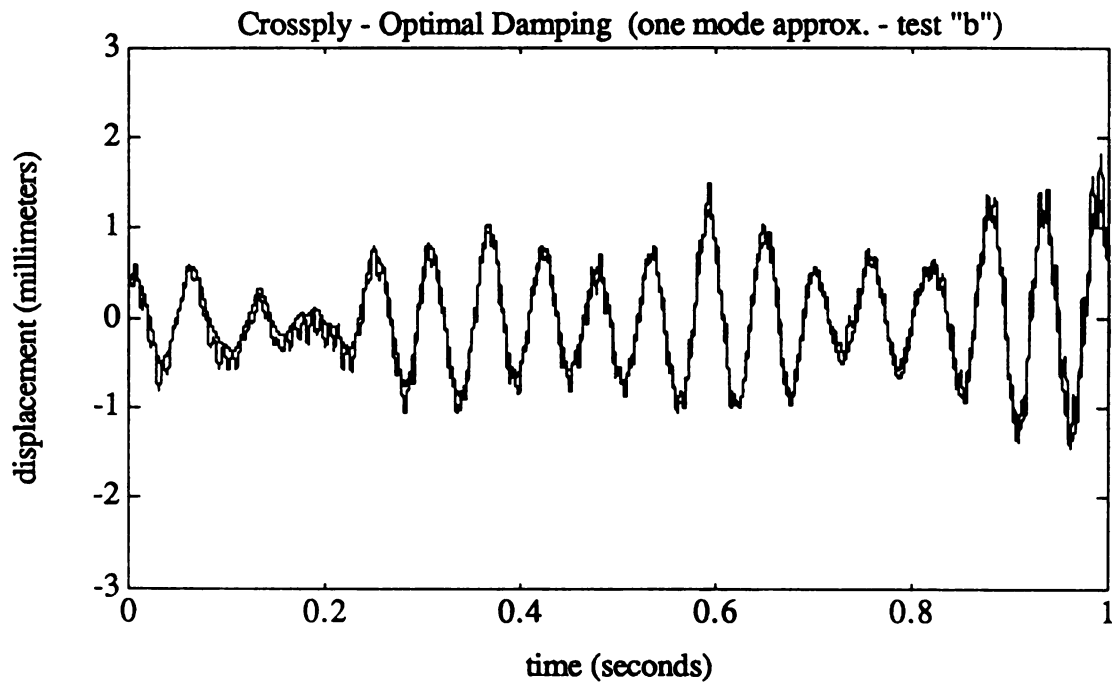


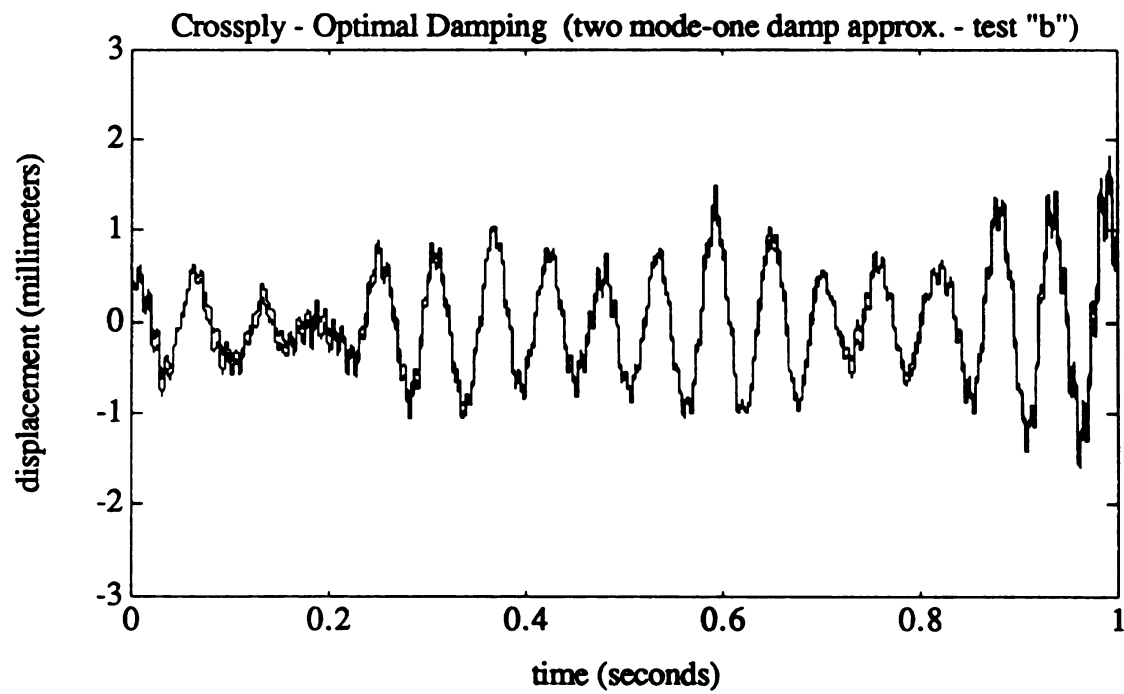
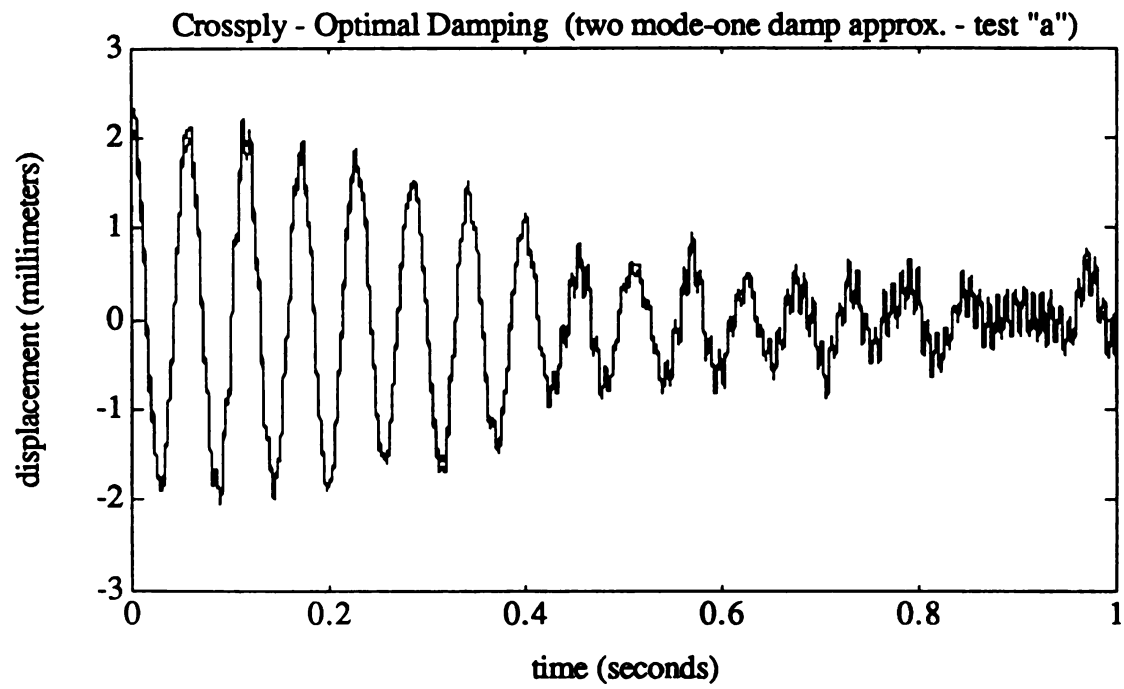


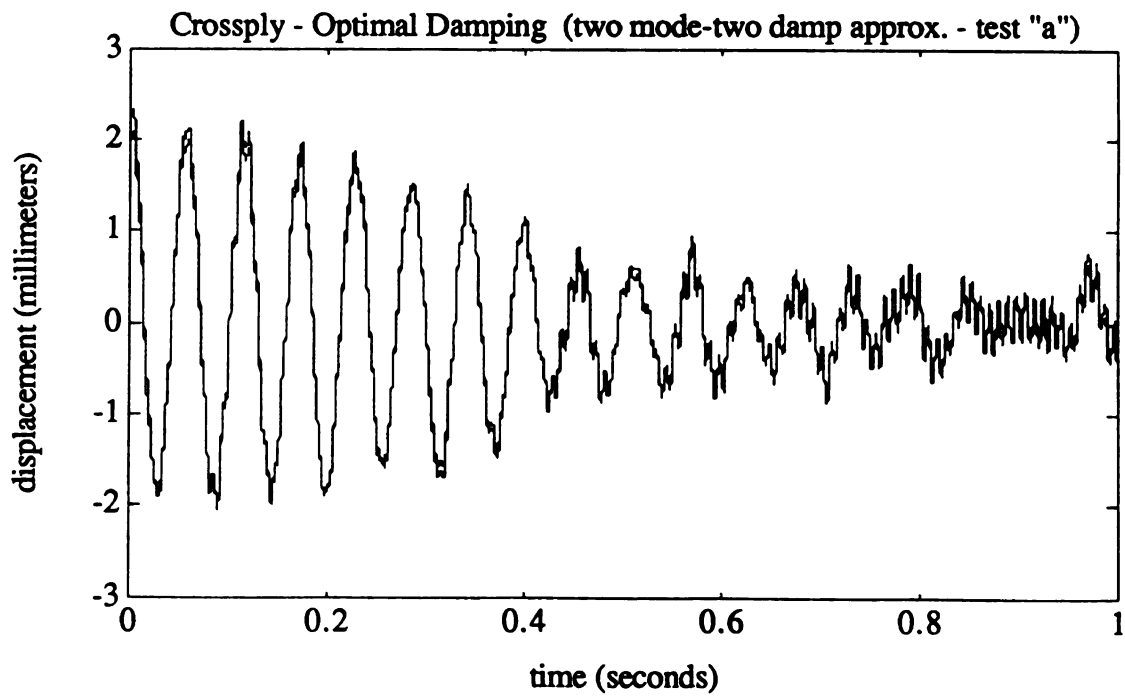
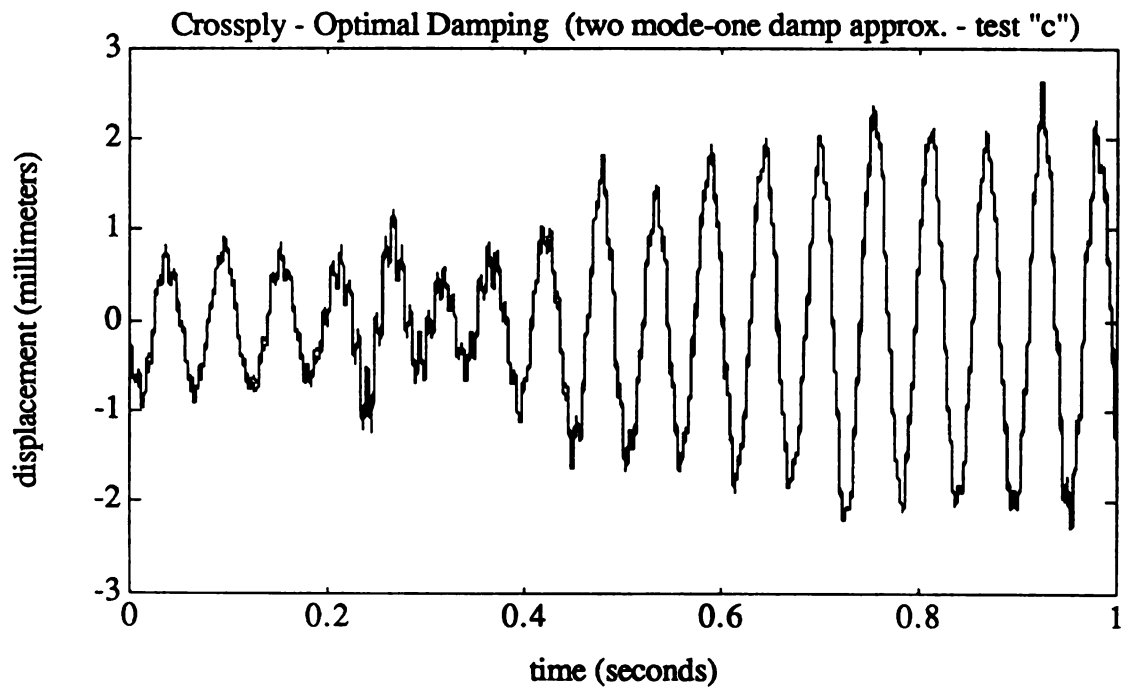


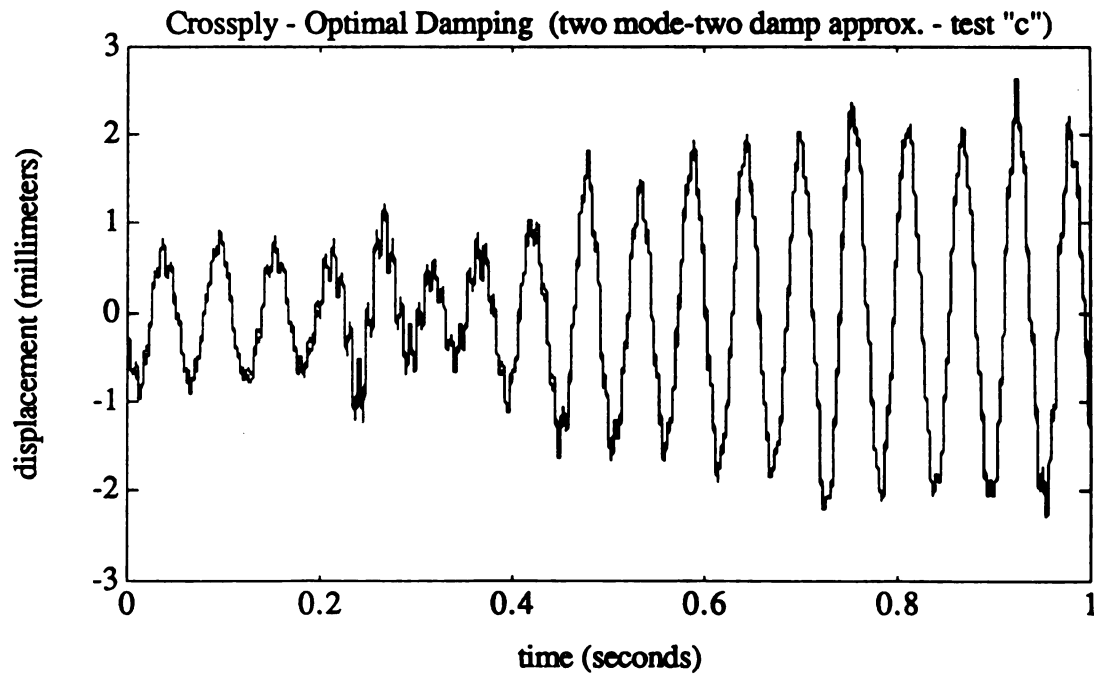
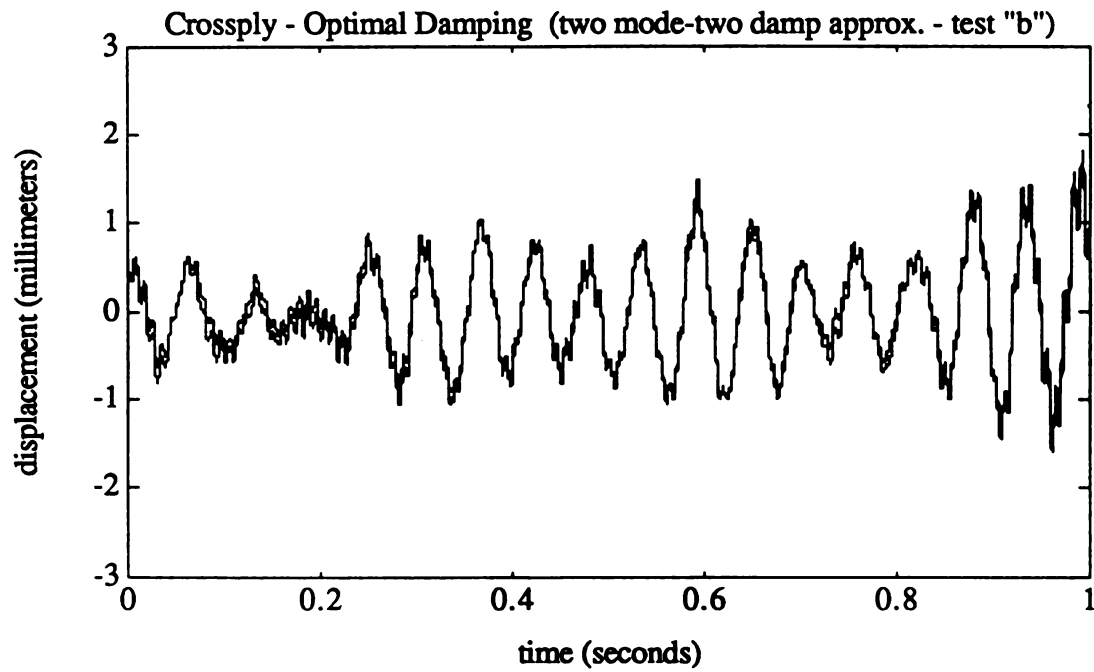


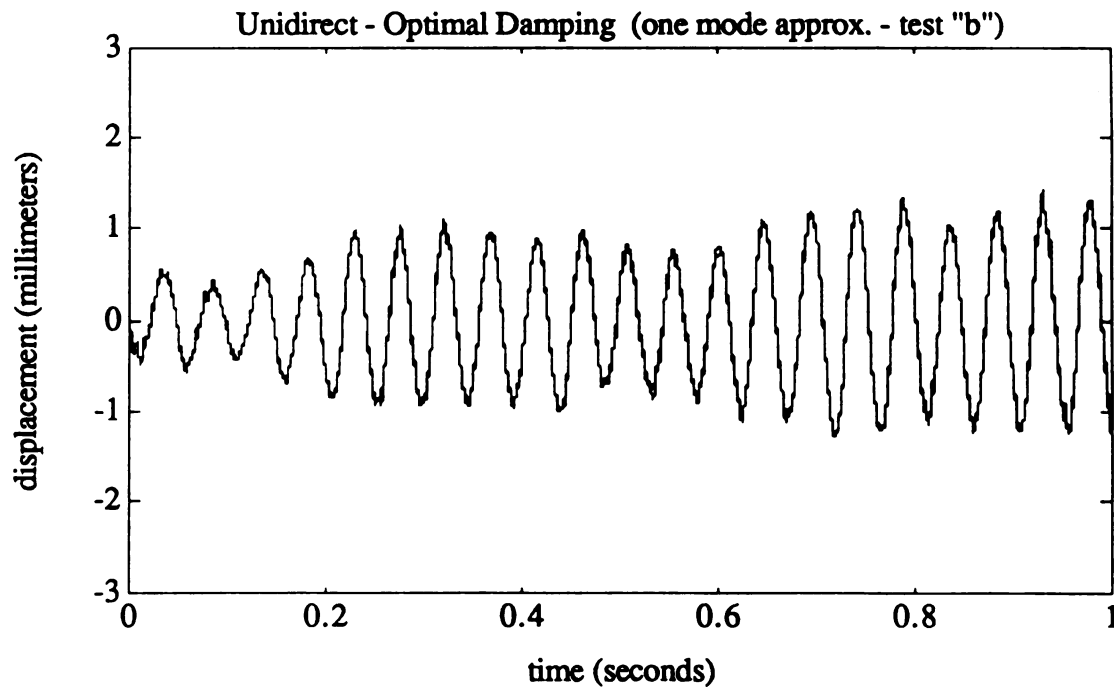
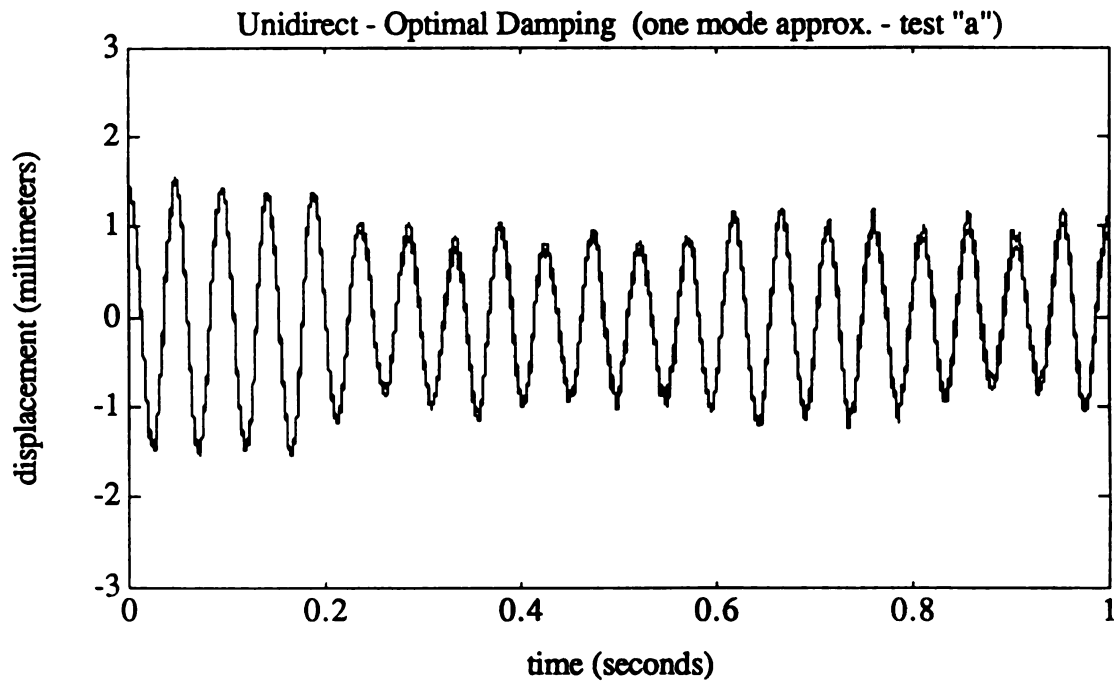


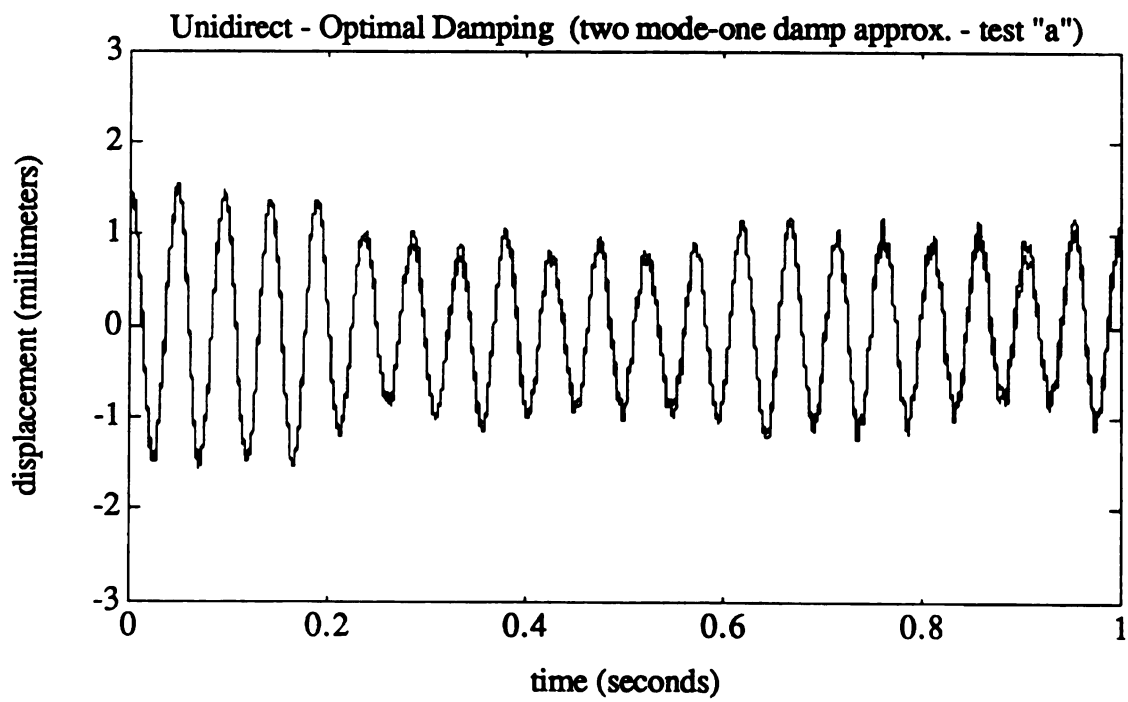
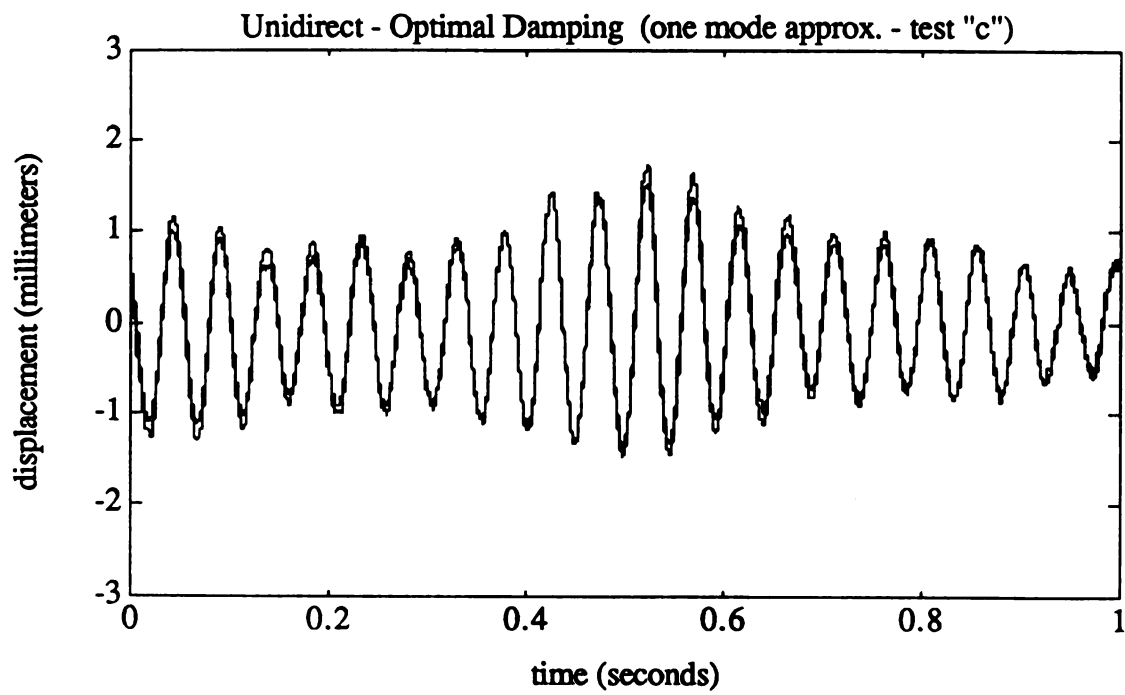


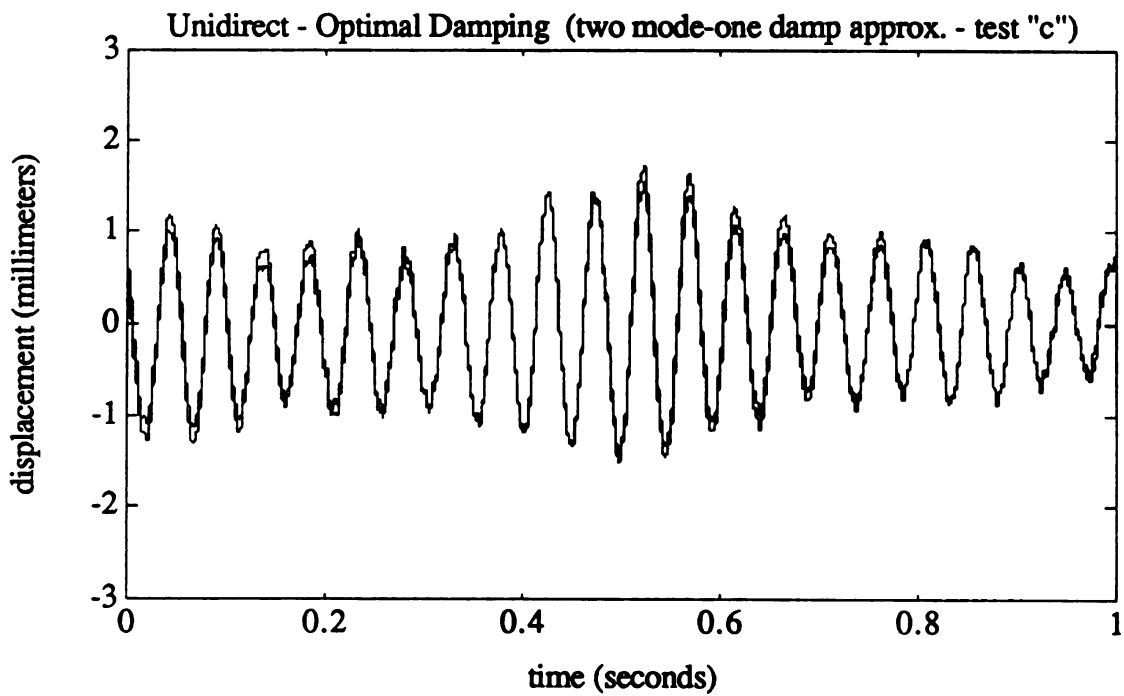
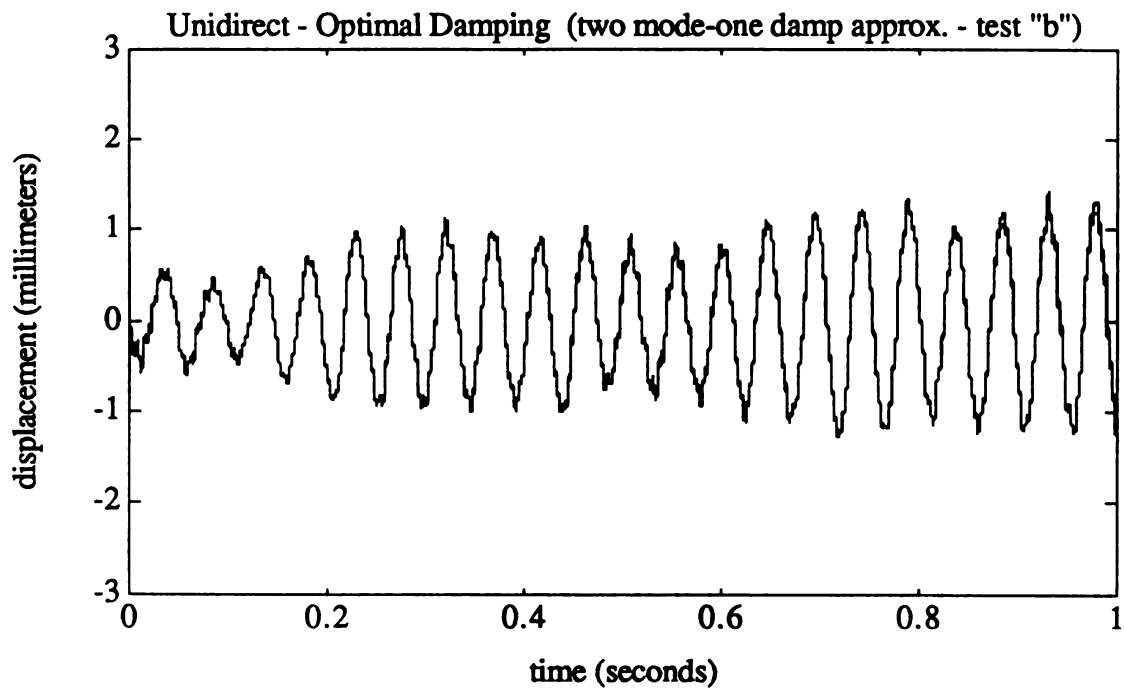


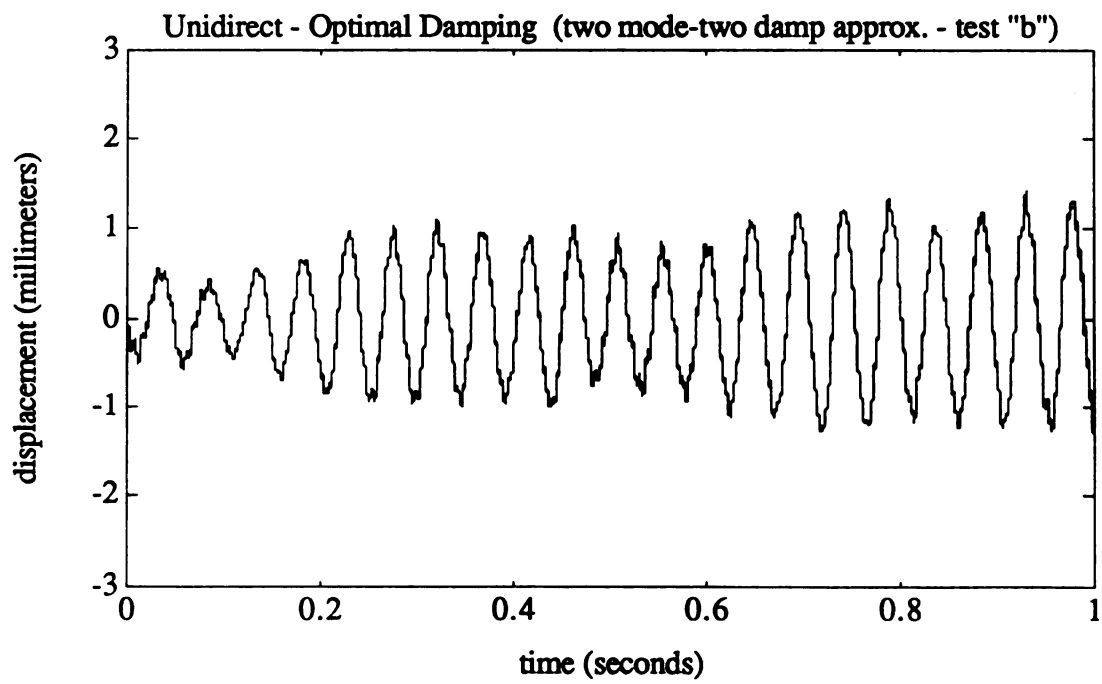
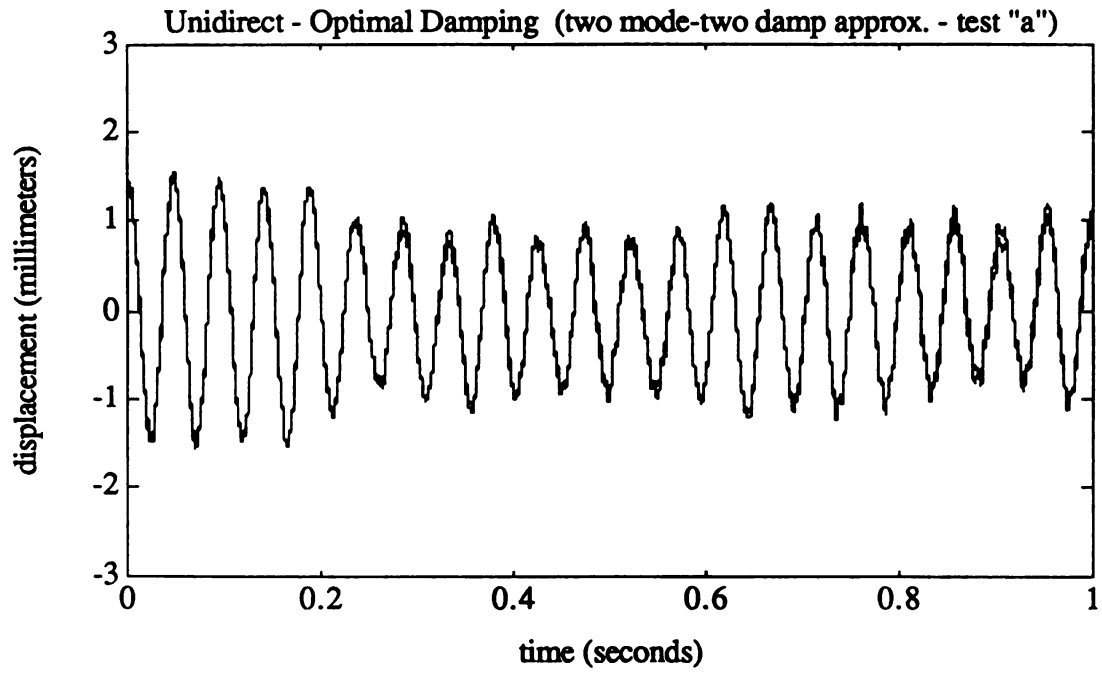


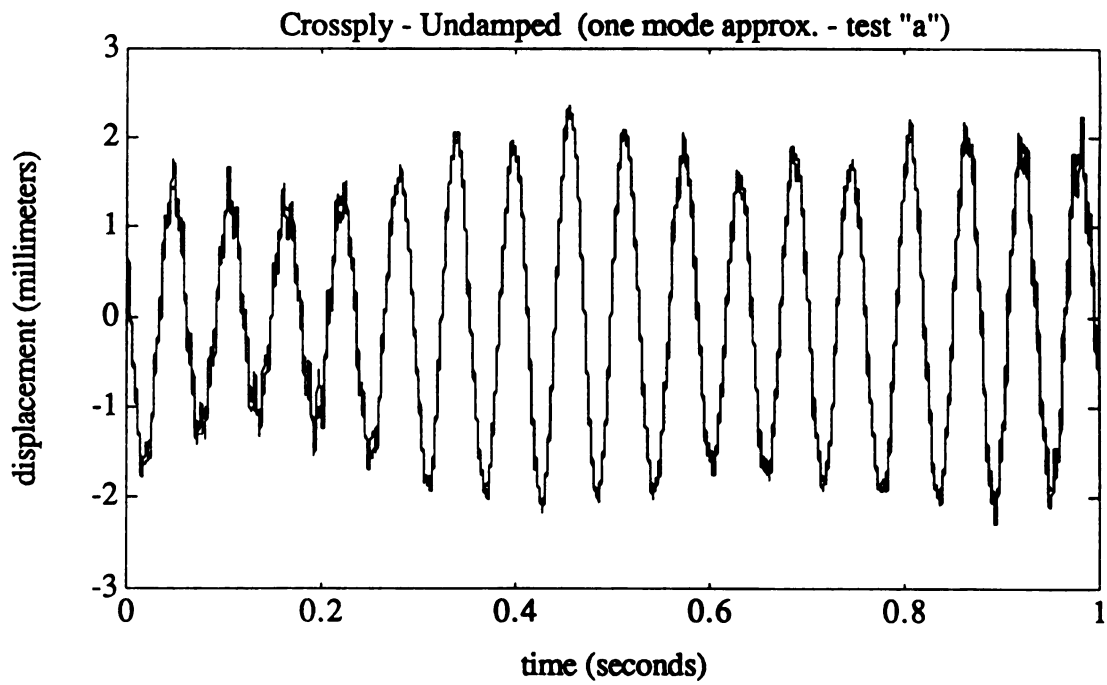
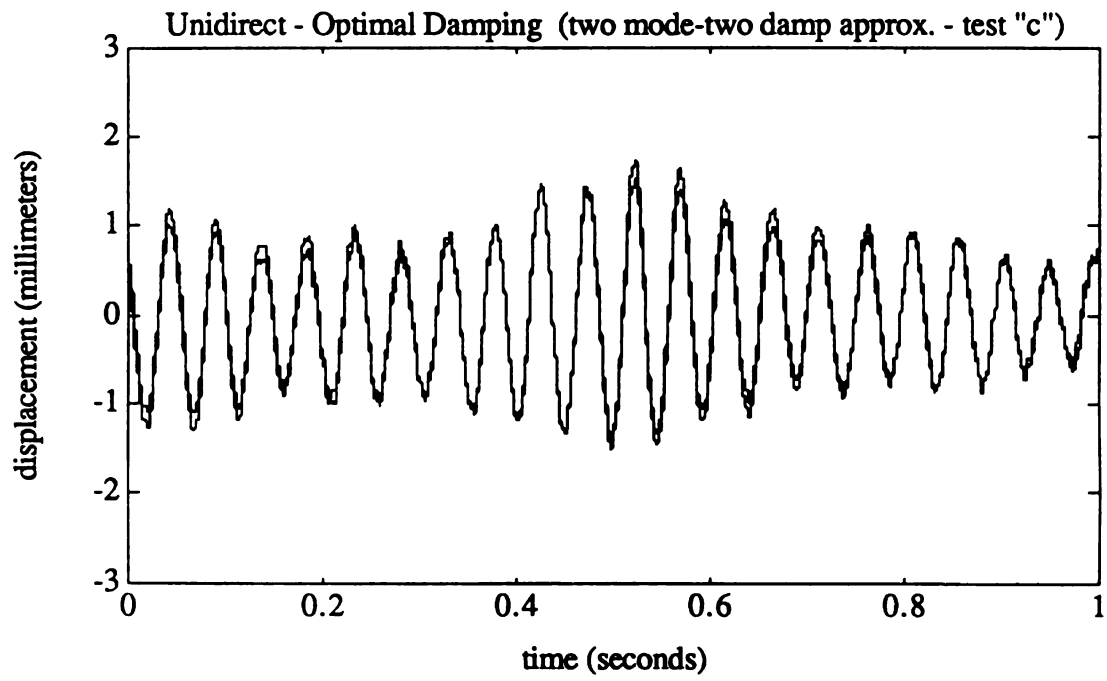


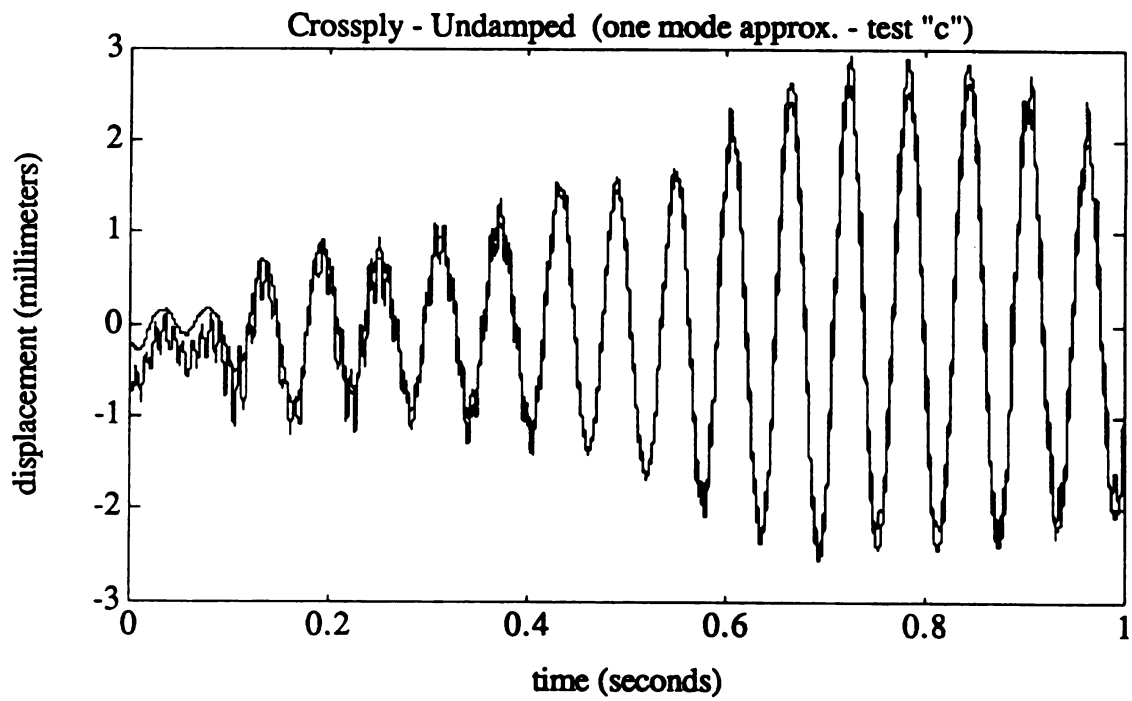
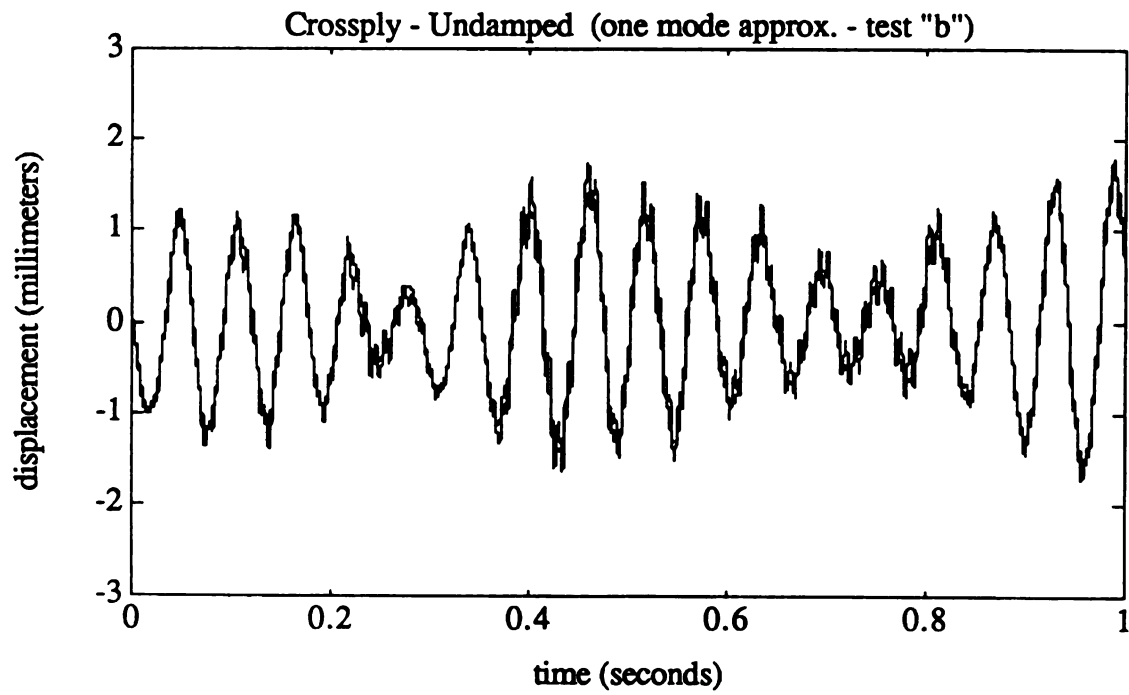


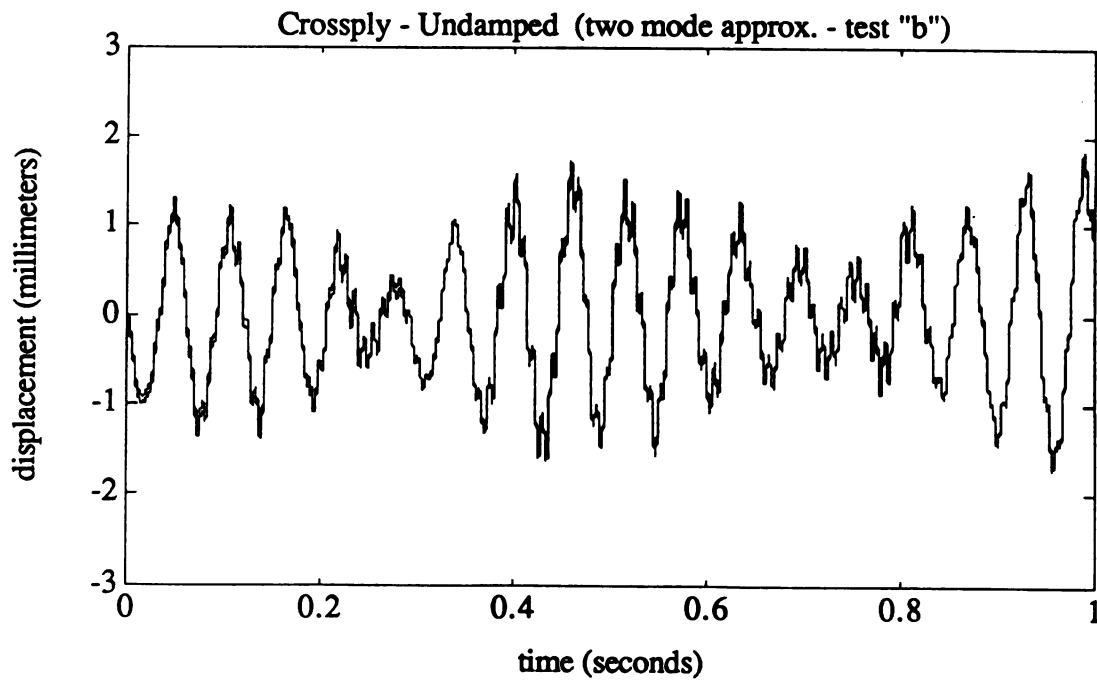
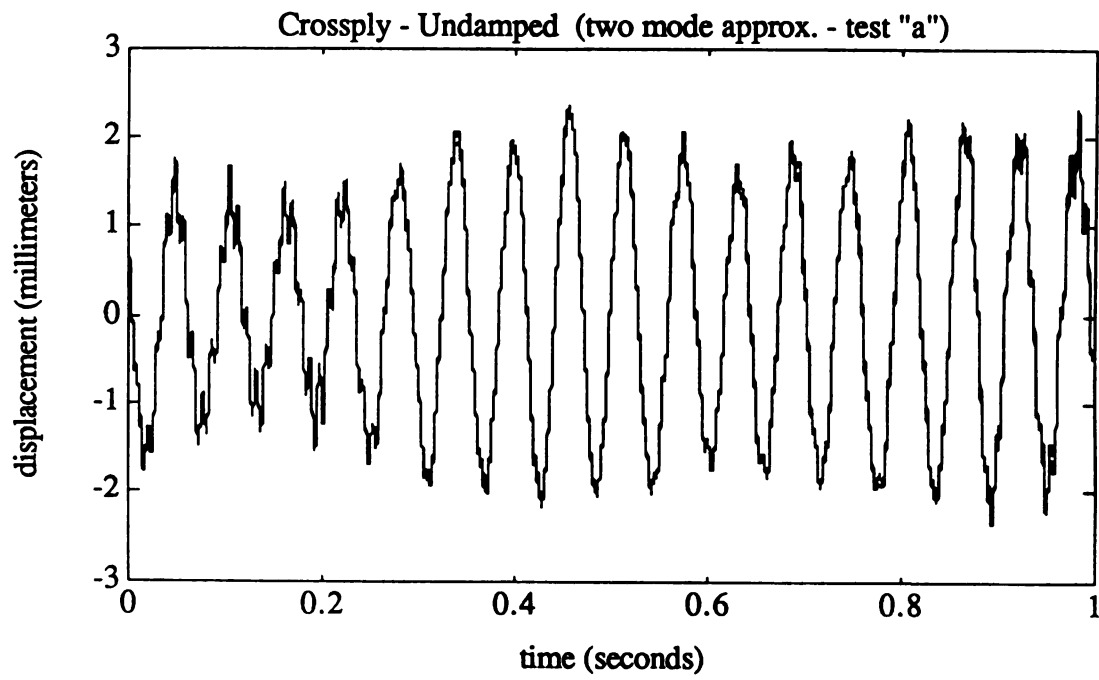


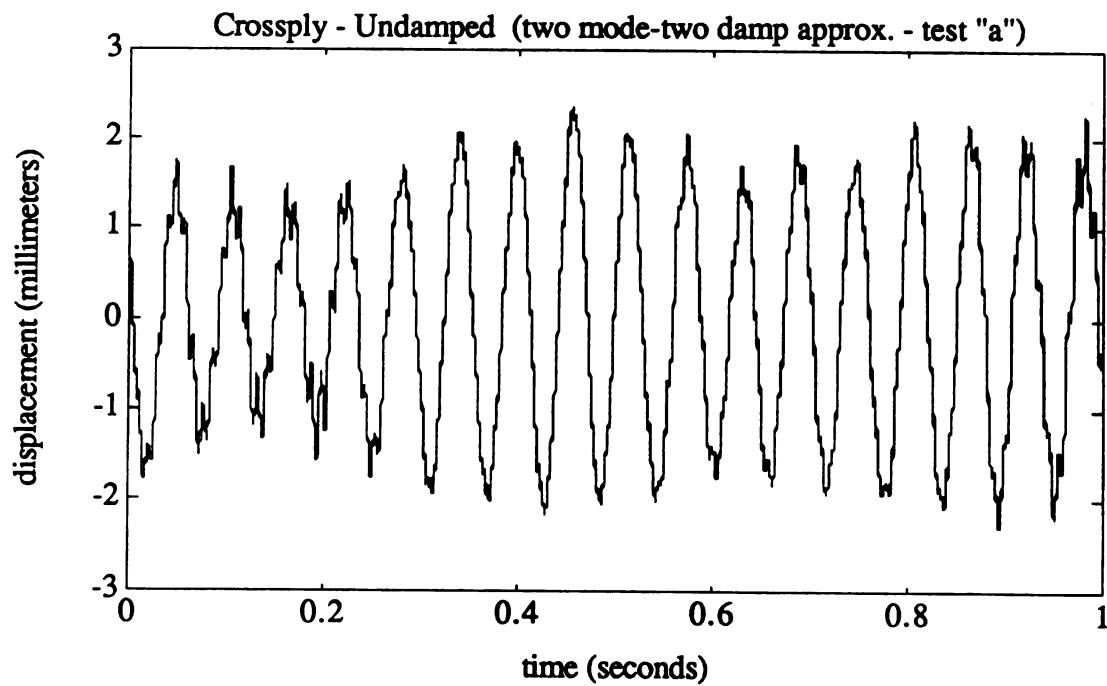
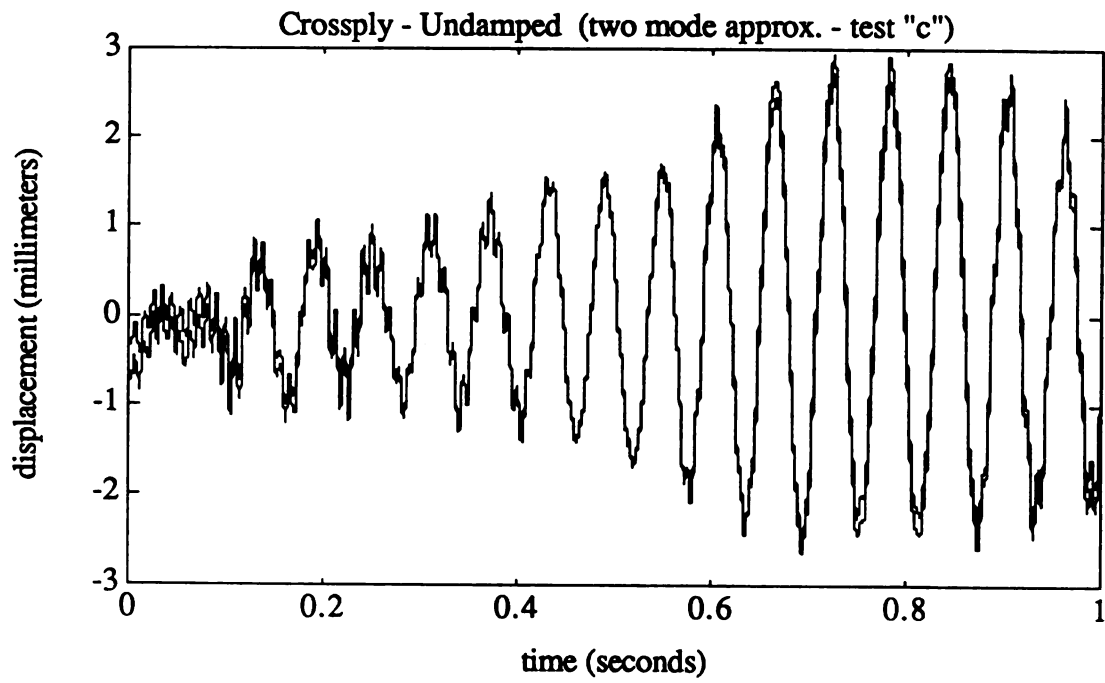


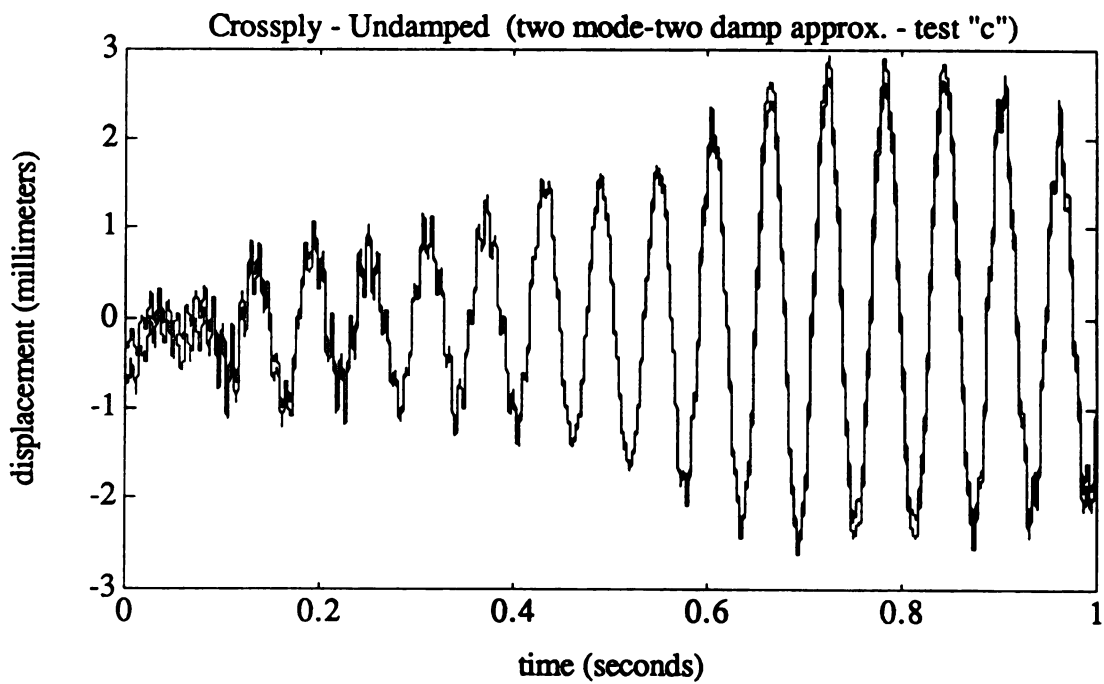
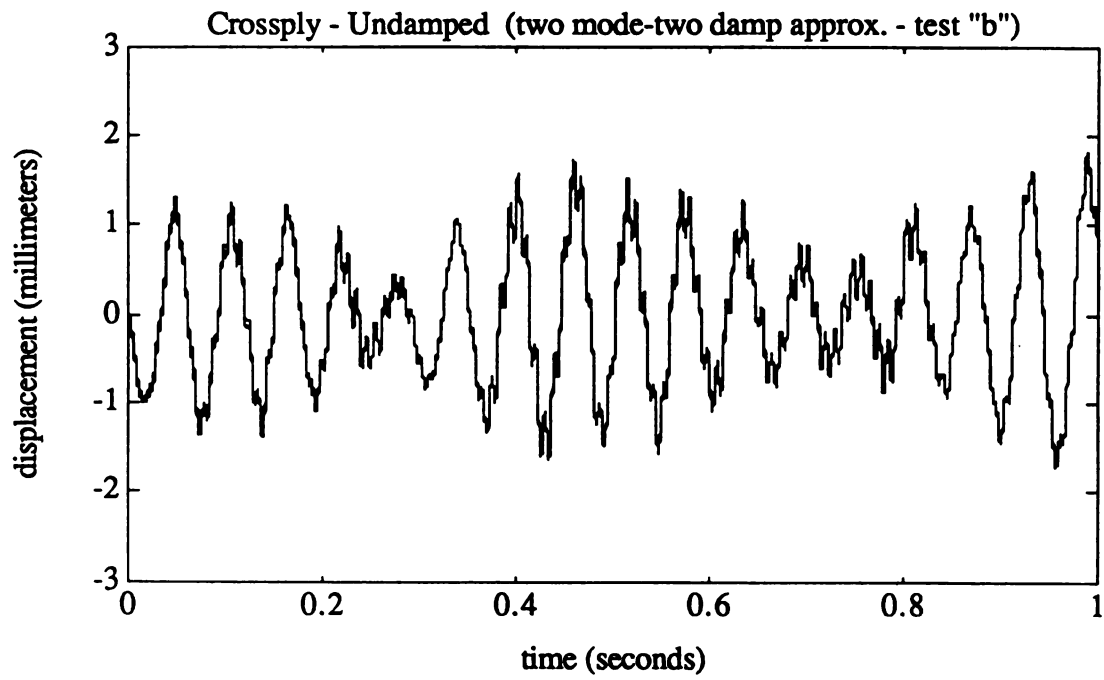


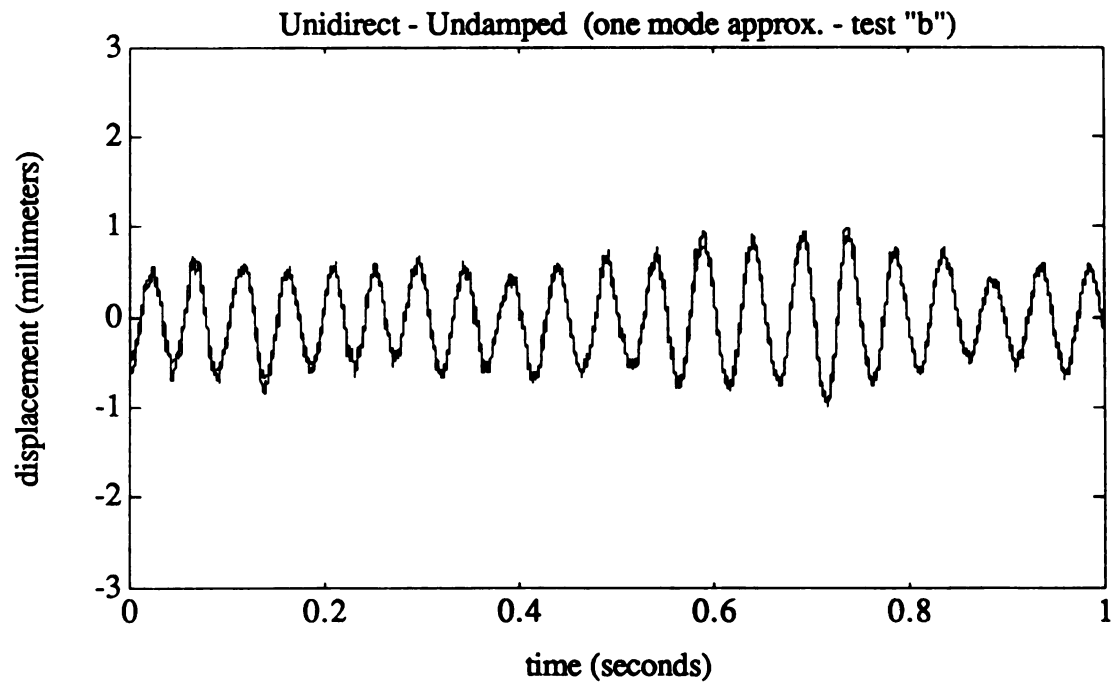
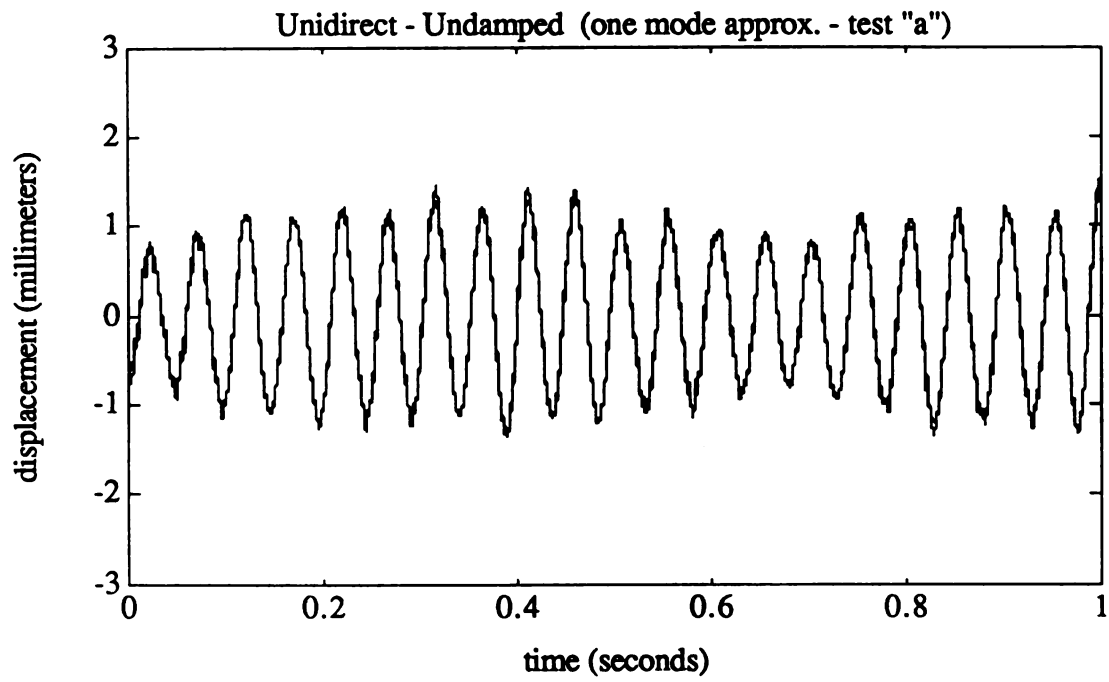


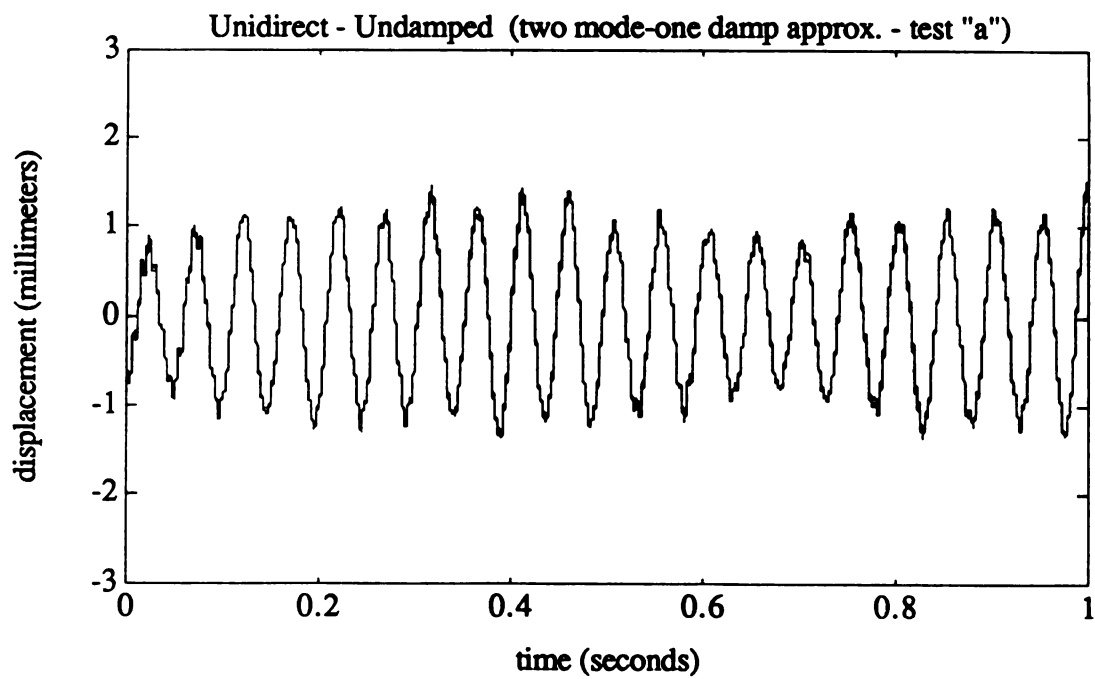
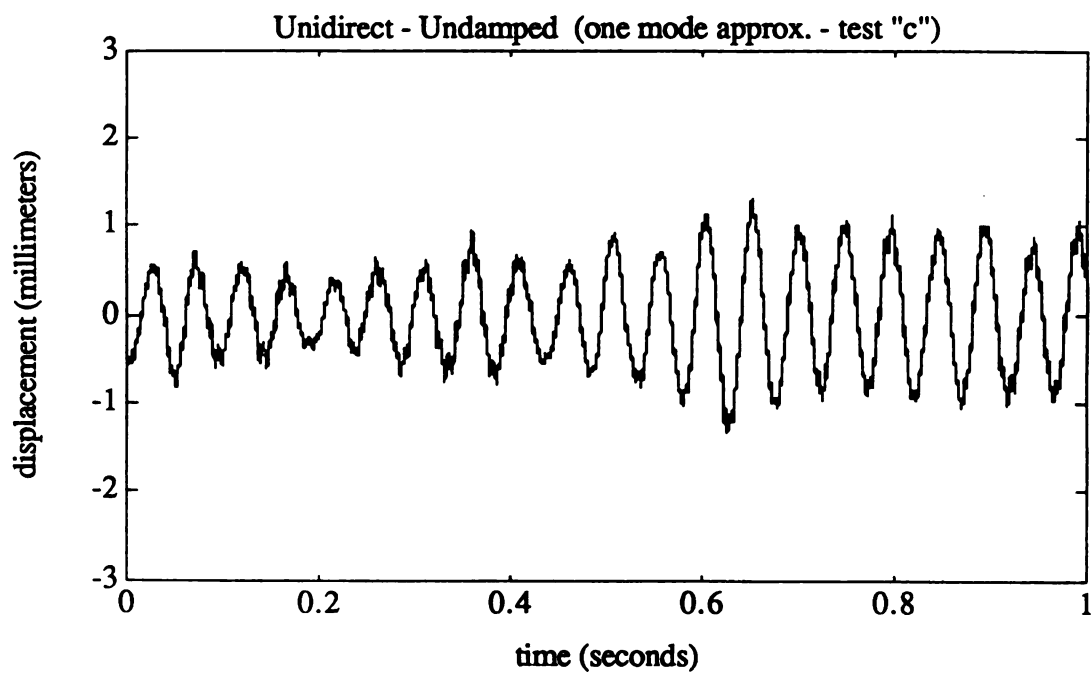


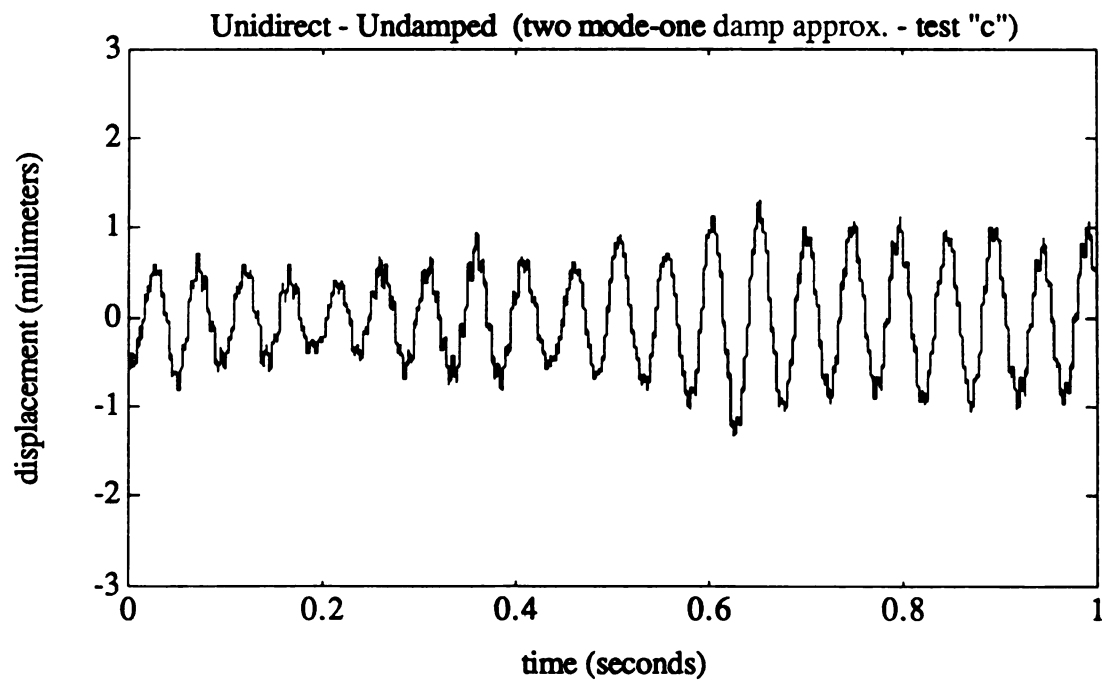
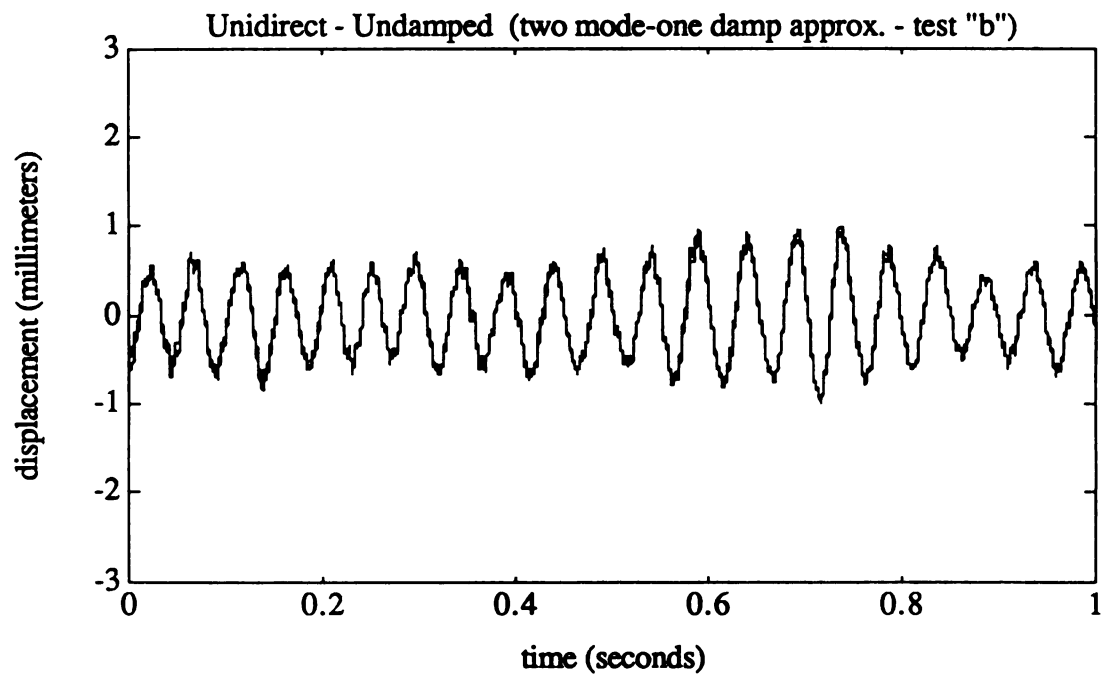


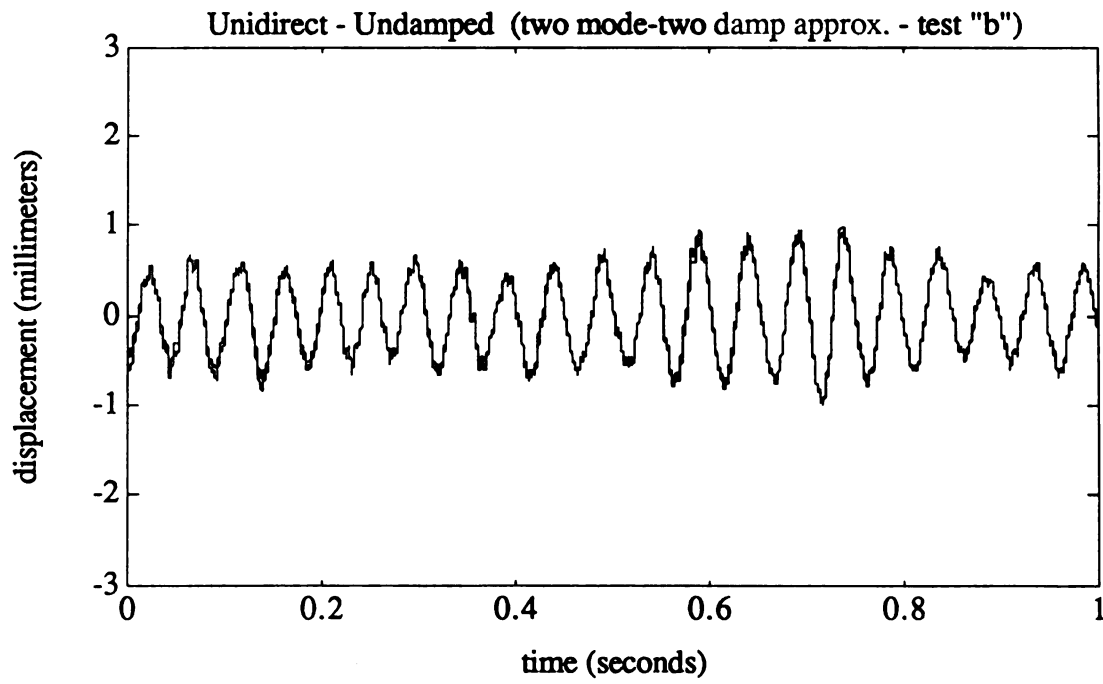
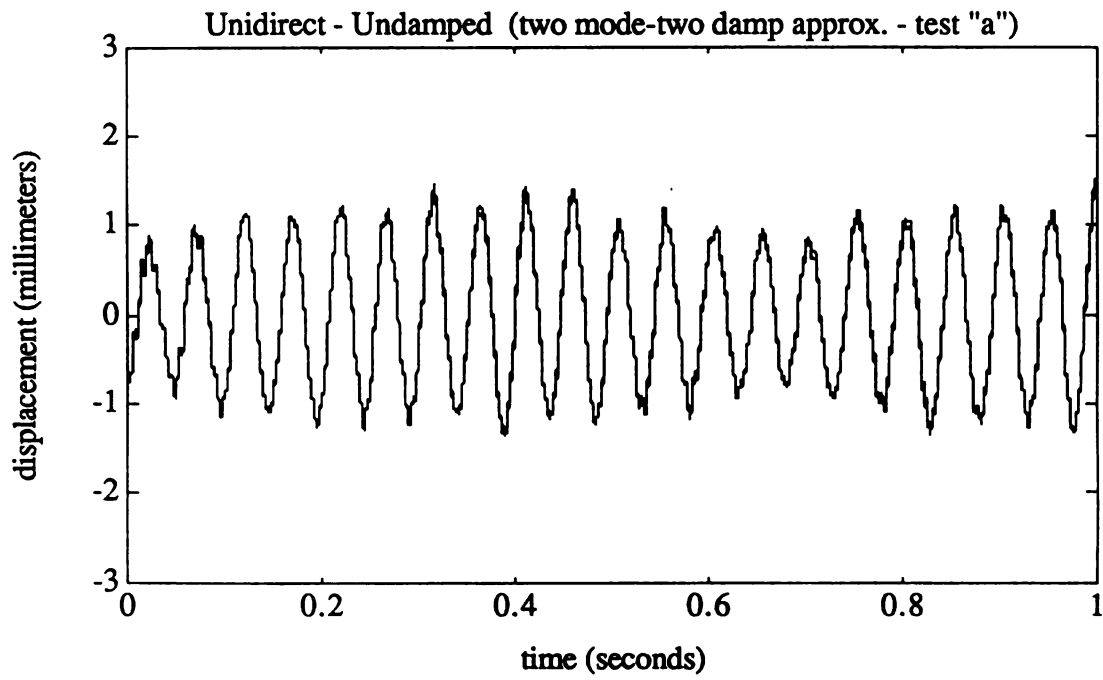


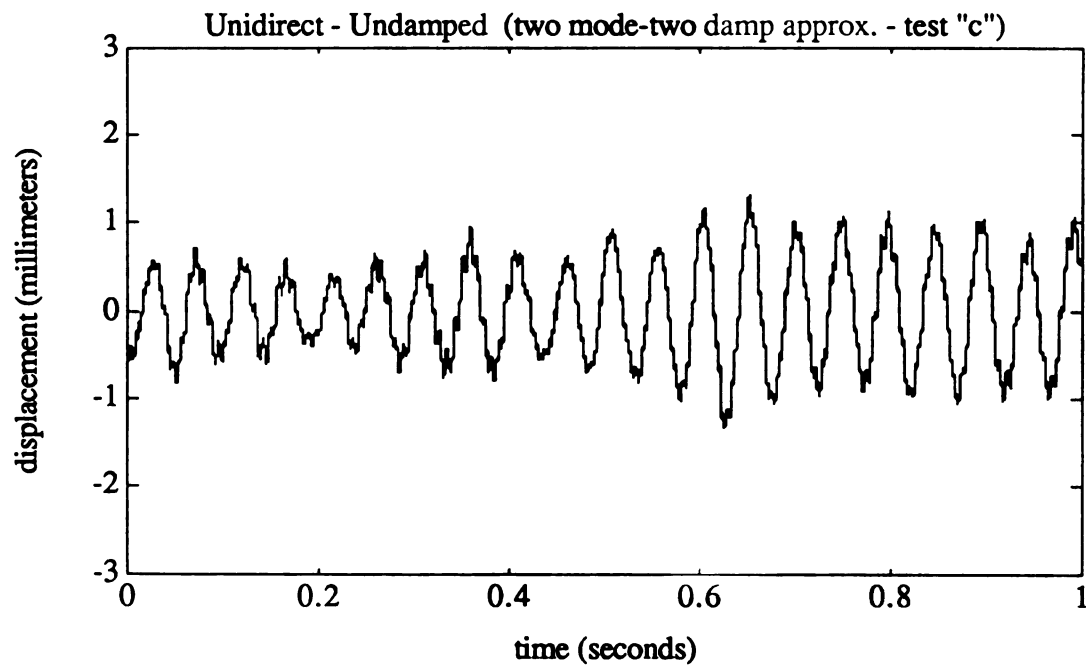












Appendix F

Time versus displacement traces for the crossply-generally damped and the aluminum 6061 specimens excited about their fourth mode resonant frequencies.

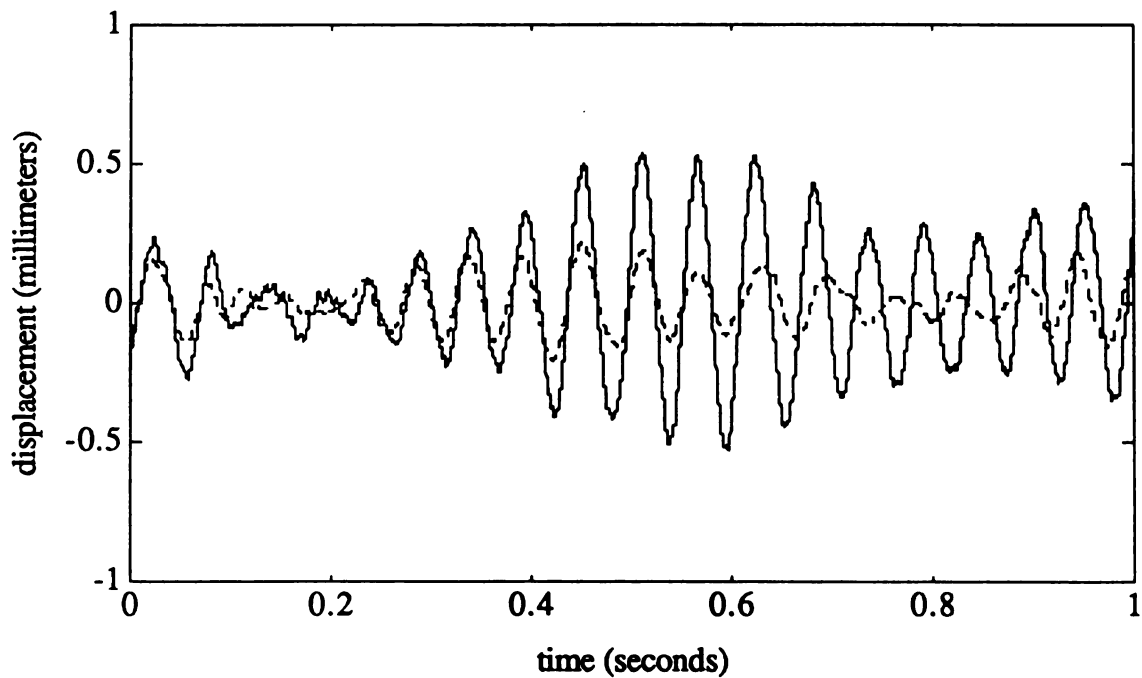


Figure F-1: Crossply-generally damped one mode approximation, test A.

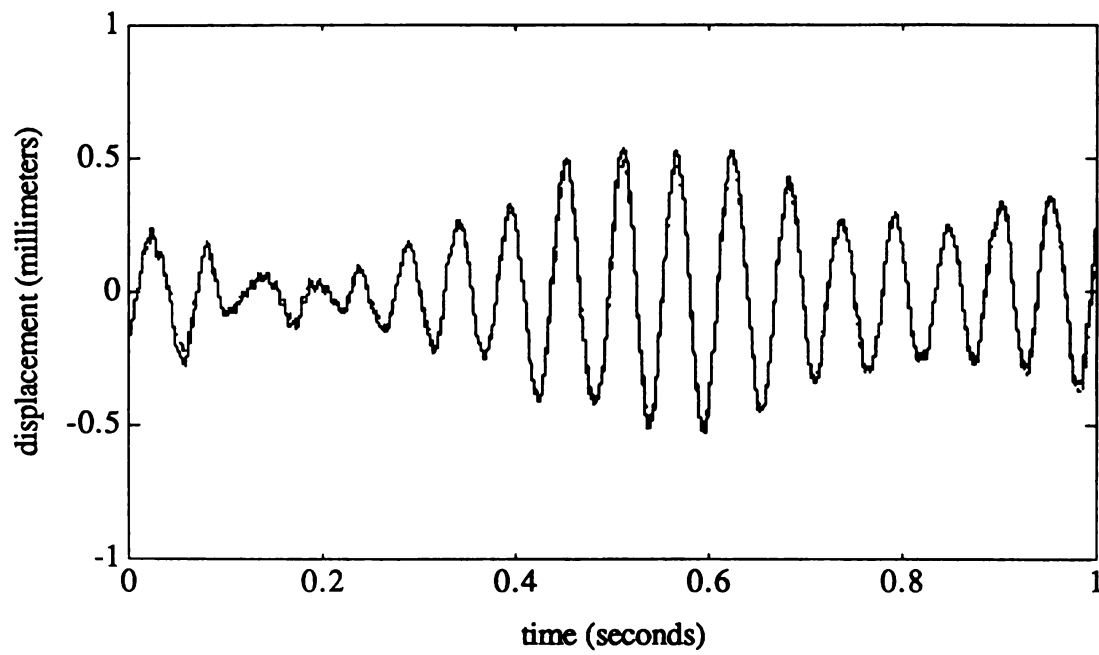


Figure F-2: Crossply-generally damped two mode approximation, test A.

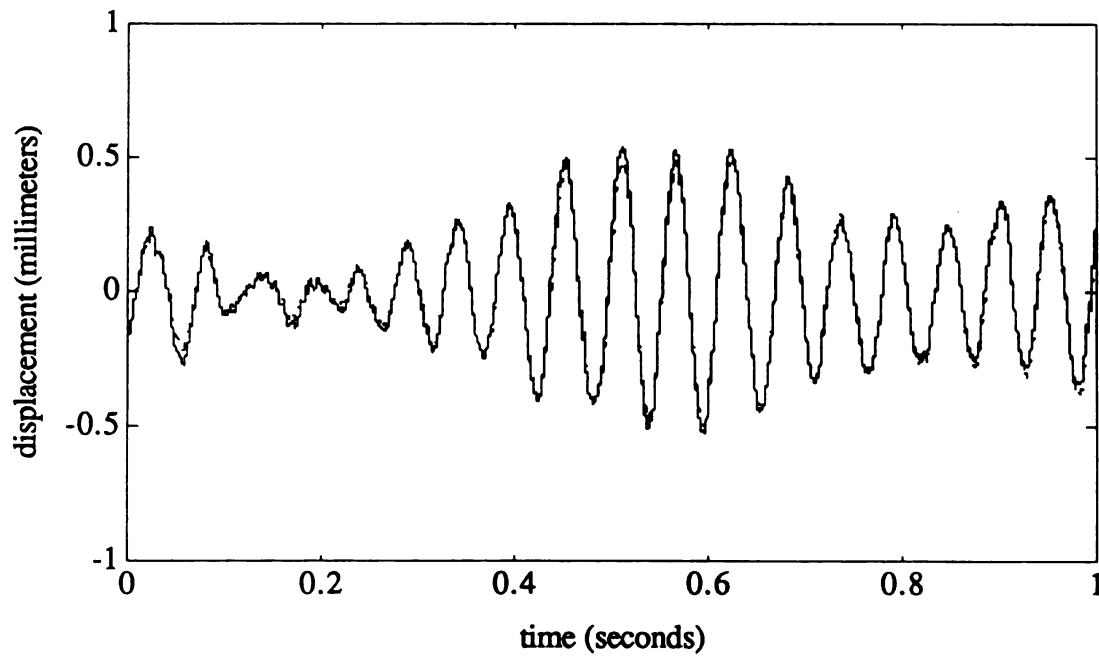


Figure F-3: Crossply-generally damped three mode approximation, test A.

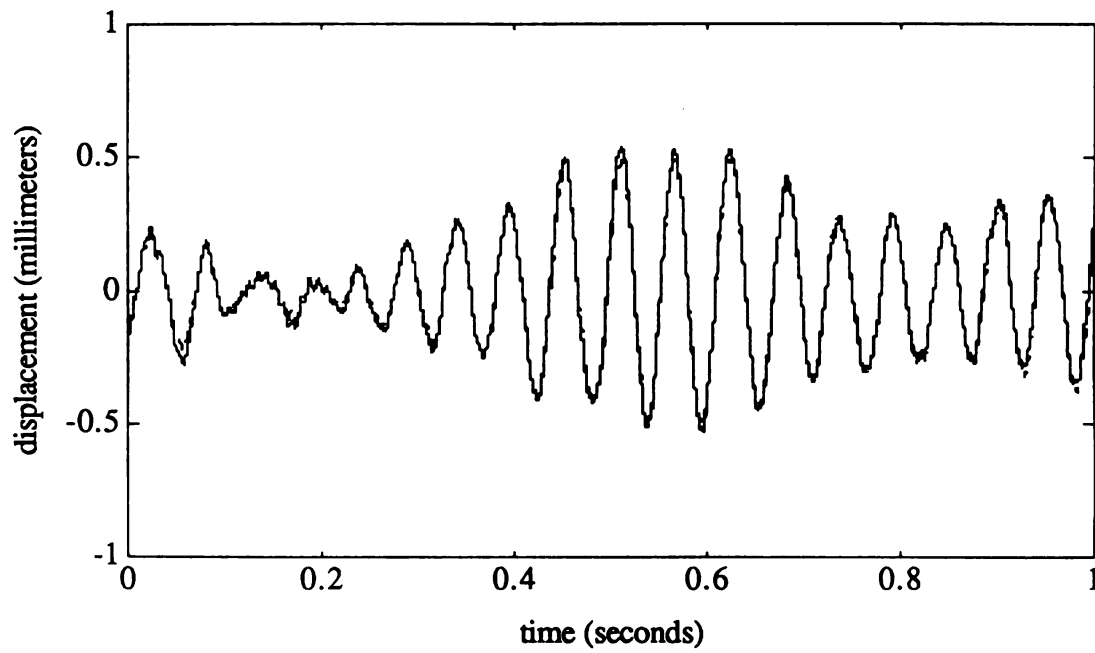


Figure F-4: Crossply-generally damped four mode approximation, test A.

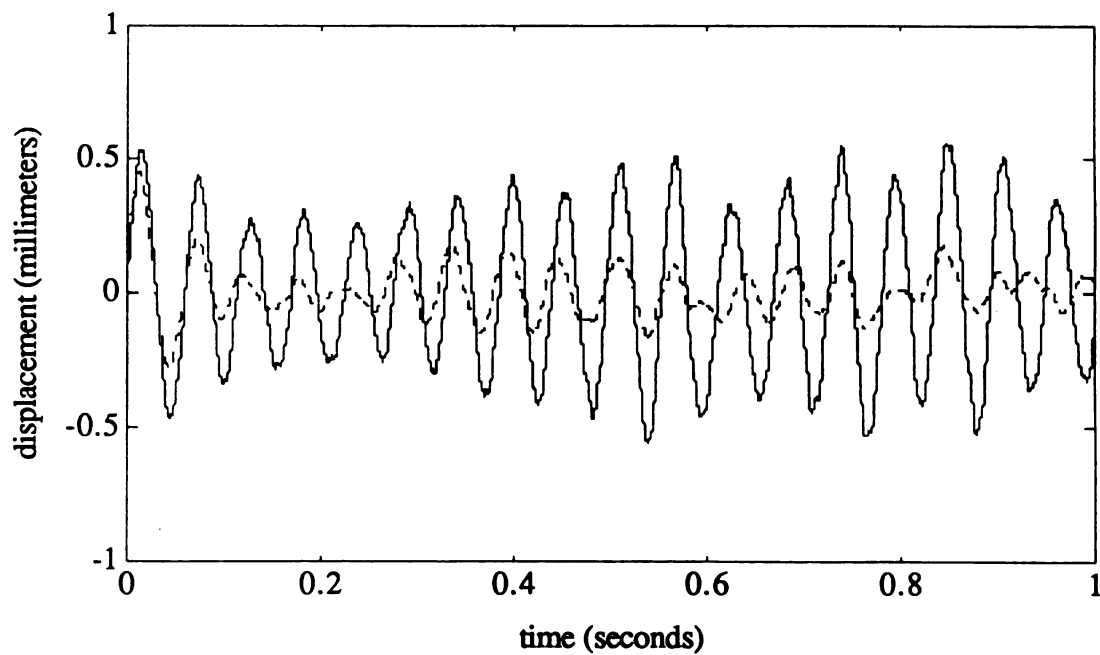


Figure F-5: Crossply-generally damped one mode approximation, test B.

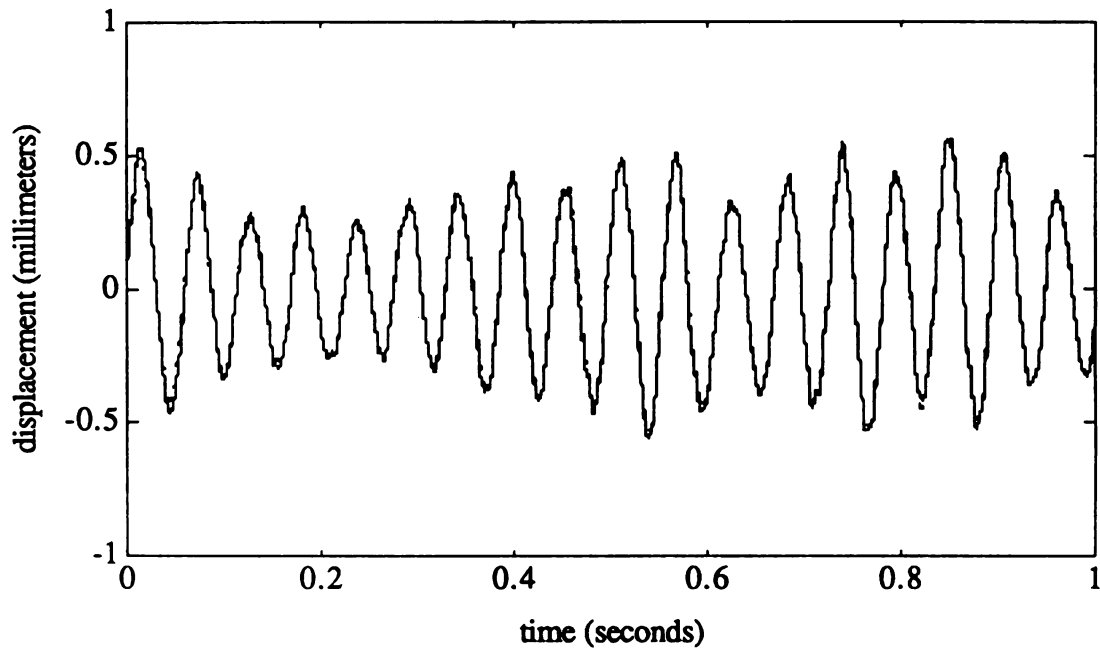


Figure F-6: Crossply-generally damped two mode approximation, test B.

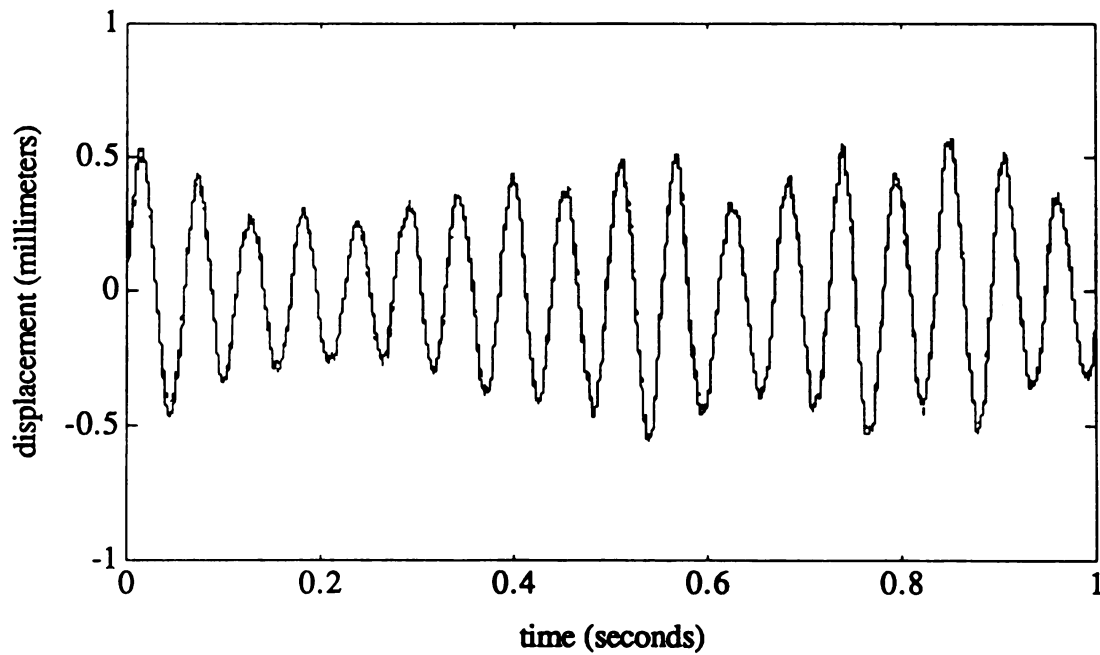


Figure F-7: Crossply-generally damped three mode approximation, test B.

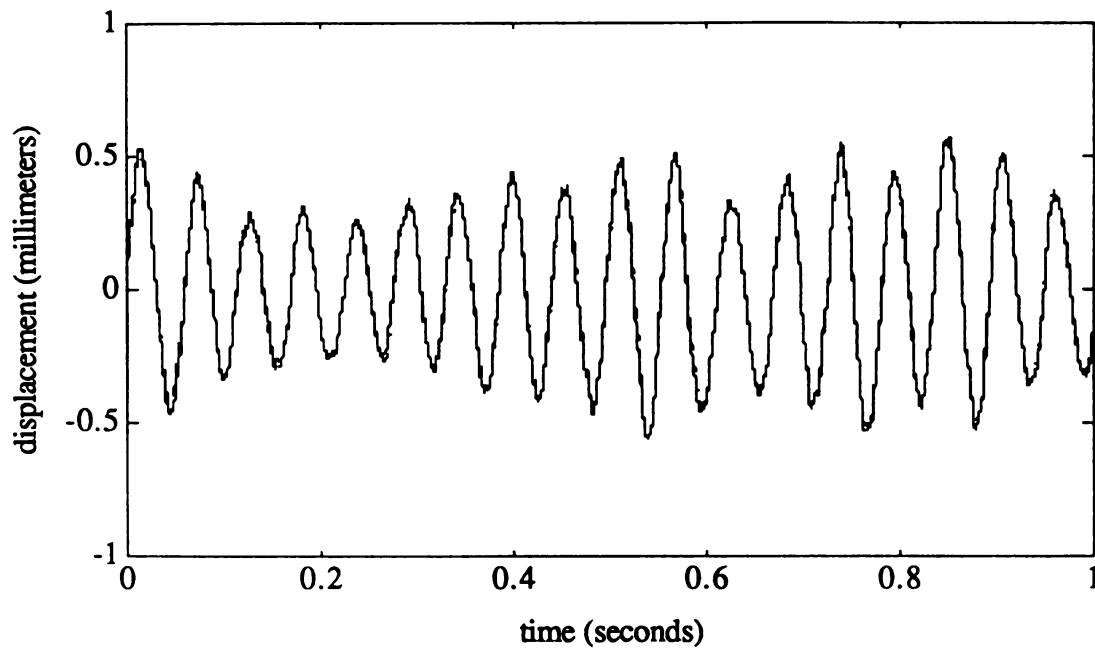


Figure F-8: Crossply-generally damped four mode approximation, test B.

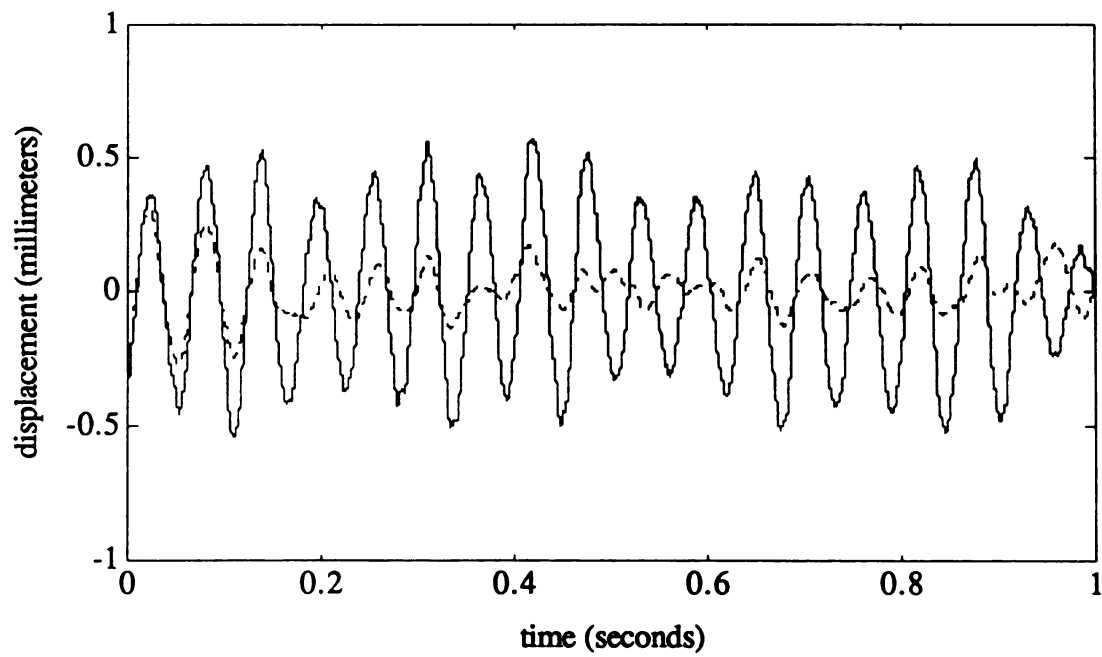


Figure F-9: Crossply-generally damped one mode approximation, test C.

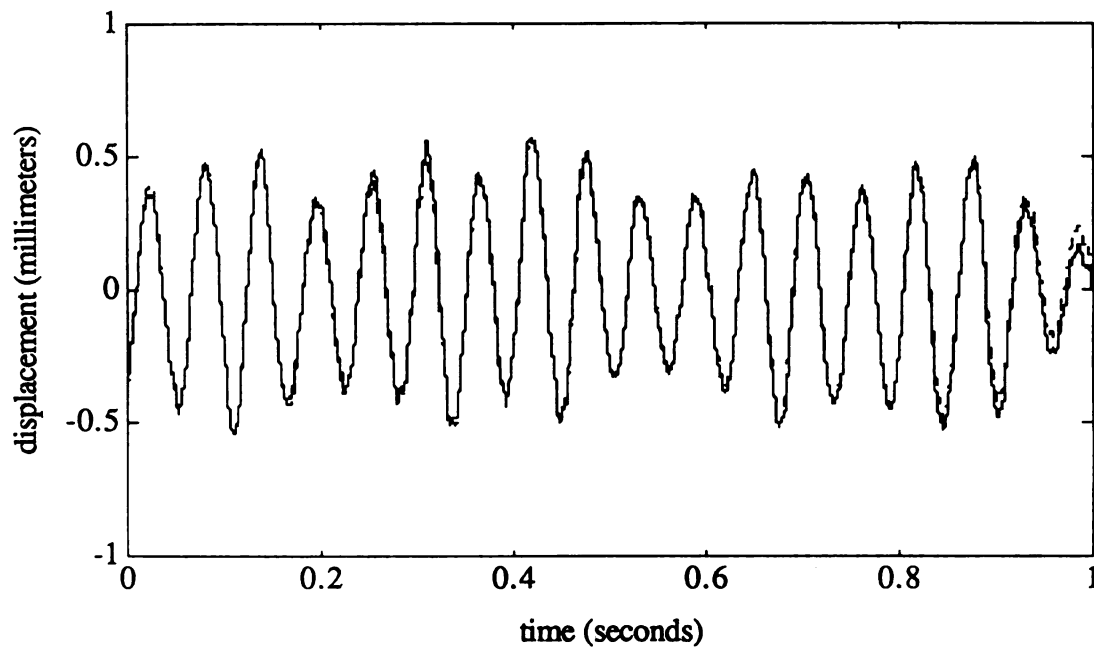


Figure F-10: Crossply-generally damped two mode approximation, test C.

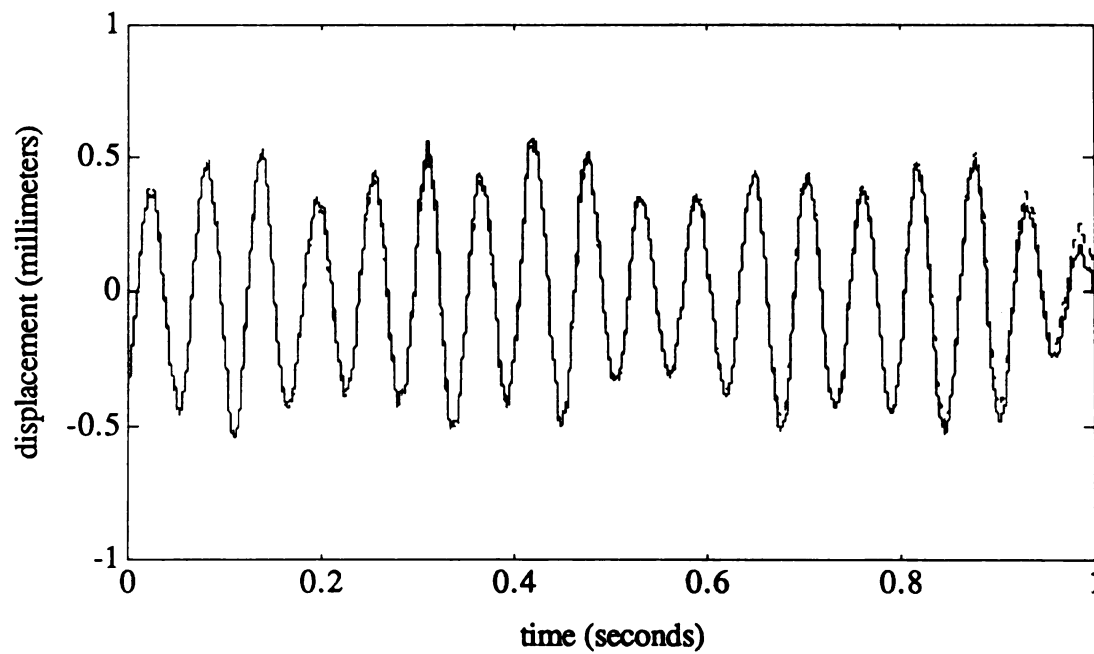


Figure F-11: Crossply-generally damped three mode approximation, test C.

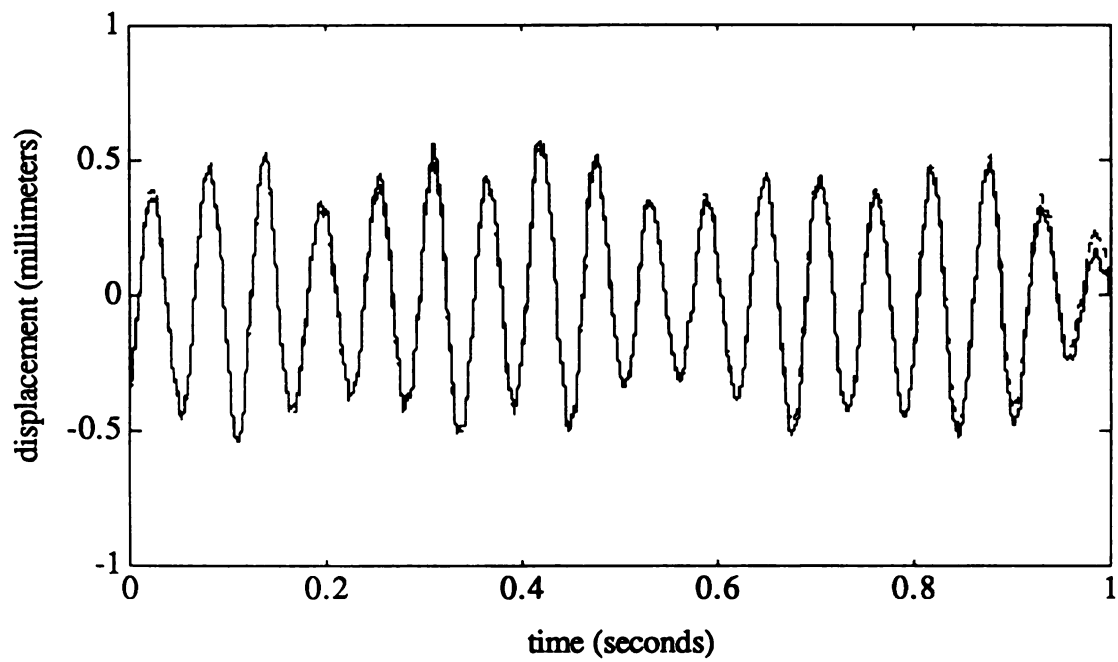


Figure F-12: Crossply-generally damped four mode approximation, test C.

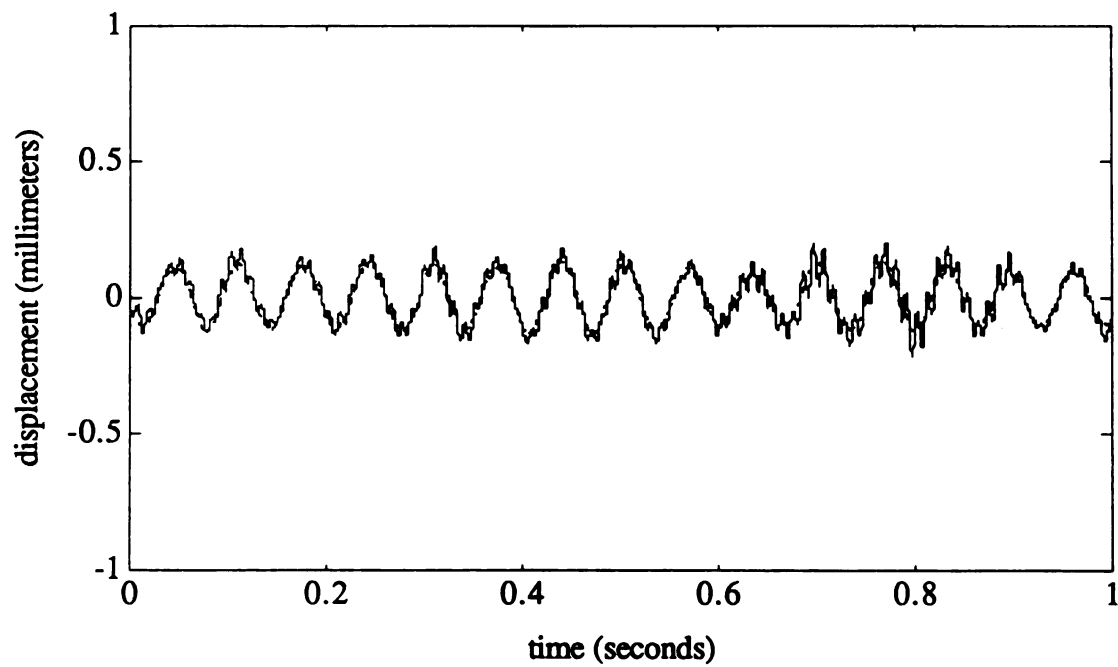


Figure F-13: Aluminum 6061 one mode approximation, test A.

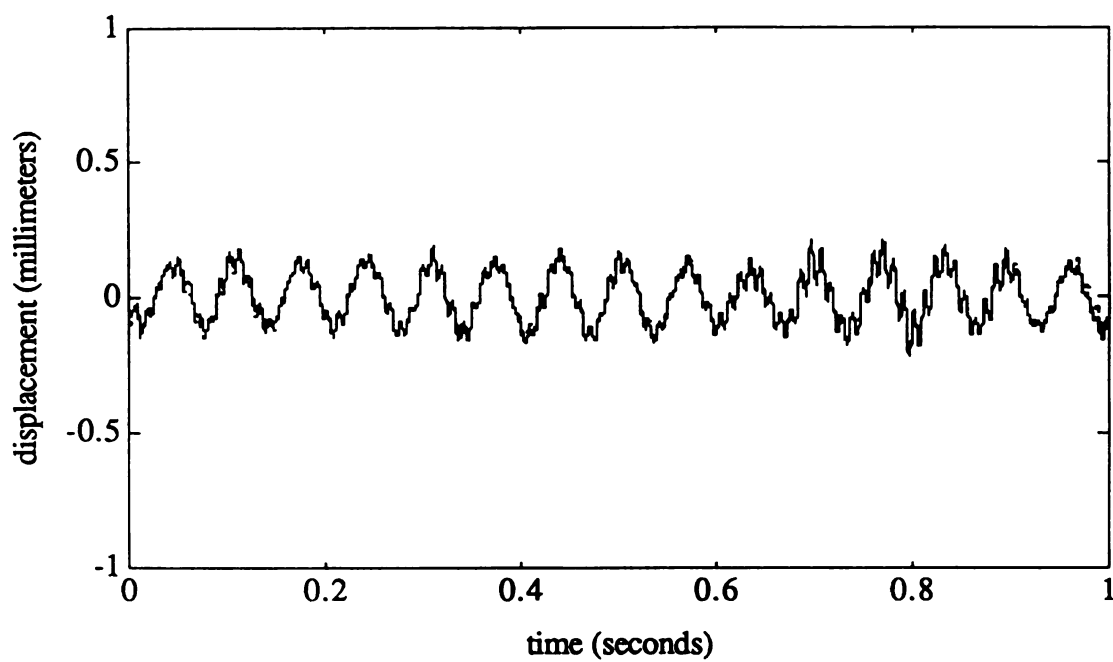


Figure F-14: Aluminum 6061 two mode approximation, test A.

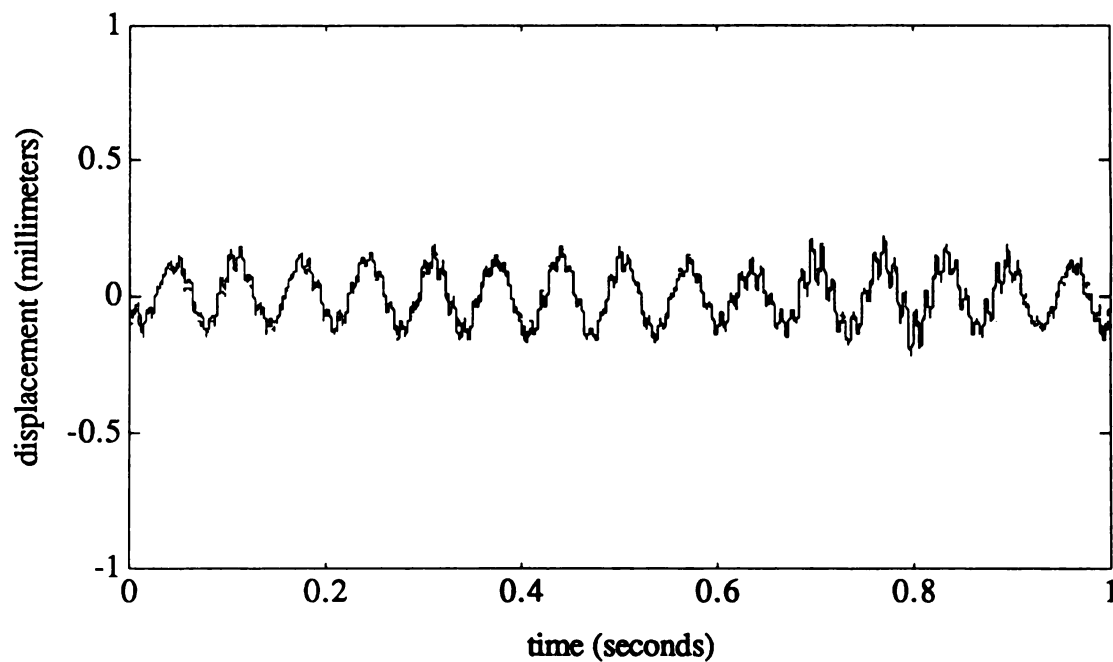


Figure F-15: Aluminum 6061 three mode approximation, test A.

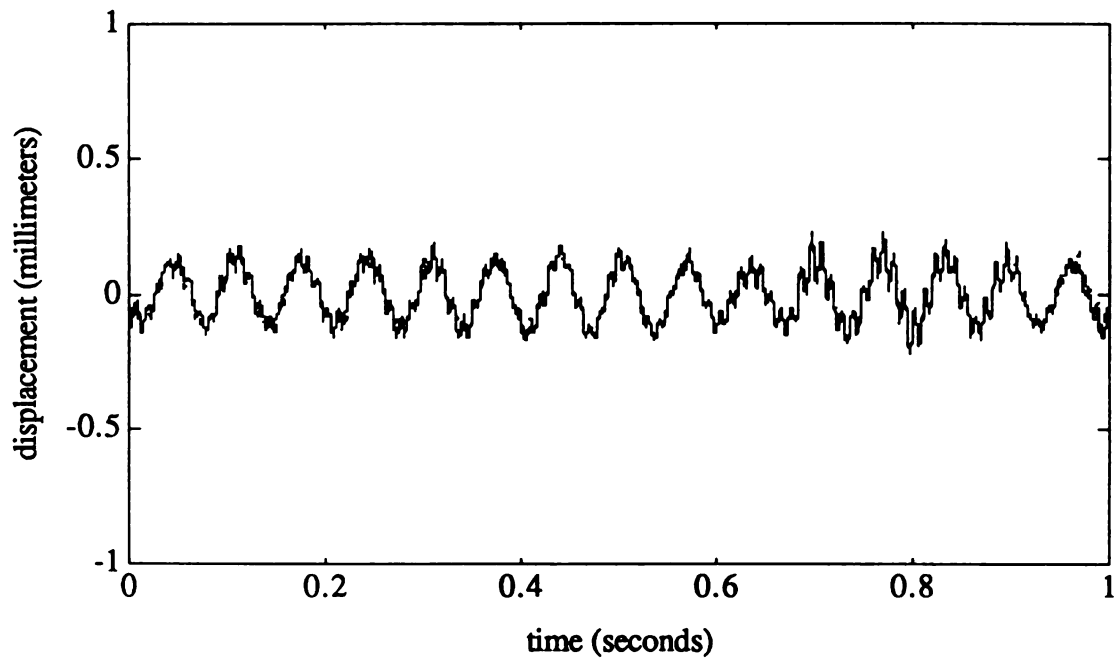


Figure F-16: Aluminum 6061 four mode approximation, test A.

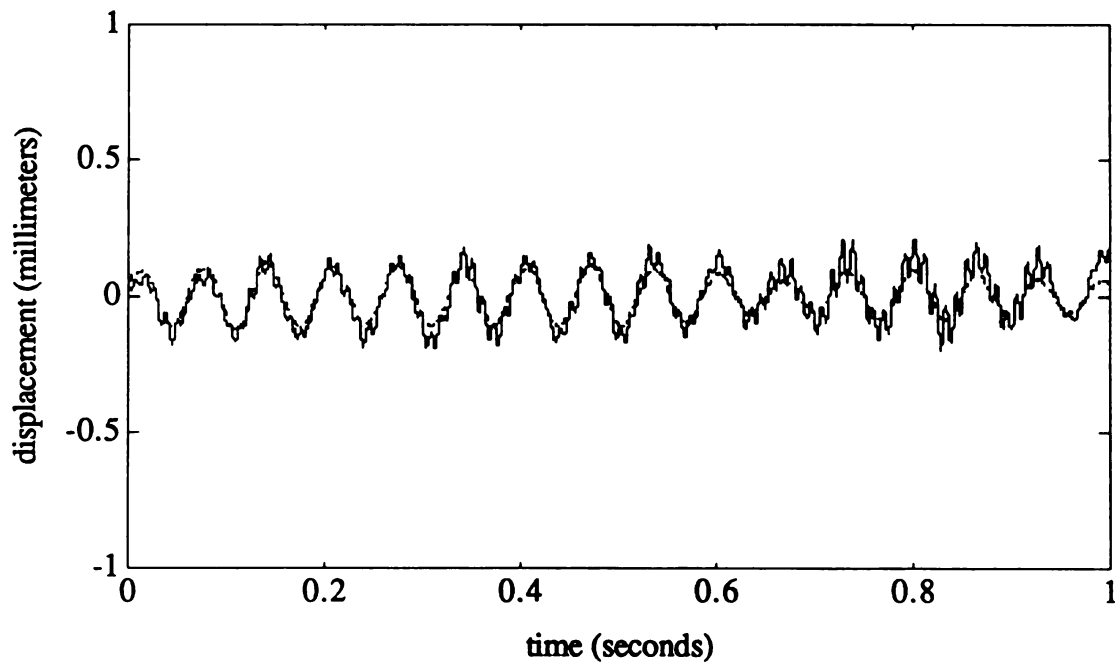


Figure F-17: Aluminum 6061 one mode approximation, test B.

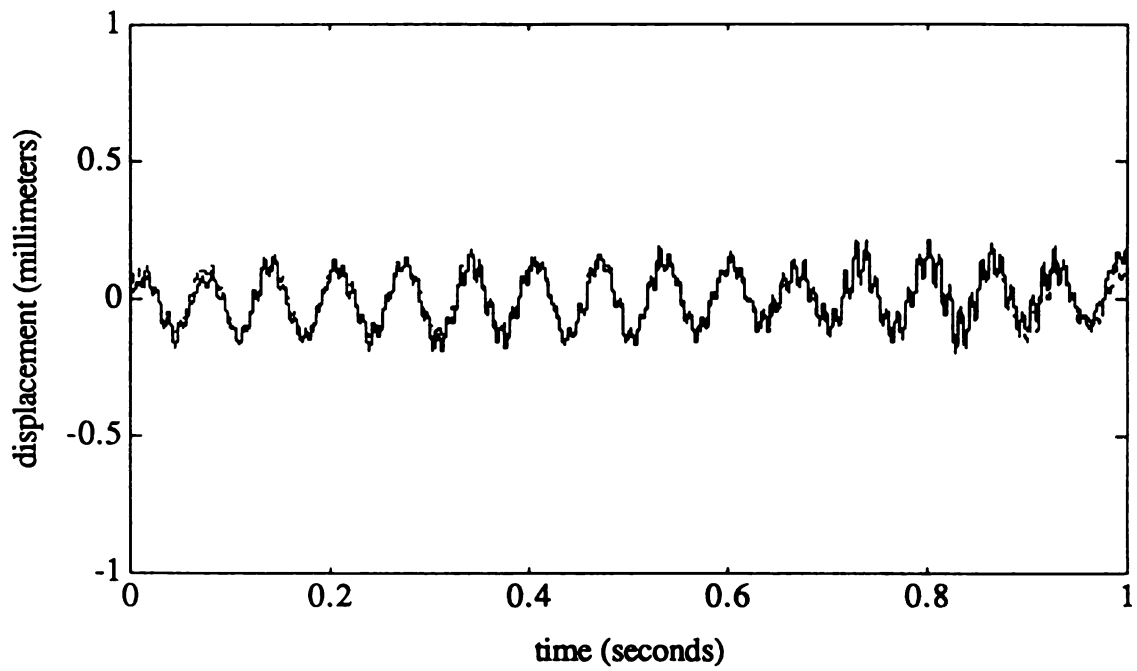


Figure F-18:Aluminum 6061 two mode approximation, test B.

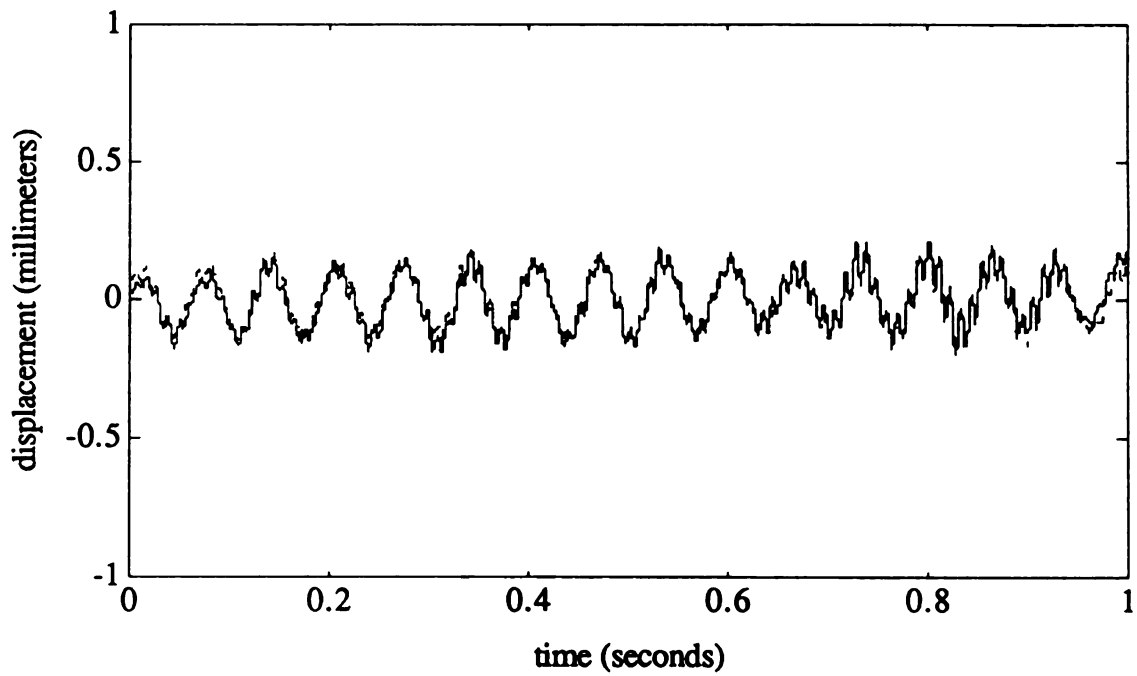


Figure F-19:Aluminum 6061 three mode approximation, test B.

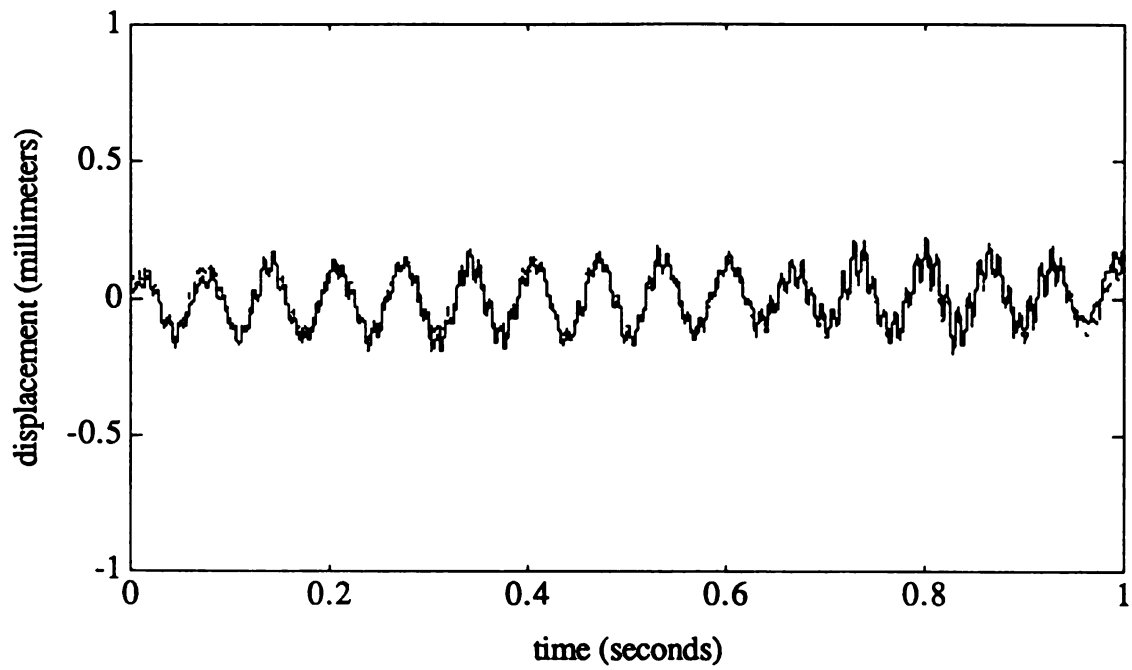


Figure F-20: Aluminum 6061 four mode approximation, test B.

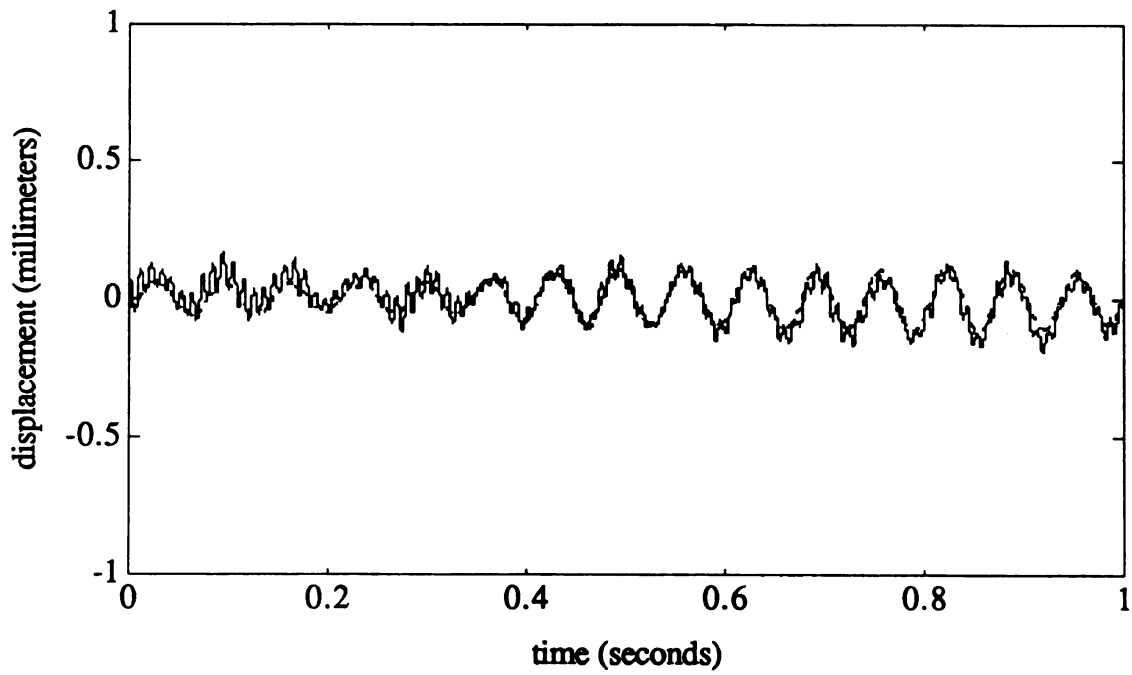


Figure F-21: Aluminum 6061 one mode approximation, test C.

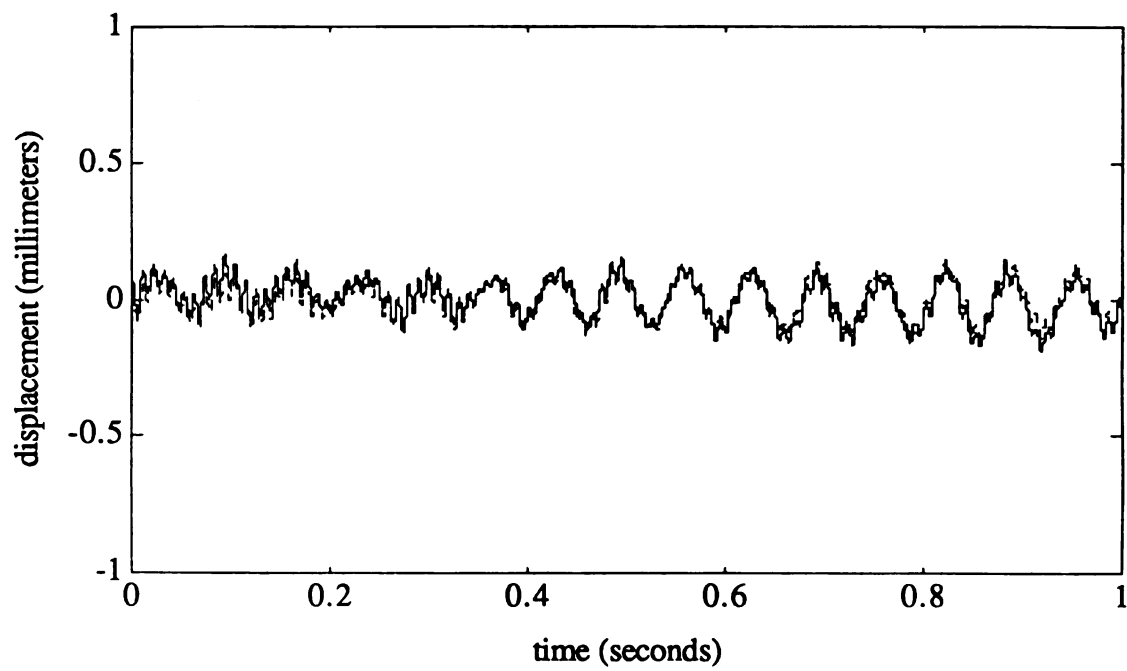


Figure F-22:Aluminum 6061 two mode approximation, test C.

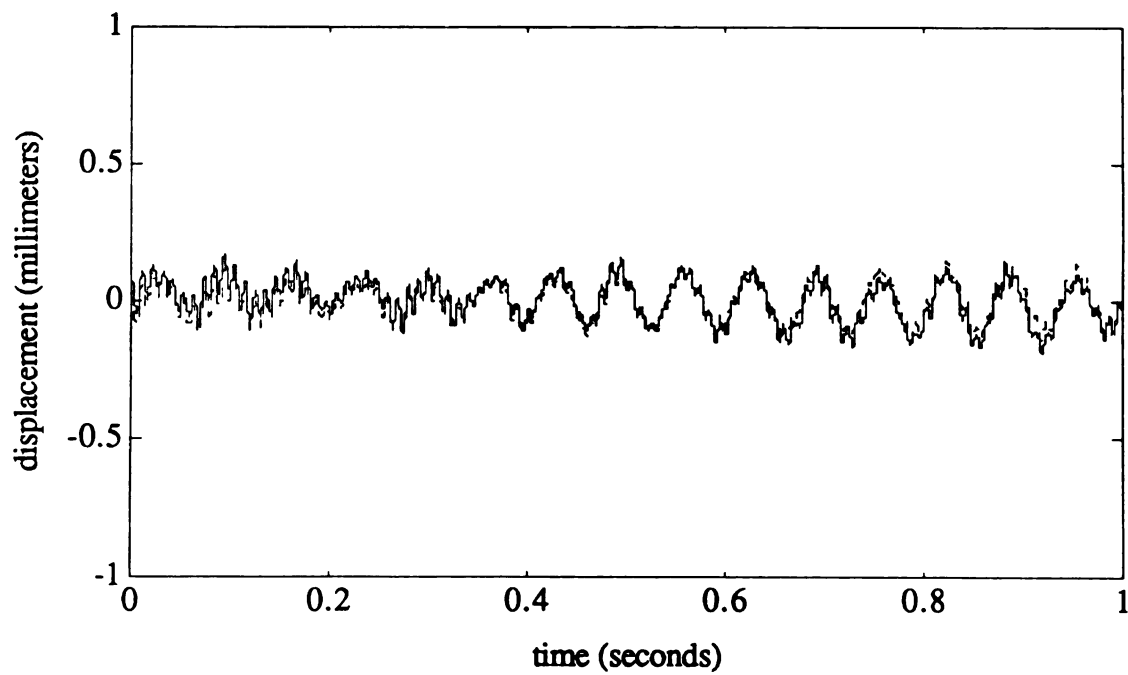


Figure F-23:Aluminum 6061 three mode approximation, test C.

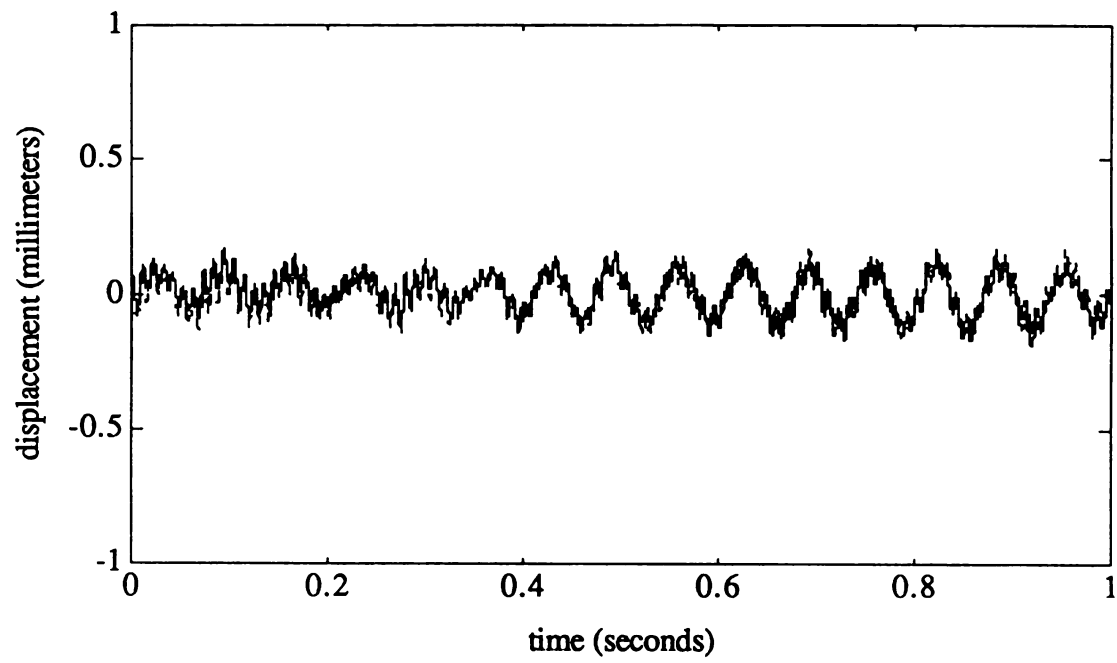


Figure F-24: Aluminum 6061 four mode approximation, test C.

MICHIGAN STATE UNIV. LIBRARIES



31293009134812